AN ABSTRACT OF THE THESIS OF

Karapetrova Evguenia for the degree of Master of Science in Material Science presented on September 22 1997. Title: Factors Influencing the Crystallization, Phase and Oxygen Vacancy Concentration in Zirconia.

Abstract approved: *Redacted for Privacy*

John A. Gardner

In order to achieve a better understanding of the processes that occur during formation and sintering of zirconia, various chemical and physical techniques were used. Along with Perturbation Angular Correlation spectroscopy, that allowed us to investigate microscopic properties inside the nanometer-size zirconia grains, such techniques as Scanning Electron Microscopy and X-ray diffraction were used for determining the size of particles before and after sintering, and Neutron Activation Analysis was employed for measuring the impurity levels in zirconia powders.

By controlling the initial conditions and heat treatment of the powders, we investigated the dependence of formation of the charged defects on the existing molecular structure and morphology of zirconia particles.

During the study, it was discovered that at low temperature the PAC frequencies of tetragonal zirconia behave very similarly for all materials that were used in this study. If stabilization is achieved by heavy doping, there are shifts and line-broadening due to the presence of dopants but no obvious differences in the essential physics. One material included in this group is Nb-doped zirconia that has no oxygen vacancies. It was concluded that there are no detectable oxygen vacancies in our pure or lightly doped tetragonal zirconia powders before they are heated into the temperature region where sintering occurs.

Vacancies are incorporated as the samples are heated above 1050°C, the temperature at which sintering becomes important. The oxygen vacancies in samples that have been heated to 1200°C remain when cooled. We see no vacancy

concentration dependence on the atmosphere for samples not doped with +5 valent elements in order to reduce the vacancy density at 1200°C. In several instances, samples that had been heated to a maximum temperature of 1050°C or 1100°C contained a vacancy density that was small (<100 ppm) but measurable. A reduced oxygen pressure increased the oxygen vacancy density by a measurable amount in these samples. Samples that are tetragonal at 800°C are well-sintered after being heated to 1200°C. Samples that are monoclinic below 1170°C are very poorly sintered at 1200°C and contain few vacancies. Flowing Cl in the system as the samples are sintering retards the densification of the grains. These samples had the smallest density of oxygen vacancies.

Factors Influencing the Crystallization, Phase and Oxygen Vacancy Concentration in Zirconia

by

Karapetrova Evguenia

A THESIS

submitted to

Oregon State University

in partial fulfillment of
the requirements for the
degree of

Master of Science

Completed September 22, 1997
Commencement June 1998

Master of Science thesis of Karapetrova Evguenia presented on September 22, 1997

APPROVED:

Redacted for Privacy

Major Professor, representing Material Science

Redacted for Privacy

Head of Department of Material Science Program

Redacted for Privacy

Dean of Graduate School

I understand that my thesis will become part of the permanent collection of Oregon State University libraries. My signature below authorizes release of my thesis to any reader upon request.

Redacted for Privacy

Karapetrova Evguenia, Author

ACKNOWLEDGMENT

I would like to take this opportunity to express my sincere gratitude to the people who supported and helped me during my work. First I wish to specially thank my adviser Prof. John A. Gardner, for his support and assistance in this very interesting study.

Special thanks to Prof. William E. Evenson for his help with the theoretical part of the PAC spectroscopy. I am very grateful for the wonderful lectures on nuclear condensed mater physics that Prof. Guenter Schatz gave to us while he was visiting.

I want to express my appreciation to Dr. Jim Sommers of Teledyne Wah Chang, Albany for many useful discussions and for providing our laboratory with source solutions for the experiments. I'd also like to thank Dr. Roger Nielson and Dr. Alfred Soeldner for their microprobe and SEM measurements. Thanks to Mr. Erwin Torne from Radiation Center for his help with NAA analysis. I appreciate the time and help of Mr. Patrick Woodward from the Chemistry department with X-ray measurements and analysis. I want to thank Mr. John Archibald for the wonderful work and furnaces that he made for our experiments.

I would like to express appreciation to the other members of our solid state group Dr. Matthew O. Zacate, Dr. Roland Platzer and Karl Shank for their support and help.

I wish to thank my committee members, Dr. Janet Tate, Dr. William Warnes and Dr. Hsiou-Lien Chen, all of whom, through their advice, have made important contributions to my work.

The financial support from the Physics Department and U. S. Department of Energy under contract number DE-FG06-85ER45191 is gratefully acknowledged.

TABLE OF CONTENTS

LIST OF FIGURES

Figure Page

Figure Page

Figure Page

Figure Page

LIST OF TABLES

LIST OF APPENDIX FIGURES

FACTORS INFLUENCING THE CRYSTALLIZATION, PHASE AND OXYGEN VACANCY CONCENTRATION IN ZIRCONIA.

1. INTRODUCTION.

Zirconia, ZrO_2, is a very important material in the production of different technical ceramics. Ultra-fine zirconia powders are used in making a number of tough ceramics. Many technological devices operating at elevated temperatures incorporate oxide components, which are required to sustain high oxygen fluxes. Examples include mixed conductors for ceramic membranes designed to separate oxygen from air, oxide electrodes for solid oxide fuel cells (SOFC), electrolyses, oxygen pumps and amperometric oxygen monitors. High oxygen flux through these devices also implies large values for the oxygen transport kinetics across the gas-solid interfaces, as it is shown on the schematic diagrams (Fig.1.1). The well-established electrolyte for these systems is $Zr_{0.9}Y_{0.1}O_{1.95}$ at 900°C.

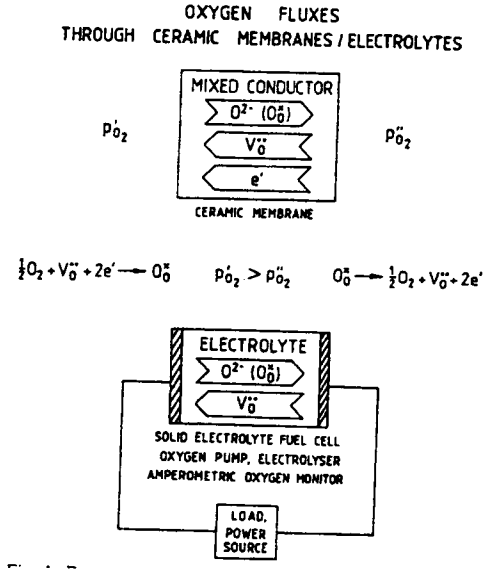

Figure.1.1 Representations of oxygen ion fluxes through system incorporating mixed conductors and oxide electrolytes.

Pure zirconia (ZrO_2) has three well-defined solid phases in equilibrium with air: monoclinic, tetragonal and cubic. The monoclinic phase is stable at temperatures below 1170°C, the tetragonal phase from 1170°C to 2370°C and the cubic phase from 2370°C to the melting point [1-3]. Pure zirconia undergoes a volume contraction on heating and a corresponding expansion on cooling, typically 3-5%, through the monoclinic-tetragonal transformation. This large volume change often results in cracking and crumbling of the zirconia sample [4]. It is very important to understand how to control the crystal structure, particle size, and reproducibility of properties in this material.

The primary focus of this project is the study of oxygen vacancies in pure zirconia and their reproducibility. Previous investigations [5-7] of tetragonal zirconia using perturbed angular correlation (PAC) spectroscopy have demonstrated the existence of a large extrinsic concentration of oxygen vacancies. Section 2.5, which is an only slightly modified version of a section from the thesis of Matt Zacate and Han-Tzong Su [6, 7], describes the results of these previous studies. The theory of Perturbed Angular Correlation spectroscopy described in Chapter 4 and 5 of this thesis closely follows the publications of G. Schatz and A. Weidinger and H. Jaeger [54,48]. Chapter 3, which is largely taken from the discussions by Y. –M. Chaing, D. Bitnie III and W. D. Kingery and W. E. Wang and D. R. Olander [49, 50], discusses the essentials of oxygen vacancy thermodynamics.

To extend the previous research some additional techniques were employed in this study. Measurements by scanning electron microscopy allowed us to investigate the dependence of the grain size and the morphology of the sintered powders on the process parameters. These parameters include the nature of the precursor, pH balance, thermal history, and influence of atmosphere. The influence of some of these parameters on the phase stabilization and different structural characteristics of tetragonal zirconia has been widely studied over the years [8-13]. A summary of these publications is given in Chapter 2. X-ray spectroscopy helped us to understand the formation and crystallization processes, and NAA analysis determined the purity of our samples. The NAA results were a very important addition to the previous results, because they showed that the charges that were causing the oxygen vacancies in our samples are not due to accidental doping.

In the course of this work, it was found that zirconia could be formed in the monoclinic or tetragonal phase depending on the nature of the process. Tetragonal crystallites can remain tetragonal or transform to the monoclinic phase below 800°C

depending on the details of how they are heat treated after formation. At temperatures below 1170°C the monoclinic phase is stable and tetragonal phase is metastable.

There are no detectable oxygen vacancies in pure or lightly Ce-doped or Nb-doped tetragonal zirconia powders at low temperatures. Vacancies are incorporated as the samples are heated above 1050°C, the temperature at which sintering becomes important. The oxygen vacancies in samples that have been heated to 1200°C remain when cooled. We see no vacancy concentration dependence on the atmosphere for samples containing a substantial number of vacancies at 1200°C. But a reduced oxygen pressure increased the oxygen vacancy density by a measurable amount in some samples at temperatures from 1050°C to 1200°C that contained only a small vacancy density (<100 ppm).

The morphology after sintering of the powders depends on the phase of zirconia at low temperature. In the course of this research, it was learned that the excess from the expected value of the oxygen vacancy concentration was not caused by the presence of impurities in the samples; this was proved by NAA experiments. The major conclusion of this research project is that the only straightforward way to explain the high concentration of oxygen vacancies in zirconia is by the existence of negatively charged extrinsic defects. These defects may be due to their inclusion in grains as the grains are sintered. The conclusion has stimulated a search for these extended defects by collaborators who use transmission electron microscopy.

2. BACKGROUND.

This chapter is a summary of the publications that are relevant to my research. The effects that are described in these papers are relevant to our experiments. The initial conditions and the method of preparation of the zirconia samples are different for nearly every experiment reported, so the temperatures and other conditions at which the specific phenomenon was observed are different for all experiments. It is therefore not always easy to make a connection between the results of one particular paper and this research. In general, though, the same physical and chemical principles are applicable to all results.

2.1 Crystallization and grain growth in zirconia.

Factors influencing formation, growth, and transformation of tetragonal zirconia have been the subject of much research in the past [9]. The most important parameters are grain size, pH balance, strength of the grains, nature of the precursor, and history of the thermal treatment. In this work we investigated the connection between these parameters and oxygen vacancies in tetragonal zirconia at 1200°C. We would like to know how the vacancies arise, when they are formed, and their dynamics.

For convenience we divided thermal processes into several temperature regions:

1. From room temperature to 400°C (Formation).
2. From 400°C to 800°C (Calcination region).
3. From 800°C to 1300°C (Sintering process).
4. Cooling down (Tetragonal to monoclinic phase transformation).

2.1.1 Formation.

It is well known that metastable t-ZrO_2 (tetragonal) can be formed in different ways from zirconia salts or from amorphous zirconium hydroxide. However, there are

still some questions concerning the structure of the amorphous zirconia precursor, as well as the mechanism of zirconia polymorph transitions. Garvie [14] suggested that tetragonal zirconia is stabilized at low temperature by surface energy effects. The experimental results obtained by ball-milling supported that hypothesis. When the grinding of the starting material sufficiently decreased the crystallite size, the m→t transition occurred [15]. In the bulk material, this transition normally occurs at 1170°C. In the milled samples, impurities also affected the phase transition m→t. Murase and Kato [16] examined the transition of tetragonal ZrO_2 by ball-milling in different atmospheres. They showed that water adsorbed on the surface of the particles affected the t→m transition of the milled samples.

From room temperature up to 400°C X-ray diffraction is not useful in determining the crystal size, because the small crystal size gives very broad lines. The data for the crystal size in this region were obtained by Raman spectroscopy [12]. The conclusion of this work is that there are three controlling regimes for the formation of crystalline ZrO_2: dissolution/precipitation at low pH, a solubility controlled regime at intermediate pH, and gel structure controlled regime at high pH. In another paper by Sato and et al. [17] it was determined that chemical formula of the amorphous zirconia precursor is:

$$Zr_{2-x}(OH)_{2x} \bullet yH_2O, x \leq 2, y \cong 1 ,$$

And at 500°C forms the metastable *t*- or *m*- phase, depending on the x value.

The mechanism of hydrolytic polymerisation of zircolnyl solutions was described in detail by A. Clearfield [10], who showed that refluxing dilute solutions of zirconyl chloride results in precipitation of colloidal zirconia in which the particles are crystallized in the monoclinic phase [18]. During refluxing the pH decreases considerably and may fall below 1. Crystallization can also be obtained by boiling slurries of freshly precipitated gelatinous, amorphous zirconia. The gel always retains some anions when precipitation occurs below pH 7, and these anions are displaced during the boiling process ($OH^- \rightarrow Cl^-$) to produce weakly acidic solutions. In this case the solid consisted of a mixture of tetragonal and monoclinic phases with decreasing amounts of the former phase as refluxing progressed. However, when amorphous, hydrous zirconia was boiled in base, it crystallized to the tetragonal phase. A mechanism was proposed [19] based on these facts and the knowledge that the tetrameric zirconyl species found in the solid [20], $[Zr(OH)2 \bullet 4H20]4^{8+}$, was also a major species in solution [21]. Refluxing ziconyl chloride solutions leads to their

hydrolytic polymerization as does addition of base to these solutions. The tetramer consists of the four metal atoms in a square with double hydroxyl bridges linking them

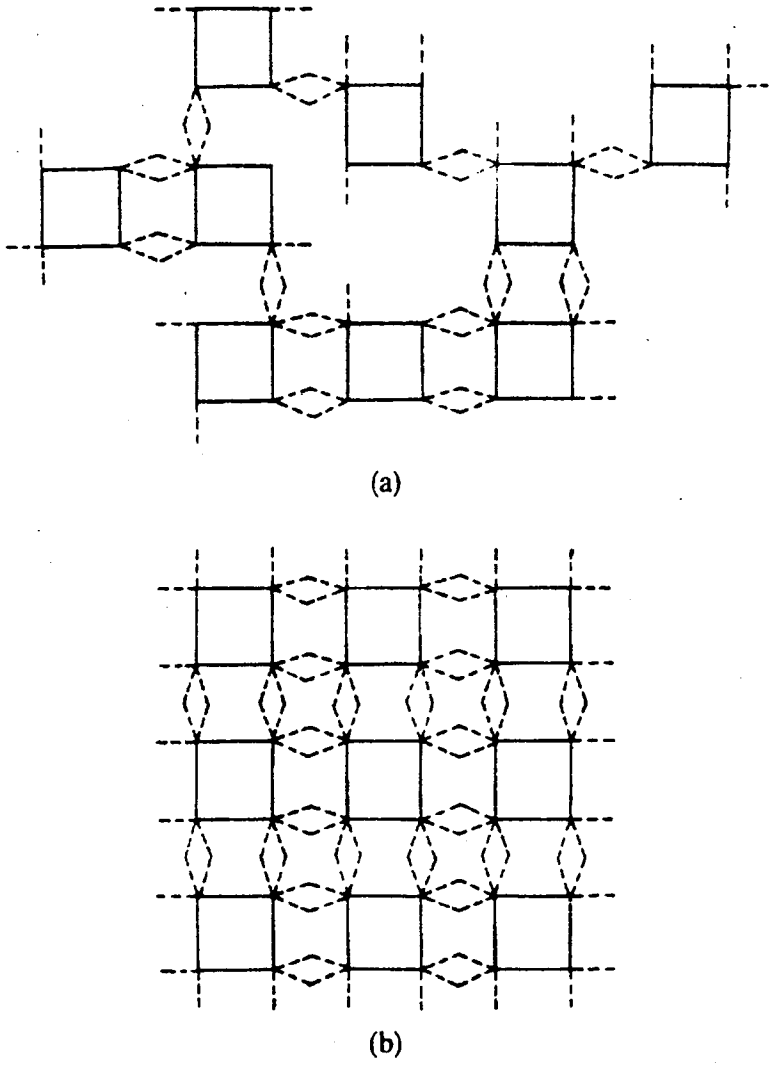

Figure 2.1 Two-dimensional representation of polymeric species formed by the aqueous tetrameric Zr(IV) complex. The solid lined squares represent the original tetrameric units, $Zr_4(OH)_8$. Each dashed line represents an -OH group formed by hydrolysis. A bent dashed line connected to two squares represents a single hydroxyl group bonded to two metal atoms. (a) Randomly formed polymer such as obtained by base addition to solution. (b) Ordered sheet polymer produced by refluxing Zr(IV) solutions.

together. The four water molecules complete the coordination sphere of each metal atom. Solutions of zirconyl chloride are highly acidic, and this certainly is due to hydrolysis,

$$[Zr(OH)_2 \bullet 4H_2O]_4^{8+} \leftrightarrow [Zr(OH)_{2+x} \bullet (4 - x)\, H_2O]_4^{(8-4x)+} + 4xH^+$$

Heating the solutions accelerates the process, shifting the equilibrium to the right [22]. Addition of the base has the same effect. It is proposed that subsequent polymerization takes place by combining of two tetrameric species to form hydroxyl bridges between them. Such linkage may occur in two different ways: by heating or by addition. Rapid addition of base increases the number of hydroxyl groups on the tetramer in a random fashion so that polymerization occurs rapidly and in many directions at once (Fig.2.1). There is no time to form an ordered array of tetramers and the result of this rapid polymerization is an amorphous gel.

In contrast, hydrolytic polymerization induce by boiling is a slow process. Therefore it was proposed that two tetramer species link up to form a third and continuation of this process leads to sheets of $Zr(OH)_4 \bullet \chi H_2O$, as shown in Fig.2.1. The water molecules are at the edges of the sheets. The sheets then come together in such a way that water splits out by condensation of hydroxyl groups, forming a fluorite structure. The growth of sheets and their assembly has been observed by electron microscopy [23]. This information was applied to the solution precipitation results. In alkaline media (above pH 13) hydrous zirconia is very slightly soluble:

$$Zr(OH)_4 \bullet \chi H_2O + OH^- \leftrightarrow Zr(OH)_5^- \bullet \chi H_2O$$

The dissolution - reprecipitation of the hydrous oxide is a slow process so that the ordered sheets can form, leading to the tetragonal phase. Thus, even at room temperature, nuclei of the tetragonal phase must form even though the solid appears amorphous to X-rays. For base precipitated oxide, in the pH range of 7-11, the longer the precipitation process takes, the greater the yield of tetragonal phase. This is also in accord with the hypothesized formation mechanism by which the tetragonal phase nucleation would be less efficient at lower pH. Rapid precipitation leads to all monoclinic ZrO_2. Thus, the randomly formed oxide particles cannot come together as sheets so that the formation of the monoclinic phase is favored on heating rather than the tetragonal.

At the other end of the pH spectrum, hydrolytic precipitation by boiling is also a slow process so one might expect to obtain the tetragonal phase. The tetragonal phase does form first, even in acid solution (pH 2 or less), but as the crystallites grow

they transform to the monoclinic phase. This transformation may result from the removal of crystal defects [24]. However, this cannot be the explanation for precipitates formed at ambient temperatures. For such cases it was proposed that at pH 2 or lower, tetragonal nuclei form, which on heating, act as a template directing the formation of tetragonal phase. At progressively higher pH values, fewer and fewer such nuclei form with the remainder forming an amorphous gel. The amorphous material then crystallizes as monoclinic ZrO_2. Figure 2.2 shows the determination of the tetragonal phase by pH.

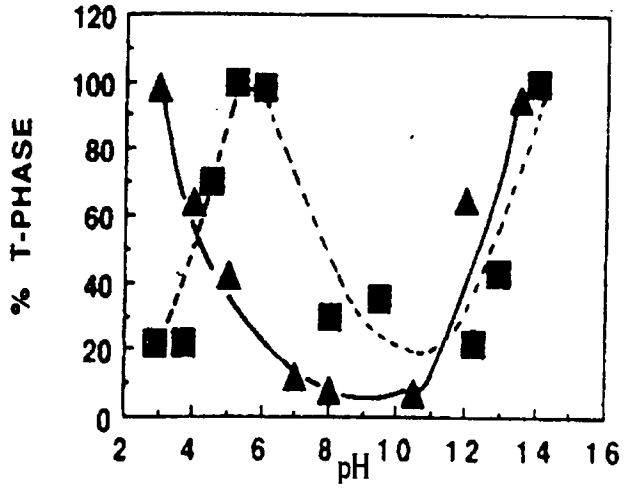

Figure 2.2 Plot showing the percentage of tetragonal phase (based on XRD peaks) vs pH (▲-from Ref. [11], ■- from Ref. [12])

Two different methods of addition of ammonium hydroxide at a pH of 10.5 were studied by R. Srinivasan and et al. [25]. Amorphous zirconia precursors were made by the precipitation of a zirconium tetrachloride solution with either slow (8h) or rapid addition of ammonium hydroxide. Following calcination at 500°C for 4 h, the rapidly precipitated precursor gave predominantly monoclinic ZrO_2 phase, while the slow precipitated precursor produced the tetragonal phase. High temperature x-ray

diffraction data was taken at 450°C showing that each amorphous precursor first crystallized in the tetragonal phase.

A study of crystallization of zirconia under hydrothermal conditions was made by M.M. Bychi and et al. [26]. Zirconia amorphous gel subjected to hydrothermal treatment transforms to crystalline material at 250°C. The morphology and size of the crystallites change with the time of the process performed in the two environments, water and water solution of NaOH. The rates of these changes are much higher in the NaOH solution. Two mechanisms of crystal growth seem to operate: coalescence of the primary crystallites in a highly oriented way, and filling the contact and facing of the particles by the dissolution-precipitation process.

Finally, it should be remarked that the presence of chelating or complexing species such as sulfates, oxalates, glycols, and the like change the polymerization pathway for the zirconium species. As a result, the products may be completely different from those obtained where only noncomplexing species, such as Cl^-, $NO3^-$, and ClO_4^- were present and this also has been observed [18,27].

G. Srefanic et al. [28] observed that zirconia salts containing Cl^-, NO_3^- or SO_4^{2-} contained metastable t-ZrO_2, which disappeared with further thermal treatment. The t-ZrO_2 to m-Zr O_2 ratios, measured by XRD, were dependent on the nature of the starting salt. The different fractions of t-ZrO_2 and m-ZrO_2 in samples obtained after the heating of $ZrOCl_2 \bullet 8H_2O$ and $ZrO(NO_3)_2 \bullet 2H_2O$ up to 400°C suggested that the structural parameters of $ZrOCl_2 \bullet 8H_2O$ were closer to t-ZrO_2 than those of $ZrO(NO_3)_2 \bullet 2H_2O$. A further increase of heating temperature showed that t-ZrO_2 formed from $ZrOCl_2 \bullet 8H_2O$ was thermally least stable, while the presence of t-ZrO_2 formed from $Zr(SO_4)_2 \bullet 4H_2O$ was found even at high temperature. Metastable t-ZrO_2 obtained by the thermal decomposition of $ZrOCl_2 \bullet 8H_2O$ and $ZrO(NO_3)_2 \bullet 2H_2O$ showed a very high sensitivity to mechanical treatment, while metastable t-ZrO_2 formed from $Zr(SO_4)_2 \bullet 4H_2O$ was stable during the same process. It was concluded that the formation of metastable t-ZrO_2 was mostly influenced by the nature of the starting salt but, once t-ZrO_2 was formed, its stability depended on the anionic impurities that remained in the oxide material.

The thermal behavior of amorphous hydrated zirconium oxide was also discussed by J. Livage. K. Doi and C. Mazieres [29]. Thet showed that crystallization was nucleated at a few favored points inside the amorphous phase and thus is not a bulk phenomenon. The particle size of the amorphous zirconia was from 1μ to 100Å.

Figure 2.3 shows the dependence of the crystallized fraction on the calcination temperature of the sample and the time the powders were kept at this temperature.

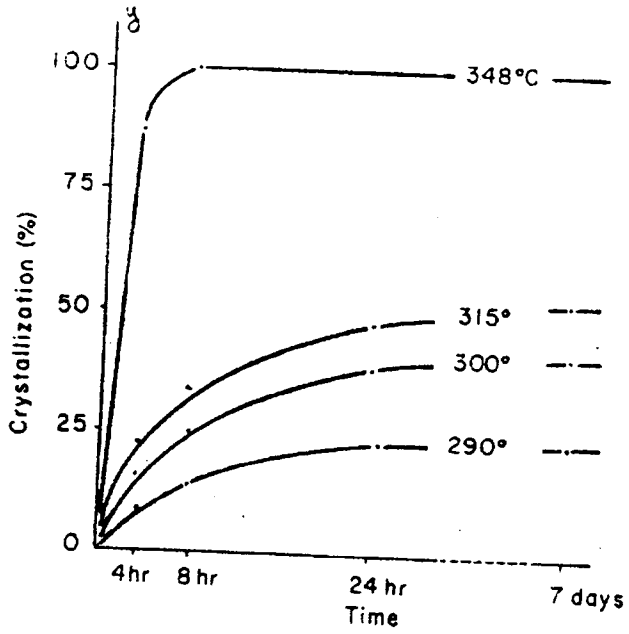

Figure 2.3 Crystallization kinetics of amorphous zirconia

The distribution function obtained by X-ray and neutron diffraction showed that the atoms were not distributed randomly in the amorphous zirconia.

2.1.2 Calcination regions (the temperature range from 400°C to 800°C).

Calcination is the common term used by ceramists for heating amorphous powders in air. The purpose of calcination is in to converting precursor solids into oxide powders.

It was found [11] that the pH of the solution from which the gel is precipitated determines the zirconia crystal phase after calcination at 600°C. Monoclinic zirconia is

produced from material precipitated in the 6.5 to 10.4 pH range; a tetragonal precursor is obtained for the 3 to 4 or 13 to 14 pH range (Fig.2.2). The calcination atmosphere, temperature history during calcination, and the presence of alkali do not appear to play a dominant role in determining the zirconia phase composition. For higher temperature, it was discovered by M. J. Readey and D.W. Readey that atmosphere does influence the grain growth [30]. The precipitates leading to nearly pure tetragonal form were obtained at pH levels above ≅ 12; it was necessary to use a strong base, NaOH or KOH, for the precipitation. The same results were obtained for both NaOH and KOH.

D. E. Collins et al. [31] described a mechanism by which the molecular configuration might influence structural features in the pyrolysis product. A sample of a zirconium alkoxide derivative, dibutoxybis (acetylacetanato) zirconium, was polymerized at 120°C and 300 millitor for 3 h to form oligomers, as characterized by gel permeation chromatography and Fourier transform infra-red spectroscopy. Pyrolysis of the precursor at 675°C in flowing 5% H_2 in N_2 followed by cooling to room temperature, produced nano-scale, tetragonal ZrO_2 considerably below the tetragonal- to - monoclinic transformation temperature (approximately 1200°C). Subsequent heat treatment of the same precursor in flowing air under otherwise identical conditions produced approximately 8 vol% monoclinic ZrO_2. It was also found that the molecular configuration of the precursor (cisoligo[dibutoxybis(acetylacetonato) zirconium (COBAZ)) and the resulting oxide after pyrolysis are intimately related. It was proposed that zirconium, within the COBAZ backbone, has an eight-fold coordination to oxygen, similar to the t-ZrO_2 unit cell; whereas terminal zirconium has seven-fold coordination. When pyrolysed in the absence of oxygen, COBAZ nucleates a completely t-ZrO_{2-x} containing oxygen vacancies retained from the COBAZ structure, particularly from the terminal zirconium positions. These vacancies play in integral role in tetragonal nucleation. When t-ZrO_{2-x} is heat treated in the presence of oxygen under otherwise identical conditions, a fractional amount of monoclinic phase develops. This introduction of oxygen diminishes the number of vacancies such that tetragonal instability occurs, facilitating monoclinic growth.

2.1.3 Sintering process (the temperature range from 800°C to 1300°C).

Sintering occurs when individual particles grow together to form a dense solid. In this temperature range some very important phenomena have been observed. At low temperature, surface diffusion is the dominant mass transport mechanism; above 1000°C densification occurs most likely via grain boundary diffusion and is retarded by reorganization processes [13]. At temperatures around 800°C, different phenomena were observed such as hopping of clusters of atoms on and off the surface of grains, and reorientation of the particles with respect to each other [32]. This reorientation can be explained in terms of a minimization of the grain-boundary energy between the two coalescing particles. This can influence the boundary between the grains.

At this temperature the influence of a HCl atmosphere was also observed, as mentioned in the previous section [30]. Pure zirconia fired in HCl shows greatly reduced shrinkage compared to the same material fired in air. One of the main microstructural differences is the much more rapid grain growth in the porous zirconia fired in HCl. The observed grain growth does not follow any simple growth law over the temperature range investigated (1100°C to 1300°C). In this range the partial pressure of $ZrCl_4$ is several orders of magnitude greater than all other vapor species and sufficiently high so that vapor transport should dominate microstructure development. The grains grow up to a limiting particle size close to the initial agglomerate size and appear to stop. The particle size that was investigated in this work is 0.3μm to 1μm.

2.1.4 Cooling down (Tetragonal to monoclinic phase transformation).

The tetragonal to monoclinic transformation on cooling down was investigated in the work of R. Srinivasan et al. [25]. It was shown that the t →m transformation in zirconia materials is not controlled by difference in crystallite size. It is therefore suggested that anionic vacancies control the tetragonal-to-monoclinic phase transformation on cooling, and that oxygen adsorption triggers this phase transformation.

In a previous investigation about the correlation between the grain size of the powder and the transition t→m temperature [33], zirconia was prepared by precipitation from a solution of zirconium tetrachloride by adding ammonium hydroxide to produce a pH of 2.95. Portions of the sample, after drying, were calcined at 500°C for various time intervals. Phase transformation was followed by X-ray

diffraction; the data shows that tetragonal phase was initially formed and it was transformed to the monoclinic phase after longer calcination. TEM particle size and XRD crystallite size show that the transformation does not appear to be due to a critical particle size effect. The TEM data show that the individual particle size does not increase significantly during the heating periods that affected the tetragonal-to-monoclinic phase change. The data do not support the view that surface energy factors stabilize the tetragonal phase of zirconia. It was suggested that the reason larger tetragonal particles transform to smaller monoclinic particles is that most tetragonal particles transform from twin-related variants of monoclinic particles.

At 1200°C, all zirconia is in the stable tetragonal phase. The anisotropic thermal expansion of the monoclinic and tetragonal phases causes crumbling of zirconia ceramics on cooling from the sintering temperature. The effect of chemical and heat treatment on the tetragonal to monoclinic transformation of zirconia was investigated by Turrilas et al. [34]. The rapid in-situ diffraction technique, synchrotron radiation-energy dispersive diffraction, was used to obtain direct information on the kinetics of the tetragonal-to-monoclinic transformation temperatures for zirconia synthesized by heating the hydroxide up to temperatures between 900°C and 1300°C. In all cases the monoclinic phase appears only during the cooling stage (The pH values of the initial samples were 8.37 and 10.35). For the heat treatment at lower temperature (generally temperatures < 1000°C) the high-pH materials have the higher transformation temperatures, whereas with higher temperature heat treatments (generally temperatures > 1000°C) the low-pH materials have the higher transformation temperatures. During the final period of heating to the maximum temperature (T_D) and the dwell time (t_D) at that maximum temperature, the oxide remains in the tetragonal state for all combinations of T_D and t_D, and pH studied. Heating rate was kept constant (50°C min^{-1}) for all measurements.

Results of this paper [34] (tab.2.1) are the following:

1) Regardless of chemical or heat treatment, the t→m transformation occurs only during the cooling stage,
2) The greater the heat treatment (combined effect of T_D and t_D), the higher the transformation temperature $T_{t\rightarrow m}$.
3) The transformation temperature is very sensitive to the top dwell temperature.
4) In separate laboratory diffraction experiments, using very restricted synthesis conditions, it was shown that the $T_{t\rightarrow m}$ (t_D) dependency is similar to the

sigmoidal variation common to most solid state time-dependent transformations [35].

5) The pH variation was somewhat unexpected: with low heat treatments, normally at a temperature of 900°C or less, the high pH materials have the higher $T_{t\rightarrow m}$. In complete contrast, with greater heat treatment, it is the low-pH material that exhibits the higher $T_{t\rightarrow m}$.
6) With heavy heat treatment (1300°C), pH difference no longer plays a role, and the dynamic transformation temperature $T_{t\rightarrow m}$ approaches the idealized value around 1170°C.

The transformation temperature can be greatly increased by the "extrinsic" effect of heat treatment as measured by the two basic variables T_D and t_D. Secondly, where the high-pH-prepared material intrinsically produces higher transformation temperatures, it is the low pH-prepared material that is more sensitive to heat treatment. The previous study [36] gave a simplified structural model to account for the more rapid crystallization, on heating, of high pH-prepared hydroxides. With high-pH

Dwell Temperature(°C)	Time Held (min.)	$T_{t\rightarrow m}$ *for pH = 8.37*	$T_{t\rightarrow m}$ *for pH = 10.35*
900	No holding	...	No transition
	10	No transition	150-<30°C
	60	100-<30°C	320-100
	420	400-100	...
1100	No holding	520-380	520-450
	10	930-850	640-580
	60	860-840	705-650
	150	890-780	...
1300	No holding	910-820	870-800
	10	925-89-	920-860
	60	970-910	920-890
	180	1010-980	...

Table 2.1 Tetragonal to monoclinic transformation temperatures as a function of thermal treatment (T_D, t_D) and hydroxide preparation (pH) from [34].

hydroxides there is more randomization in the linking of polymerized tetrameric units, producing more numerous, highly strained embryonic nuclei for the crystallizing tetragonal phase. We might imagine that this "intrinsic" preference could persist, with lower heat treatment, so that high-pH material also forms more numerous/strained monoclinic nuclei as well, prior to or during cooling. The increases in the crystallite size appear to correlate linearly with $T_{t\rightarrow m}$ in similar fashion for both low and high pH preparations. While this seems to confirm a connection between crystallite size growth and extrinsic effects, it still does not explain why the low pH material should be so much more sensitive to heat treatment.

2.2 Effect of dopants on the crystal structure of zirconia.

Microstructure development during non-isothermal and isothermal sintering has been studied for tetragonal zirconia ceramics (TZP) containing various amounts of Y and Ce [37]. Smaller grain sizes were obtained when Ce-TZP was doped with yttrium. This could be attributed to segregation of yttrium to the grain boundaries, thus causing an impurity drag. With increasing temperature, the grain growth in the Ce-TZP samples became faster, which could be attributed to the absence of a dragging force. The slow grain growth at low temperature in the Ce-TZP samples was attributed to slow diffusion kinetics of the diffusing species (trivalent and tetravalent cerium). The critical grain size for retention of the tetragonal phase at room temperature is larger in the Y, Ce-TZP system compared to the Y-TZP and Ce-TZP systems. The chemical stability increased by doping Y-TZP with cerium. Y, Ce-TZP and Y-TZP show the same compaction behavior. Although a similar picture was obtained for the Ce-TZP powders, the agglomerates seem to be slightly weaker. The existence of trivalent cerium in Ce-TZP could be demonstrated using (quantitative) TGA and (qualitative) IR measurements. The reduction reaction started significantly at about 1200°C, but a slight reduction might occur at lower temperatures. The exact temperature depends on the porosity. In dense Ce-TZP (at 1400°C) about 10% of the cerium was reduced. Up to about 1200°C, the non-isothermal grain growth behavior was comparable for all the compaction studies. Between 1000°C and 1200°C, the grain growth in Y-containing samples was retarded by a developing impurity drag force caused by segregation of yttrium to the grain boundaries. The intrinsic grain growth in Ce-TZP is relatively

slow, due to the slow kinetics of the diffusing species Ce^{3+} Ce^{4+} compared to Y^{3+}. At higher temperature the grain growth in Ce-TZP is fast, due to the absence of an effective grain growth retarding mechanism.

2.3 Nonstoichiometry.

Nonstoichiometry has been investigated in a number of works [29,31,38,39]. It was suggested that the nano-crystallite, metastable t-ZrO_{2-x}, should have lattice parameters similar to those of doped zirconia at room temperature. The probability of transformation to the monoclinic phase during this onset of nucleation may be relatively small due to the crystallite size [40]. Upon further heat treatment in the presence of oxygen, the anionic vacancies fill as depicted in Fig. 2.3.1. A sufficient decrease in the number of these vacancies should facilitate

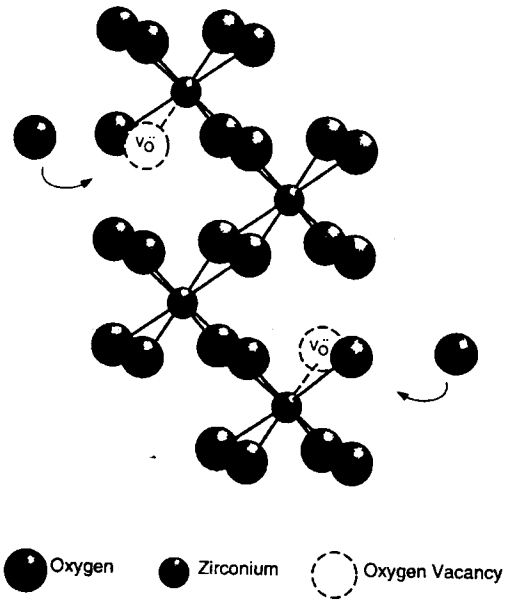

Figure 2.3.1 Schematic of oxygen movement into oxygen vacancies that act as dopants to stabilize the tetragonal phase of zirconia during crystallization of a zirconium- based polymer. The polymer is at a point in pyrolysis in which the organic material has decomposed

instability in the metastable tetragonal phase. Because the metastable phenomenon also occurs in the zirconyl chloride system, which is devoid of residual carbon, its actual influence is questionable; however, evidence that carbon may stabilize nonstoichiometry has been found in the literature and cannot be ignored [41]. The structural anisotropy at high temperature (from 1000°C and above) was investigated in work by P. Aldebert and J.-P. Traverse [42]. The data is represented in Tab. 2.3.1.

Temp. (°C)	a_p (10^{-1} nm)	c (10^{-1} nm)	c/a_p	$V_p = (a_p^2 c)/2$ or $a_p^3/2$ (10^{-1} nm^3)
		Neutral atmosphere		
1160	5.1435 (11)[†]	5.2689 (11)	1.0244 (5)	69 70 (4)
1355	5.1458 (9)	5.2864 (10)	1.0255 (4)	70.24 (4)
1545	5.1656 (7)	5.2969 (10)	1.0254 (4)	70.67 (3)
1695	5.1729 (6)	5.3051 (10)	1.0256 (4)	70.98 (3)
1925	5.1887 (17)	5.3180 (18)	1.0249 (7)	71.59 (7)
2025	5.1934 (13)	5.3200 (14)	1.0244 (6)	71.74 (5)
2165	5.2022 (20)	5.3175 (19)	1.0222 (8)	71.95 (8)
2290 (tet. + C)	5.261 (5)		]	72.81 (21)
2410 (C)[‡]	5.269 (6)		]	73.14 (25)
		Reducing atmosphere		
1135	5.1418 (10)	5.2685 (11)	1.0246 (5)	69.64 (4)
1335	5.1530 (7)	5.2836 (8)	1.0253 (3)	70.15 (3)
1500	5.1624 (6)	5.2938 (6)	1.0255 (3)	70.54 (2)
1715	5.1752 (7)	5.3093 (7)	1.0259 (3)	71.10 (3)
1895	5.1873 (12)	5.3193 (13)	1.0254 (5)	71.57 (5)
1990	5.2013 (7)	5.3033 (8)	1.0196 (3)	71.74 (3)
2115 (C)[‡]	5.2438 (10)		]	72.10 (4)
2230 (C)[‡]	5.247 (3)		]	72.23 (12)

[*]Subscripts F and p denote pseudofluorite cell and primitive cells, respectively. [†]Uncertainties given are estimated standard deviations. [‡]For cubic ZrO_2 a_F is fluorite cell parameter and V_p is equal to half the fluorite cell volume.

Table 2.3.1 Cell parameters and cell volume for tetragonal ZrO_2.

2.4 Water and alcohol influence.

Washing and rinsing zirconia samples with both water and alcohol was carried out, but no significant difference was found in PAC measurements.

In 1990, Mary Sue Kaliszewski and Arthyr H. Heuer [43] found that alcohol could be used to control agglomeration during wet milling of powders. It is possible that the higher surface tension of water compared to alcohol leads to higher capillary forces and thus hard agglomerates in water-washed powders. However, as pointed out by M. J. Readey and et al. [44], capillary forces vary inversely with the particle size,

and since the effect of alcohol washing does not appear to be size dependent, surface tension is probably not a controlling factor determining the strength of agglomerates. Likewise, solubility issues do not seem germane.

Ethanol interaction with hydrous ZrO_2 during washing results in the replacement of hydroxyl groups with ethoxy groups. Jones and Norman [45] demonstrated that methanol washing of ZrO_2 gels removed coordinated water and the terminal hydroxyl groups of the gels. It was also found in this paper that the removal of the ethoxy groups does not result in Zr-O-Zr bond formation between particles.

Water was used with the zirconia samples in studies by C. E. Scott and J. S. Reed [46]. As much as 1 wt% chlorine residue was found in commercial, submicron yttria-stabilised zirconia powders prepared from chloride precursors. Approximately 95% of the chlorine was removed as Cl^- ions by an aqueous laundering technique of admixing distilled water, centrifuging, decanting, admixing fresh water, etc. The $[Cl^-]$ in decants was analyzed using a specific-ion electrode; results indicated that maximum chlorine was removed when the powders were laundered as a dilute suspension. The influence of water was also studied in the work of Tsugio Sato and Masahiko Shimada [47]. Sintering and phase transformation of ceria-doped tetragonal ZrO_2 polycrystals were investigated using coprecipitated fine-grained zirconia powders containing 8% to 12 mol% CeO_2 as starting materials. The rate of grain growth of ceria-doped zirconia was faster than that of yttria-doped zirconia. The tetragonal to monoclinic phase transformation in ceria-doped zirconia ceramics was observed over the range 80° to 300°C. The phase transformation was greatly accelerated by low-temperature annealing in water. The rate of the phase transformation decreased with increasing CeO_2 concentration and with decreasing grain size.

2.5 Previous PAC study of zirconia.

Phase transitions in zirconia have been studied using Hf PAC, and oxygen vacancies have been studied using In PAC. Typical Hf PAC data for pure zirconia are shown in Fig. 2.5.1. Since hafnium has the same valence as zirconium, one does not expect hafnium to attract point defects in the material. Hafnium's daughter, tantalum, is 1+ with respect to the lattice and can, in principle, attract negatively charged point

defects. If an appreciable quantity of negative defects with high enough mobility is present, the tantalum can trap the defects before emitting its γ-rays. This is not the case for the temperatures at which zirconia has been measured. Consequently, the electric field gradient measured by PAC is due entirely to the lattice. The measured electric field gradient should be axially symmetric in the tetragonal phase and non-axially symmetric in the monoclinic phase, as is observed [48]. The monoclinic to tetragonal and tetragonal to monoclinic phase transition was observed by PAC (Fig. 2.5.2)

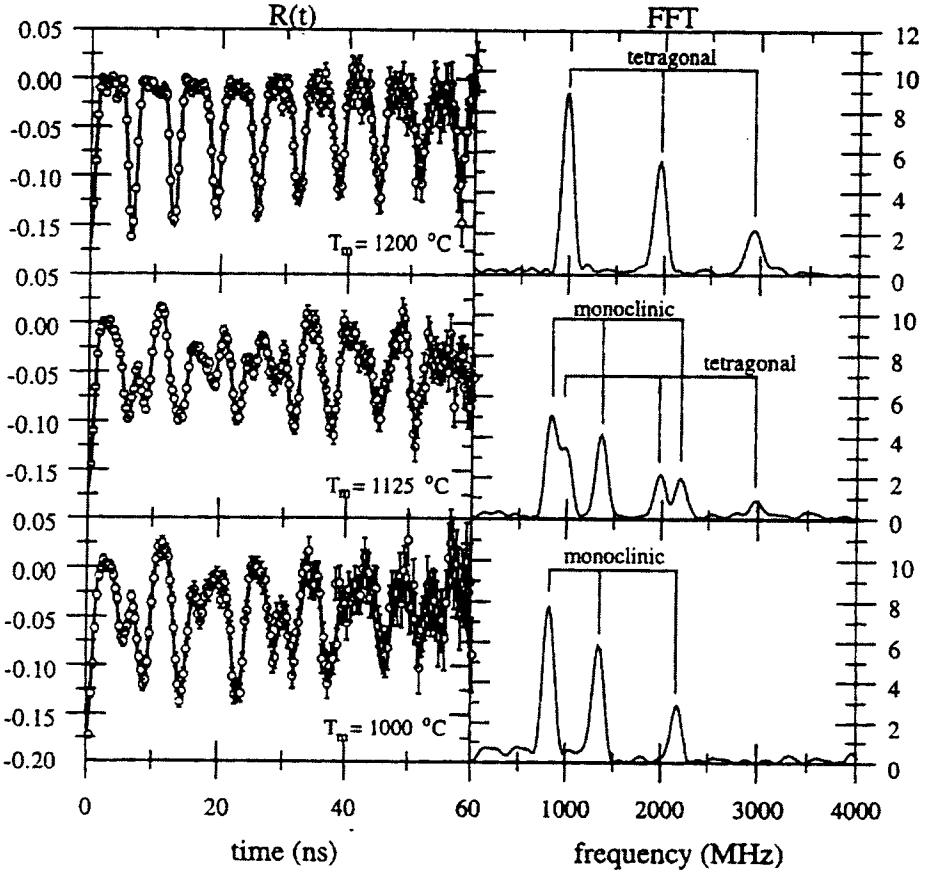

Figure 2.5.1 Typical Hf PAC spectra for zirconium dioxide. The plot shows spectra for tetragonal (top), monoclinic zirconia (bottom), and a mixture of both (middle)

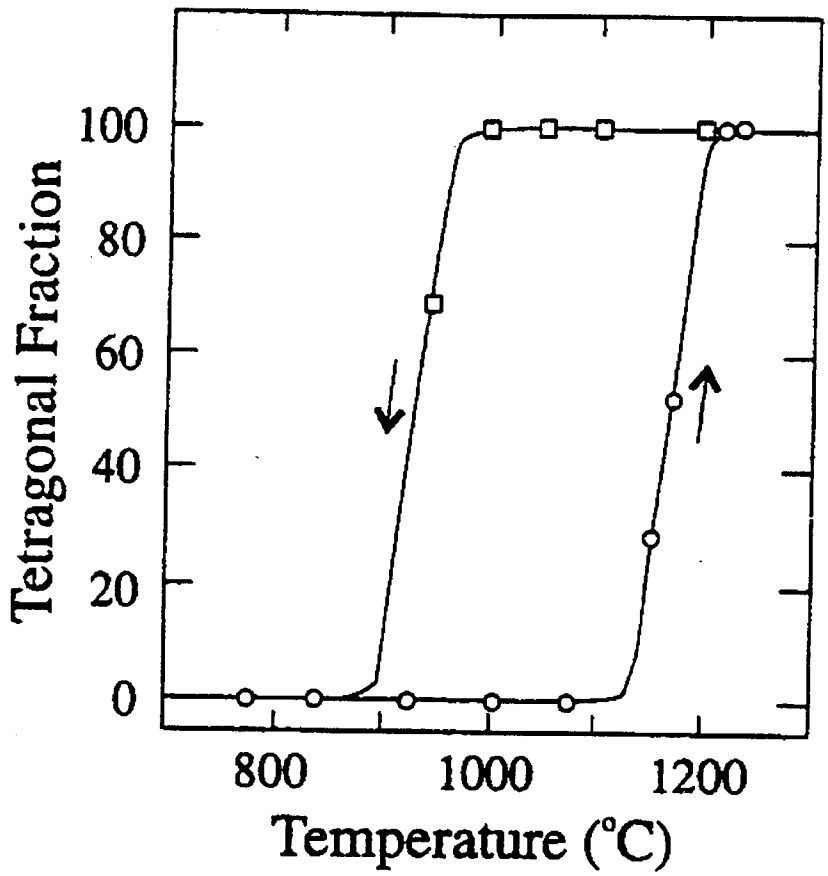

Figure.2.5.2 Tetragonal/monoclinic transition in zirconia as observed by PAC [48].

Indium PAC can also resolve the monoclinic and tetragonal phases as shown in Fig. 2.5.3.

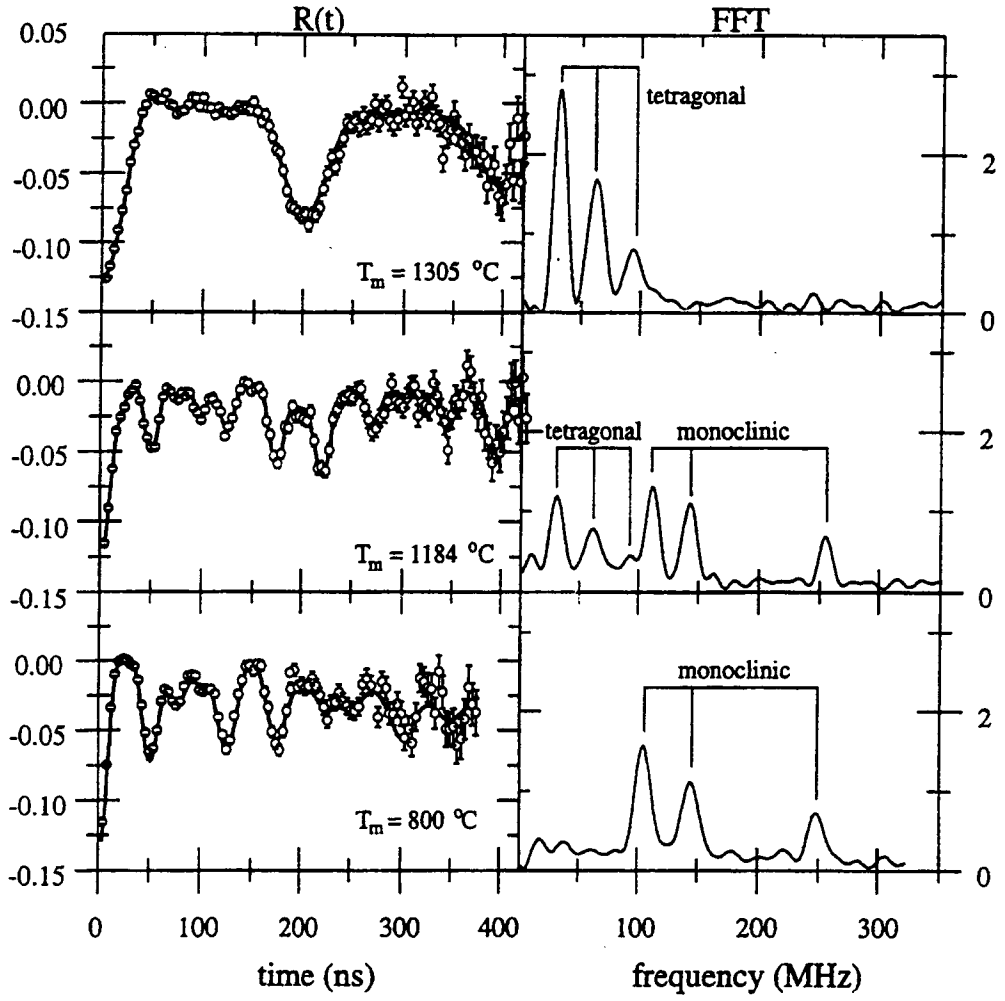

Figure 2.5.3 Typical In PAC spectra for zirconium dioxide. The figure shows spectra for tetragonal zirconia (top), monoclinic zirconia (bottom) , and mixture of both (middle)

Since indium and its daughter cadmium have lower valences than zirconium, the probes attract oxygen vacancies and the observed electric field gradient is affected. The tetragonal phase interaction frequency changes depending on the concentration of oxygen vacancies (Fig. 2.5.4)

In order to assign a value to the tetragonal phase interaction, zirconia samples were doped with 0.5% niobium to eliminate oxygen vacancies. The oxygen vacancy-free hyperfine parameters for tetragonal phase in zirconia at 1200°C are: ω_1=38.5(3) Mrad/s and η=0.19(1). The shift in frequency depended on the concentration of oxygen vacancies in the tetragonal phase and was explained using a simple model. At high measurement temperatures the oxygen vacancies move very rapidly, and it was

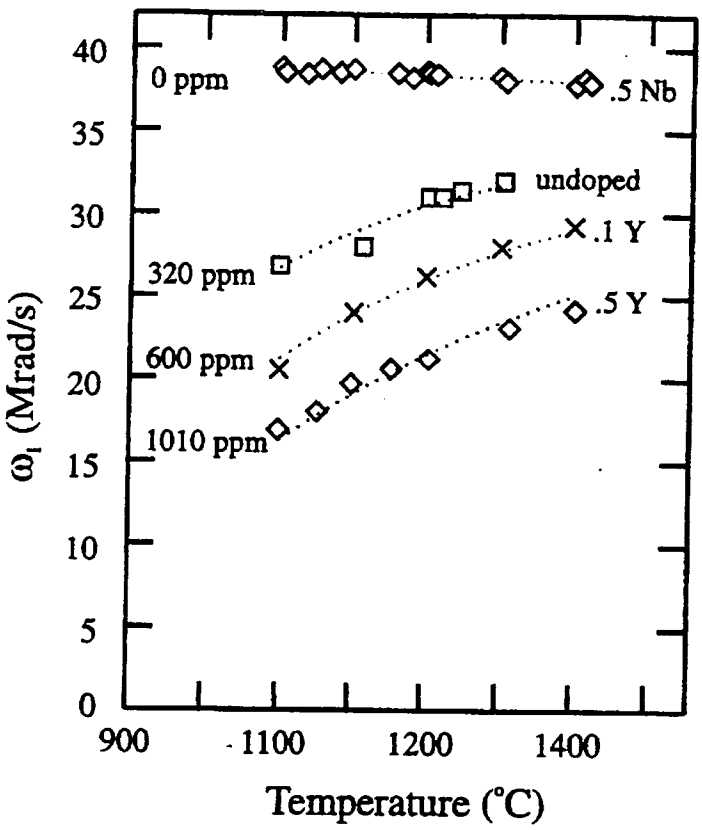

Figure 2.5.4 Tetragonal phase frequencies versus temperature [5]. The interaction frequency (ω_1) depends on the measurement temperature and the concentration of oxygen vacancies. The curves are from fits using equation 2.5.1 to determine the concentration of oxygen vacancies given the frequency and temperature.

assumed that when an oxygen vacancy was trapped by a probe, its rapid motion about the probe averaged to a very small electric field gradient interaction. When oxygen vacancy was not trapped by a probe, the electric field gradient interaction was due to the lattice. The observed interaction frequency should then be an average of the two electric field gradients, weighted by the fraction of time the oxygen vacancy spent trapped.

$$\omega_{observed} = f\omega_{V_o} + (1-f)\omega_{lattice} \tag{2.5.1}$$

where f is the trapping fraction or average occupancy of oxygen vacancies around the cadmium probe, ω_{V_o} is the interaction frequency when an oxygen vacancy is next to the probe, and $\omega_{lattice}$ is the interaction frequency with the lattice. The trapping fraction of oxygen vacancies is:

$$f = \frac{1}{\frac{1}{CN} e^{-E_A/kT} + 1} \tag{2.5.2}$$

where N is the number of trap sites about the probe (8 for near-neighbor positions), C is the concentration of oxygen vacancies, E_A is the association energy, k is Boltzmann's constant and T is the temperature in Kelvin. The PAC fits also required a Marshall-Meares-type damping parameter. Fits using such a model gave best results when N=24 (next-near-neighbor oxygen vacancies) and ω_o=0 Mrad/s (i.e. the lattice is locally cubic as a result of the trapped vacancy). Values of 0.44(3) eV were obtained for the association energy [5].

3. FORMATION OF OXYGEN VACANCIES.

Equilibration of ionic solids in an environment of gas that is also a constituent of the solid plays an important role in determining defect structure [49]. The reduction of an oxide can be described as the removal of oxygen to the gas phase, leaving behind oxygen vacancies:

$$O_o^x = \frac{1}{2}O_2(g) + V_o^{\bullet\bullet} + 2e'$$

where $V_o^{\bullet\bullet}$ represents doubly positive charged (+2) oxygen vacancies (' for negative charge, x for neutrality).

Two electrons that were associated with the O^{2-} ion are released within the solid. The equilibrium constant for this interaction is:

$$K_r = n^2\left[V_o^{\bullet\bullet}\right]P_{o_2}^{1/2} = K_R^o \exp\left(-\frac{\Delta g_R}{kT}\right)$$

where the oxygen partial pressure P_{o_2} is equivalent to oxygen activity, n is concentration of the electrons [e'], K_R^o is a constant, and Δg_R is the free energy of reduction. The concentration of oxygen ions on their proper sites, $\left[O_o^x\right]$, has been left out since it is assumed that the concentration of vacancies is dilute. All of the above represents the compensation of the doubly positive charged oxygen vacancies by two electrons at low oxygen potentials. At high oxygen potentials, completely ionized zirconium vacancies, $V_{Zr}^{''''}$, are the major defects [50-53]. The second defect formation reaction is

$$O_{2(g)} = 2O_o^x + V_{Zr}^{''''} + 4h^{\cdot}$$

where h' is the concentration of holes.

The Schottky defect equilibrium relates the concentration of the two point defects:

$$nyll = 2V_o^{\bullet\bullet} + V_{Zr}^{''''}$$

The equilibrium constants for the second and third reactions are following:

$$K_2 = \frac{\left[V_{Zr}^{''''}\right][h]^4}{P_{O_2}}; K_3 = \left[V_{Zr}^{''''}\right]\left[V_o^{\bullet\bullet}\right]^2$$

where $O_o^x \cong 2$ is assumed. Then $x \cong \pm\left(2\left[V_{Zr}^{''''}\right]-\left[V_o^{\bullet\bullet}\right]\right)$, the sign here is chosen so that x is positive in both ZrO_{2-x} and ZrO_{2+x}. The charge neutrality condition completes the defect relations:

$$2\left[V_o^{\bullet\bullet}\right]+[h']=4\left[V_{Zr}^{''''}\right]+n;and$$
$$2x=\pm(h-n)$$

These equations can be solved for the five unknowns n, h, $V_{Zr}^{''''}, V_o^{\bullet\bullet}$ and the oxygen pressure P_{O2}. For the case of oxygen vacancies in ZrO_{2-x}, $x > 10^{-5}$, the concentrationa of positive holes and cation vacancies are negligible so we can write :

$$\left[V_o^{\bullet\bullet}\right]=\frac{n}{2}=x$$

Then K_r can be obtain

$$K_r \cong 2x^3 P_{O_2}^{1/2}$$

Using the additional calculations made by Xue [52] one can get

$$\ln P_{O_2} = -6\ln x + 2.58 - \frac{136000}{T}$$

4. INTRODUCTION TO PAC.

The primary technique used in this study was perturbed angular correlation (PAC) spectroscopy. PAC allowed us to investigate microscopic properties inside the nanometer size zirconia grains The PAC technique involves measurement of internal fields with the help of radioactive probe atoms. These local fields, magnetic dipole or electric field gradient produce a magnetic precession of the probe atom's nuclear spin, so the precession frequency ω is proportional to the strength of the field at the nucleus. The change of the nuclear spin orientation with time is directly observable by detecting two γ-rays from a decay cascade. Conservation of angular momentum connects the orientation of the nuclear spin with the angular distribution of the emitted γ-rays. The change of the spin orientation with the time interval between the cascade γ-rays reflects the spin precession frequency ω. Thus when ever a radioactive probe atom decays, the information about the field strength at its lattice site can be studied by measuring the frequency ω. The information obtained in this way is microscopic and local in its nature, since the field strength decreases rapidly with increasing distance from the probe atom.

Radioactive tracer ^{111}In is used in this study as a nuclear probe to investigate the structural temperature-dependent changes in zirconia. ^{111}In , which has a half-life of 2.83 days, decays to ^{111}Cd by electron capture and emits radiation. The scheme of this decay is shown in Figure 4.1. The I=7/2 state of ^{111}Cd decays to an intermediate I=5/2

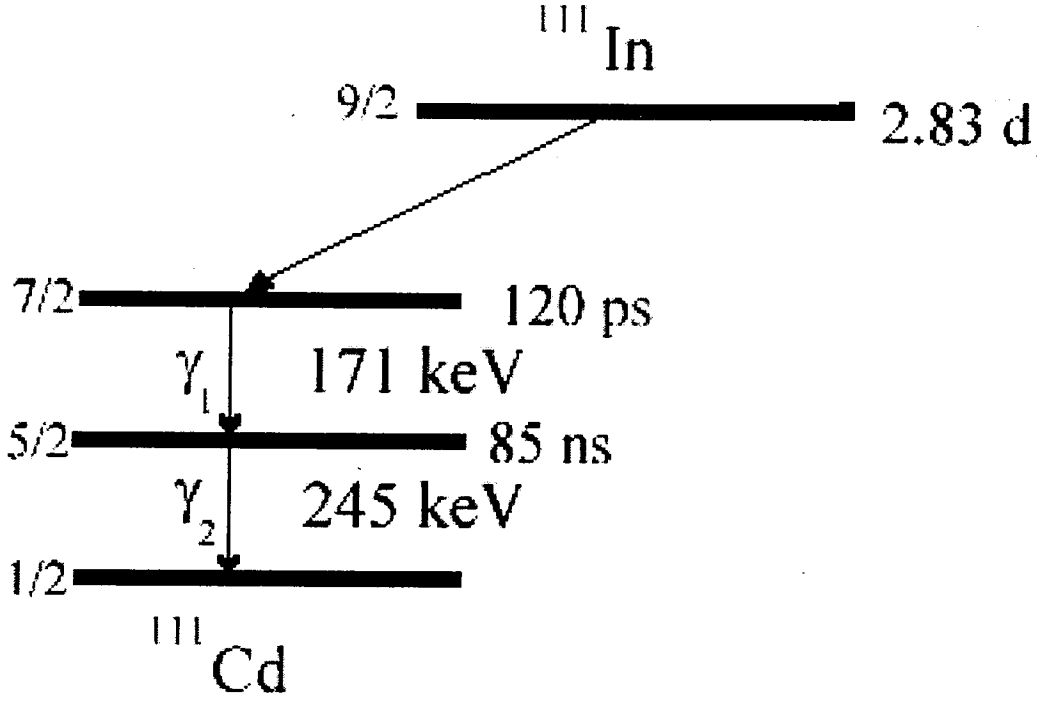

Figure 4.1 Decay scheme of ^{111}In.

excited state by emitting a γ-ray. The spin-5/2 state is characterized by an 85-nanosecond half-life. Then cadmium decays to its ground state spin-1/2 by emitting a second γ-ray. ^{111}In and then ^{111}Cd sit in zirconium lattice sites as substitutional dopants. Zr is +4, and in zirconium oxide, ZrO_2, each atom of +4 zirconia is neutralized by two oxygen atoms of charge -2 each (Figure 4.2). The defect free zirconium oxide lattice is neutral, and if there are no additional

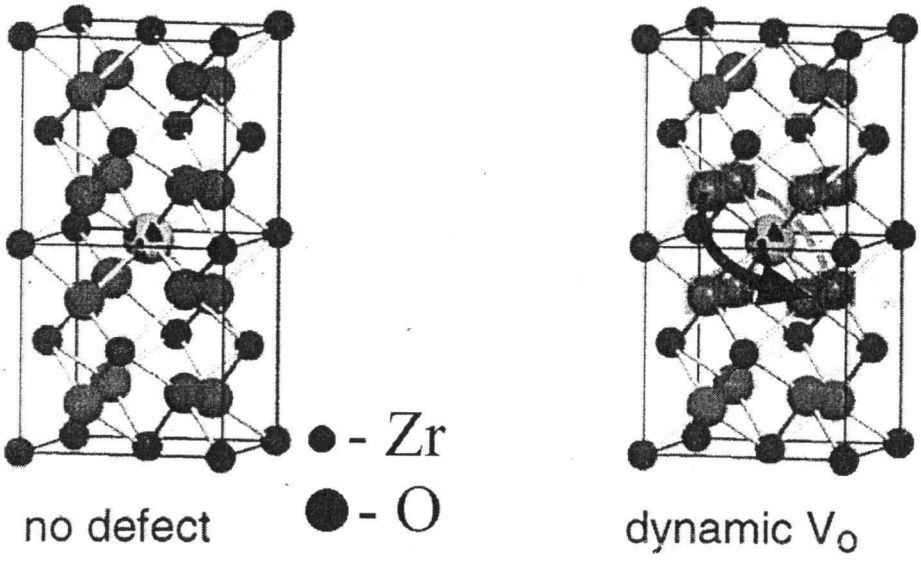

Figure 4.2. Fluorite-like tetragonal zirconia unit cell with radioactive probe atom on the substitutional zirconia site (left). Dynamics of the oxygen vacancy (right).

charges present, there is no efg at a probe site. But if there are charged defects in the lattice that can produce an efg, the angles and times between successive radiations will be perturbed, because the interaction of the nuclear moment and the efg results in splitting the nuclear energy levels. The strength and symmetry of the efg obtained through PAC measurements from the frequencies ω_1 and ω_2. From these frequencies we can also deduce the concentration of defects and the structure of the PAC sample.

4.1 General theory of the electric quadrupole interaction.

Perturbed angular correlation spectroscopy analyses the directions of detection versus time of the two γ-rays from Cd. The theory of PAC is described in various publications [54,55]. The transition amplitudes for the γ-emission from the initial to the intermediate state, and from the intermediate to the final state, depend on the following matrix elements (fig. 4.1.1)

$$< I, M, \vec{k}_1, \sigma_1 | \mathrm{H}_1 | I_i, M_i > \text{ and } < I_f, M_f, \vec{k}_2, \sigma_2 | \mathrm{H}_2 | I, M >,$$

where k_i and σ_i are the wave vector and polarization of γ_i (i = 1, 2).

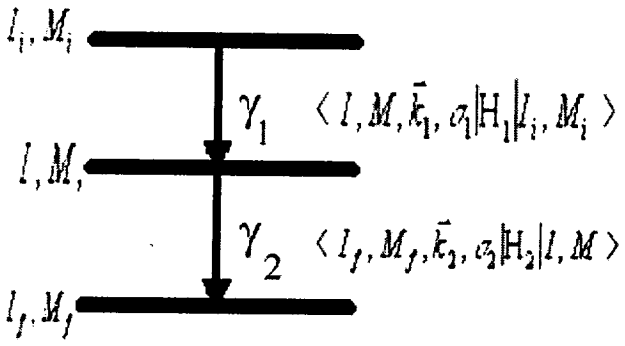

Figure 4.1.1 Schematic representation of γ-γ cascade.

If the nucleus is subject to interactions with an efg, this can cause splitting of the intermediate state with nuclear spin 5/2. In this case, the energy for different M ($\pm 5/2, \pm 3/2, \pm 1/2$) states can be calculated (only for η=0):

$$E_Q = \frac{3M^2 - I(I+1)}{4I(2I-1)} eQV_{zz}, \tag{4.1.1}$$

where V_{zz} is the z-component of the electric field gradient in Cartesian coordinates. The coordinate system is chosen so that $|V_{zz}| \geq |V_{yy}| \geq |V_{xx}|$. I is nuclear spin, Q is the electric quadrupole moment of the nucleus describing its deviation from spherical shape, and is defined as

$$Q = \frac{2}{5}(c^2 - a^2)Ze, \tag{4.1.2}$$

where *Ze* is the charge of the nucleus, *c* is the length of a spheroid semi-axis parallel to the z-axis, and *a* is the length of the semi-axes perpendicular to the z-axis. Because of the M^2 dependence of E_Q, +M and -M states are degenerate.

$$E_Q(M=\pm\frac{1}{2}) = -\frac{1}{5}eQV_{zz} \tag{4.1.3}$$

$$E_Q(M=\pm\frac{3}{2}) = -\frac{1}{20}eQV_{zz} \tag{4.1.4}$$

$$E_Q(M=\pm\frac{5}{2}) = \frac{1}{4}eQV_{zz} \tag{4.1.5}$$

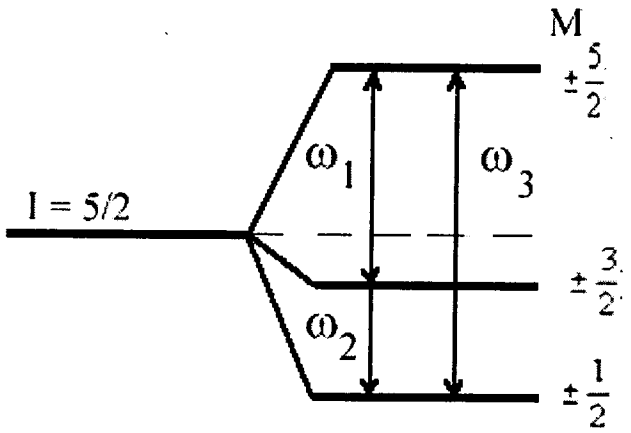

Figure. 4.1.2 Energy splitting of an I = 5/2 nuclear level under the influence of an axially symmetric quadrupole interaction.

Thus the distance between splitting levels depends on the strength of the efg. Laplace's equation requires $V_{xx}+V_{yy}+V_{xx}=0$; therefore , only two parameters are required to characterize it. So the efg can be expressed in terms of V_{zz} and an asymmetry parameter η.

$$\eta = \frac{V_{xx}-V_{yy}}{V_{zz}} \tag{4.1.6}$$

For a non-symmetric efg the matrix element E_Q cannot be calculated in the form (4.1.1). In that case the Hamiltonian is generally diagonalized numerically, because the algebraic complexity of this diagonalizaton is daunting.

The transition energy between two sublevels M and M' (only for η=0) is

$$E_Q(M) - E_Q(M') = \frac{3eQV_{zz}}{4I(2I-1)}\left|M^2 - M'^2\right| = 3\left|M^2 - M'^2\right|\hbar\omega_Q ; \qquad (4.1.7)$$

$$\omega_Q = \frac{eQV_{zz}}{4I(2I-1)\hbar}, \qquad (4.1.8)$$

Our intermediate state with angular momentum I=5/2 has a certain life time τ_N=85ns. If the nucleus is a subject to hyperfine interactions, the population or phase of the intermediate state can change substantially before the second γ-ray is emitted.

4.2 Angular dependence.

In order to calculate the probability of detecting a γ-ray in particular direction, we need to consider a vector potential **A,** which must satisfy Maxwell's equations. Since the wavelength of the γ-ray is far smaller than the distance between nucleus and detector, the electromagnetic wave describing the γ-ray can be represented as a plane wave with wave-vector **k**. On the other hand the wavelength of the γ-ray is larger than its nuclear source. The transition occurs between states with different angular momentum, and thus it is convenient to represent the vector potential in terms of spherical harmonics. The expression for **A** is complicated and can be found in [7]. It is used to calculate the interaction Hamiltonian operator for the emission of γ-rays. The vector potential **A** at point **r** and time *t* can be expressed as a multiplication of three parts: one radial, one time dependent and another angular dependent. Let's look at the part represented by vector spherical harmonics:

$$X_l^m(\theta,\varphi) = \frac{1}{\sqrt{l(l+1)}} LY_{lm}(\theta,\varphi) \qquad (4.2.1)$$

where $Y_{lm}(\theta,\varphi)$ is the spherical harmonic function and **L** is the angular momentum operator, $L = -i\hbar(r \times \nabla)$. Using the Maxwell equations and Poynting theorem one can find that the angular dependence of the radiation is proportional to $\left|LY_l^m\right|^2$. Using quantum mechanical notation:

$$\begin{aligned} L_+ &= L_x + iL_y \\ L_- &= L_x - iL_y \\ L_z &= L_z \end{aligned} \tag{4.2.2}$$

$$\begin{aligned} L_+ Y_l^m &= \hbar\sqrt{(l-m)(l+m+1)}\,Y_l^{m+1} \\ L_- Y_l^m &= \hbar\sqrt{(l+m)(l-m+1)}\,Y_l^{m-1} \\ L_z Y_l^m &= \hbar m Y_l^m \end{aligned} \tag{4.2.3}$$

and using the relations

$$\left|Y_l^m(\theta,\varphi)\right|^2 = \sum_k \frac{2l+1}{4\pi}(2k+1)\begin{pmatrix} l & l & k \\ m & -m & 0 \end{pmatrix}\begin{pmatrix} l & l & k \\ 0 & 0 & 0 \end{pmatrix} P_k(\cos\theta) \tag{4.2.4}$$

where $P_k(\cos\theta)$ are the Legendre polynomials, we can calculate the angular distribution $\left|LY_l^m\right|^2$. It will include Clebsch-Gordan coefficients, which are not equal to zero under the following special conditions (selection rules):

$$\begin{aligned} \Delta l &= l_f - l_i = \pm 1 \\ \Delta m &= m_f - m_i = -1,0,+1 \end{aligned} \tag{4.2.5}$$

Therefore there are only a limited number of transitions.

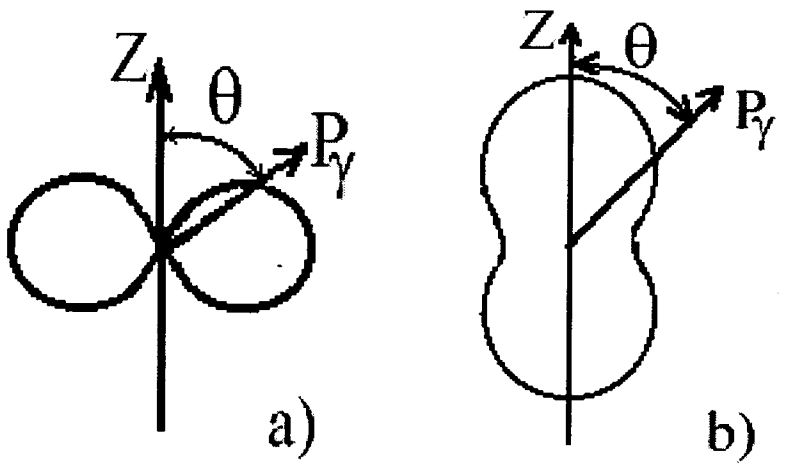

Figure 4.2.1. Emission pattern of dipole l=1 radiation. a) Δm = 0, b) Δm = ± 1

The photon has angular momentum **L** = 1. The two angular distributions displayed in Fig. 4.2.1 show the probability to find a photon along the direction $\mathbf{P}_\gamma$. The photon, as a massless particle, never has its angular momentum vector pointing perpendicular to its flight direction. As we can see from Fig. 4.2.1 if **L** is in the z direction, then transitions with m = 0 have **L** primarily perpendicular to $\mathbf{P}_\gamma$, and m = ± 1 is responsible for the case when **L** is parallel to $\mathbf{P}_\gamma$. This relationship between the direction of **L** and the flight direction $\mathbf{P}_\gamma$ of a photon can provide the information about the orientation of the nuclear spin **I**, because of conservation of angular momentum. Let's look at the nucleus produced via the β-decay of a mother isotope in its excited state E_i with $\mathbf{I}_i = 0$. The nucleus can lose its energy and finally reach its ground state E_f with the final spin $\mathbf{I}_f = 0$ by emitting a γ-γ cascade consisting of two photons with energies $E_{\gamma_1} = E_i - E$ and $E_{\gamma_2} = E - E_f$. As can be seen in Fig. 4.2.2, the transition with Δm = 0 can not occur because the m=0 intermediate state is empty.

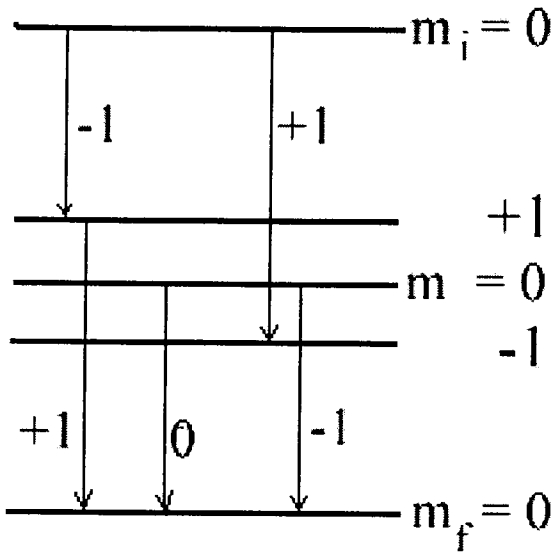

Figure 4.2.2 Quantum numbers describing the level scheme of a nucleus that emits a γ-γ cascade.

In this case, the angular distribution for the second γ for m = ± 1 has form shown in Fig. 4.2.1 (b) and is described by the formula:

$$W(\theta) \approx 1/2(1+\cos^2\theta) \qquad (4.2.6)$$

Now if we vary the angle θ between two radiations the correlation between the first and second γ-rays will be cos2θ dependent, and the general formula for this angular dependence is shown in Fig. 4.2.3.

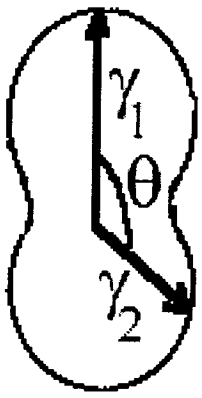

$$W(\theta) = 1 + \sum_{k=2}^{k_{max}} A_{kk} P_k(\cos\theta)$$

Figure. 4.2.3 W(θ) angular correlation function of γ-γ radiation.

where k=2,4,...k_{max}, and k_{max} is determined by the smallest of the three angular momenta **I**, $\mathbf{L_1}$ and $\mathbf{L_2}$. The angular correlation coefficient A_{kk} describes the deviation of the coincidence probability from the isotropic case W(θ) = 1. Since the transition probabilities between nuclear states decrease with increasing angular momentum of the emitted ray, we shall usually meet cases with L = 1 or 2, so that k_{max} does not become larger than 4. For ^{111}In $A_{22} = -0.18, A_{44} = -0.0015, A_{24} = -0.206, A_{42} = -0.0013$ [54].

So far we have discussed only unperturbed γ-γ angular correlation. The population of the m states created by first γ remains unchanged until the emission of second γ. But

hyperfine interactions change this situation and the angular correlation function W(θ) has additional coefficients responsible for this perturbation.

4.3 Perturbed angular correlation.

The presence of a field creates a torque which acts on the nuclear spin and makes it rotate about the field direction. The frequency ω of this rotation is proportional to the strength of the field. If the spin rotates through an angle Δθ, the emission of the second gamma will be delayed by the time Δt = Δθ/ω with respect to the first gamma. Therefore the intermediate nuclear state of the probe atom has to exist for some time, that is characterized by a mean lifetime τ. In another words, the γ_2-rays will be emitted from sublevels with populations that exist at the time of the decay. The intermediate state is under the influence of the time-dependent operator $U(t) = \exp(-\frac{i}{\hbar}\mathrm{H}t)$, where H is the interaction Hamiltonian. Due to this fact the angular distribution can be written as follows:

$$W(\theta,t) = 1 + \sum_k A_{kk} G_{kk}(t) P_k(\cos\theta) \qquad (4.3.1)$$

A perturbation factor $G_{kk}(t) \approx \exp\left[\frac{i}{\hbar}\left(E_Q(M) - E_Q(M')\right)t\right]$, where the difference between the two energies is given by equation 4.1.7 (only for η=0).

The PAC probes in real crystal in static field have slightly different environment. This fact causes a spread in the PAC frequency. The distribution of efg magnitude is characterized by a relative width δ=ΔVzz/Vzz. The static frequency distribution function most often represented as a Gaussian or Lorentzian distribution.
In the time-dependent perturbation the perturbation function can be written in a form: $G_{kk}(t)=e^{-\lambda t}$. Where λ is a damping parameter related to an actual fluctuation rated of the efg. The formulas explaining these parameters can be found in [6,7].

Time dependence can be detected as wiggles on the spectrum $N(\theta,t) = N_0 \exp(t/\tau) W(\theta,t)$ (Fig.4.3.1).

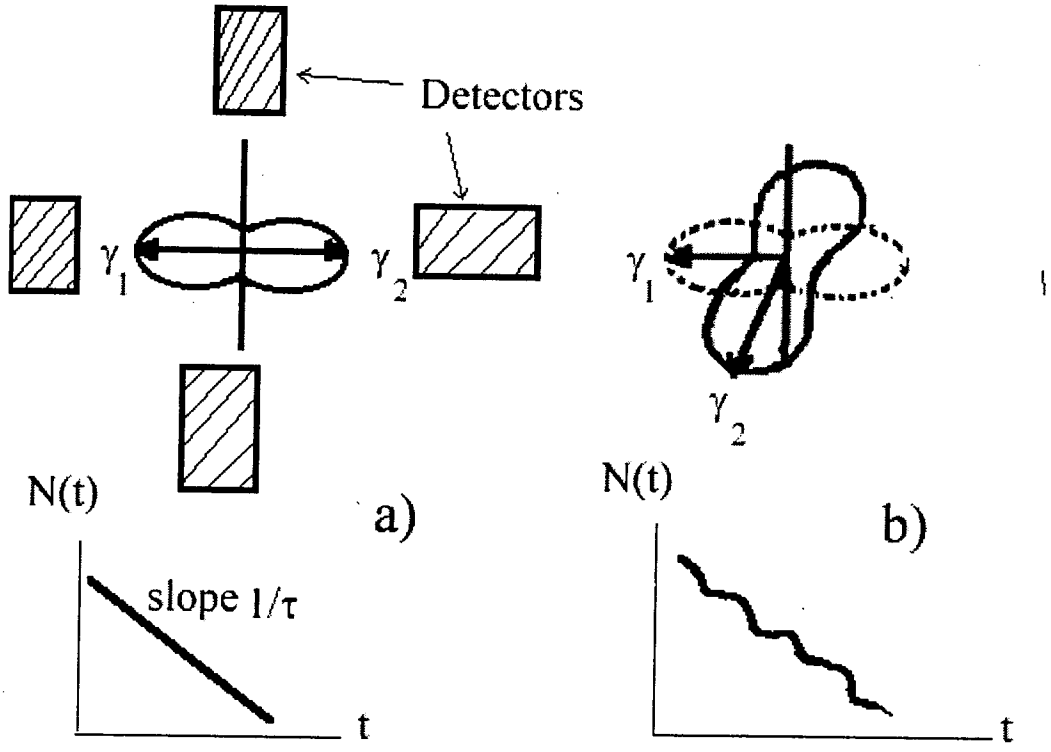

Figure.4.3.1 Time dependence of the coincidence count rates N(t) for an unpertutbed a) and perturbed b) γ-γ angular correlation, where τ is the mean lifetime of the intermediate nuclear state.

4.4 Data Recording.

Let us assume that detector 1 in Fig. 4.4.1 is tuned to record the first photon of the γ-γ cascade, and detector 2 to record the second one. Two signals are derived from each detector. The anode signal is transformed to a digital timing pulse by a constant fraction discriminator. This time signal is delayed and sent to a coincidence circuit which allows it to pass if the γ-ray has the desired value. The energy of the γ-ray is determined by the detector dynode signal. This signal is amplified and sent to a single-channel analyzer which selects those signals with the desired energies. After the coincidence, the signal contains both time and energy information. The signals from the coincidence circuits are used to start and stop a TAC (time-to-amplitude converter).

Its output is an analog signal the height of which is converted to a digital value by an ADC and stored in a multichannel analyzer.

Usually, the spectrometer consists of four detectors set in a plane at 90° angular separation. Each detector can be used for both start and stop detection. These combinations give a total of 12 possible pairs of start and stop signals. The counting rate ratio has the following form:

$R(t) = 2\dfrac{\sqrt{N_{02}N_{13}} - \sqrt{N_{03}N_{12}}}{\sqrt{N_{02}N_{13}} + 2\sqrt{N_{03}N_{12}}}$, which leads to $R(t) \approx A_2 G_2$. Thus from experimental measurements we can determine the perturbation factor.

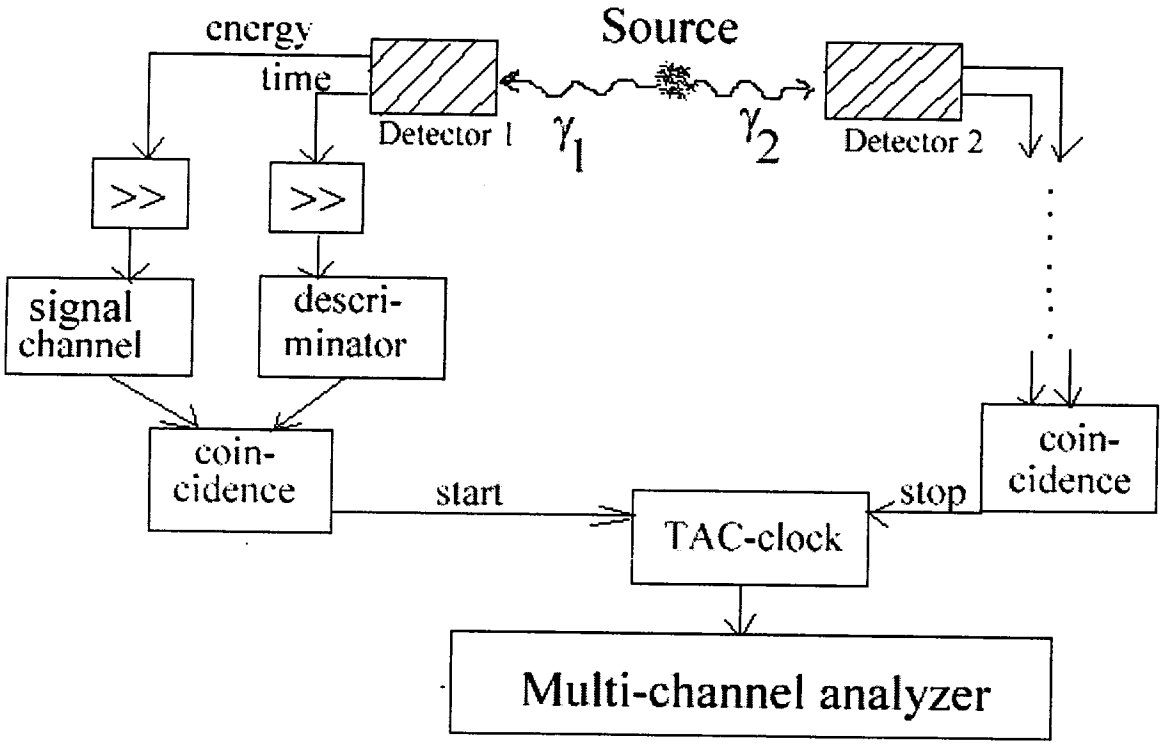

Figure 4.4.1 Experimental apparatus for a time-differential perturbed angular correlation measurement.

4.5 Analysis.

Once PAC spectra are obtained, the physical quantities are extracted by performing least squares fits with a theoretical function that contains the physical parameters. The least squares fits provide estimates for uncertainties in the fitting parameters. The quality of the fit is described by the chi-squared parameters. The best fits have chi-squared ≤ 1. The analysis program used in this study employs Marquardt's algorithm [56].

5. SPECTROMETER.

Four spectrometers were used in the course of this work. All four are eight sector slow-fast coincidence spectrometers. Three are equipped with BaF detectors, while the fourth is outfitted with NaI detectors. The spectrometers are slightly modified versions of the spectrometer design by Jaeger et al. [57].

Each spectrometer station has a furnace allowing *in situ* measurements of samples at temperatures as high as 1200°C. The PAC furnace's outer shell is water-cooled and has a radius of about 3 cm to allow the PAC detectors to be placed near the desired sample-to-detector measuring distance of 5 cm. The heating element used is 18 gauge Kanthal A-1 [58] which allows high temperature operation in air. The heating element is wrapped lengthwise around in a 1.25cm outer diameter, high purity alumina tube. The heating element was fed through 1.5mm inner diameter alumina tubes with 0.7 mm thick walls to insulate the element windings from one another. The heating element in insulating tubes was then wrapped in an yttria-stabilized zirconia felt [Type ZYF-50, Zircar Products, Inc., 110 North Main Street, Florida, New York 10921] for heat insulation. The typical power required to reach 1200°C is around 500 watts. For heat treating samples while not being measured or heat processing samples at higher temperatures, a Linberg box furnace capable of 1900°C operation [Furnace model no. 51214, power supply and temperature control by model no 59246. Lindberg, a unit of General Signal, 304 Hart Street, Watertown, WI 53094] with $MoSi_2$ heating elements was used.

For samples requiring processing under special atmospheric conditions, a pumping station was used to seal the samples in quartz or platinum tubes.

6. SAMPLE PREPARATION.

Since we wanted to investigate the influence of preparation parameters on the reproducibility of the oxygen vacancy concentration in our samples different sample preparation methods were used in this study. Most of the samples included radioactive ^{111}In for purpose of the PAC measurement. It was purchased from Dupont as a solution of $^{111}InCl_3$. All of the test tubes and all of the instruments that were used in the process of sample making were soaked over night in nitric acid (diluted 20%) and rinsed several times with deionized water.

Method #1. Precipitation method used for Ce-doped and pure zirconia samples. This method was developed by Dr. James A. Sommers at Teledyne Wah Chang Laboratories in Albany, Oregon.

Step1: A drop of ^{111}In(about 10μCi) was added to 2 ml zirconium oxychloride or nitrate solution.

Step2: The resulting solution was purred into 20 ml of diluted NH_4OH (20%) solution with constant stirring. The resulting hydrous oxide was formed as white flakes.

Step3: The sample was washed with dilute NH_4OH and filtered.

Step4: It was Dried under the heat lamp until most of the liquid had been driven off and a fine white powder remained.

Method #2. The same as #1, only step 1 is different. It was changed in order to eliminate Cl in our samples, and was used only with nitrate source solutions. A different method for the activity transfer was used. This procedure is described in the PhD thesis of Dennis Tom, and was shown by neutron activation analysis to reduce Cl contamination from the $^{111}InCl_3$ solution.

Step 1: The solution of $^{111}InCl_3$ was placed on a clean quartz chip and dried at 70°C. A clean quartz tube was sealed at one end with an oxygen-hydrogen torch and a quartz chip with the $^{111}InCl_3$ dried on it was placed inside. The tube was then evacuated and backfilled with H_2 gas and sealed with the oxygen-hydrogen torch. The encapsulated quartz tube was subjected to a temperature gradient of 700°C with the empty end at 300°C. The $^{111}InCl_3$ dissociated. The chlorine combined with the hydrogen gas to form HCl , and the ^{111}In transferred to the

empty end of the tube. An efficiency of 80% was achieved in such a transfer of activity. The efficiency of the transfer is measured by forming a window about a centimeter wide with two lead bricks and measuring the starting activity at a distance of 10 cm with a Geiger-Mueller counter. After the transfer, the same window technique was used to measure the activity on the empty end of the tube. The two numbers are compared and a percent efficiency was calculated. After the transfer, the quartz tube was broken. The source solution was added to the end of the tube where ^{111}In had been transferred.

Steps 2-4 from method #1 are then followed.

Method #3. This method was suggested by Erwin Torne of the OSU Radiation center. This procedure was made to launder Cl from the samples. A similar method for washing the Cl from the samples originated at Alfred University in 1978. They used triply distilled water. Powders were put into plastic jars 1/4 filled with Teflon beads and agitated on a wrist action shaker for 5 minutes. The slurry was centrifuged in plastic tubes at 2400 rpm for 60-90 minutes and the decant was measured and stored. The powder concentrate was returned to the mixing jar, equal volumes of water and decant were added and the agitation/centrifugation process was repeated 10 times. In these experiments as much as 1wt% chlorine residue was found in zirconia powders prepared from chloride precursors. Approximately 95% of the chlorine was removed as Cl^- ions by an aqueous laundering technique of admixing distilled water, centrifuging, decanting, admixing fresh water, etc. This may suggest that Cl is located mostly on the surface of the particles. In the method which was used in this study, the zirconia powders, prepared by method #1. Following steps:

Step 1: The powders were redissolved in diluted Nitric acid (of various concentrations). The test tube with powder and acid was placed under the heat lamp to speed the process, and then cooled down after 10 hours of heating.

Step 2 Diluted ammonia NH_4OH (of various concentrations) was added. Again the white flakes precipitated and the supernatant was centrifuged.

Step 3: After centrifuge the white gel was on the bottom of the tube and on the top was clear liquid. The liquid was separated, and checked for remaining zirconia by adding ammonia to the liquid. If some zirconia were still in solution the white flakes again would appear.

Step 4:The gel on the bottom of the tube was again redissolved in the acid and steps 2

and 3 were repeated. Redissolving was done 3 times. Then the white gel was washed from the test tube with ammonia onto filter paper and dried under the heat lamp. This washing approach reduced the Cl concentration from 4000ppm to 300ppm. (This was shown by neutron activation analysis.) The dry redissolved zirconia looked like translucent big crystals, but after calcining at high temperatures (800°C and higher) it reverted back to the expected white powder.

Method#4: Boiling method.

Step 1 from method #1 was performed. Then deionized water was added. For reasons of safety, the " hot tub" method was used: the cup with the radioactive solution was put into a bigger cup with water, and then the two cups together were put on the hot plate. Slowly boiling the water away resulted in the formation of white crystals on the bottom of the cup. It was found that these samples had the highest percentage of Cl concentration in them (4wt%).

Method#5: Using a sample preparation bomb.

The special sample preparation bomb was used.

Step 1. 5 ml. of source solution was added to the 10 ml. of water and placed in the 25ml bomb.

Step 2. The bomb with the liquid in it was taken up to 190°C and kept at this temperature for 24 hours, and then cooled down. A white powder formed on the bottom of the teflon cylinder.

Step 3. The water from the top was pumped away, and was checked for the presence of zirconia by adding ammonia. All zirconia from the source solution was on the bottom of the bomb.

Step 4. Then the bomb with the wet powder was put under the heat lamp, and the water was evaporated overnight. The solid white disk of dry zirconia that remained was used for the experiments. After calcining at high temperature (above 600°C) these samples were similar in form to pieces of a broken plate , as it was put into the quartz tubes, unlike the other samples which formed loose white powders at high temperatures. The bomb technique was not used for radioactive experiments. Its only purpose was to grow big grains at low temperatures. The samples were used in X-ray measurements and EMPA (Electron Microprobe analysis)

7. DATA

This chapter represents the data for different techniques and different preparation methods of zirconia powders. This chapter does not include explanations for the observed phenomena or parameters, which are shown on the figures. The physical significance of the PAC parameters can be found in Sections 2.5 and Chapter 4 or in the work of previous investigators [5-7,48,54].

Briefly, PAC frequency ω_1 is a function of the strength of the time average electric field gradient (efg) at our probe atom, and from ω_1 one can calculate using formulas in Section 2.5 the oxygen vacancy concentration at a given temperature. PAC probes may also experience slightly different efg, since the material is not perfectly homogeneous. This inhomogeneity can cause a small spread of PAC frequencies, which is accounted for by "delta" broadening. The efg can also be time dependent. This case was first studied by Abragam and Pound [62] The dynamic frequency line broadening is accounted for by "lambda". "Eta" describes asymmetry of the efg, and can be calculated from formula (4.1.6).

Different methods of preparation are discussed in Chapter 5. The discussion and implications of the data are given in Chapter 8.

7.1 Ce-doped zirconia.

We can study oxygen vacancies only in tetragonal zirconia. We started our research with Ce-doped zirconia powders, because it was well known that a small amount of Ce stabilizes zirconia in the tetragonal phase below the phase transition region , and at this time we did not know how else to stabilize zirconia below 1200°C.

All of the Ce-doped samples were prepared by method #1, which is described in Chapter 5.

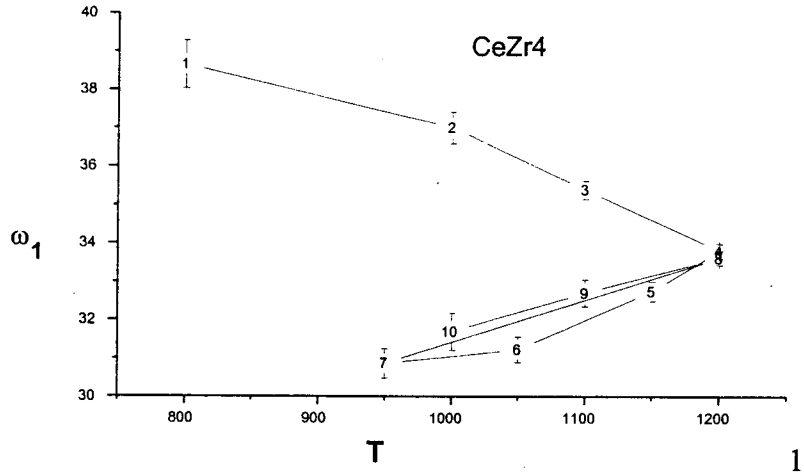

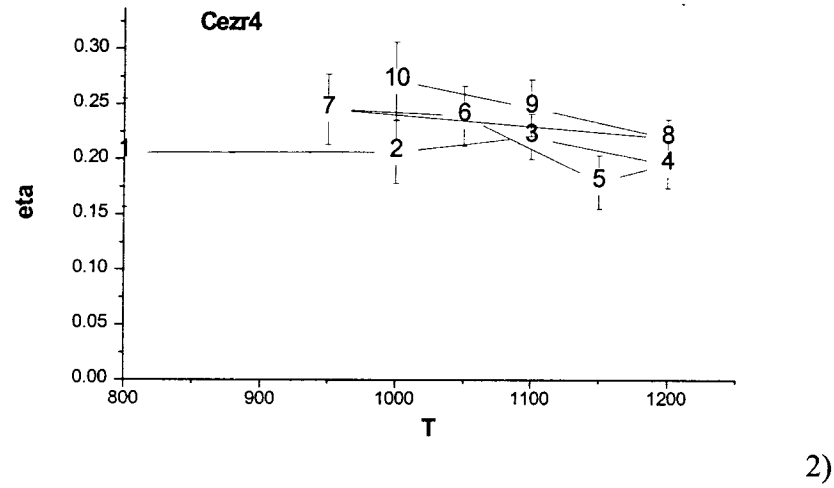

Figure.7.1.1 Temperature dependence of frequencies 1) and asymmetry parameter eta 2) for sample CrZr4 - 1% Ce doped zirconia.

The first figure shows the temperature dependence of the PAC frequencies of the tetragonal site after the sample was heated to 1200°C and then cooled down. This sample shows that the frequencies were reproduced as the sample was heated up back to 1200°C from 950°C .

The second figure shows the temperature dependence of eta for Ce-doped zirconia samples. Eta is non-zero even at 1200°C and stays constant in the region from 800°C to 1200°C. Lines get very broad below 1200°C as the temperatures go down.

The spectra at these temperatures were fitted with lambda broadening (the plot of the lambda parameter vs. temperature for several samples is shown and discussed in chapter 7.7)

Eta should be zero if the PAC probe is in a site of tetragonal symmetry. We do not understand whether the non-zero eta indicates that the lattice is actually not tetragonal or if there is local relaxation around the PAC probe that breaks axial symmetry.

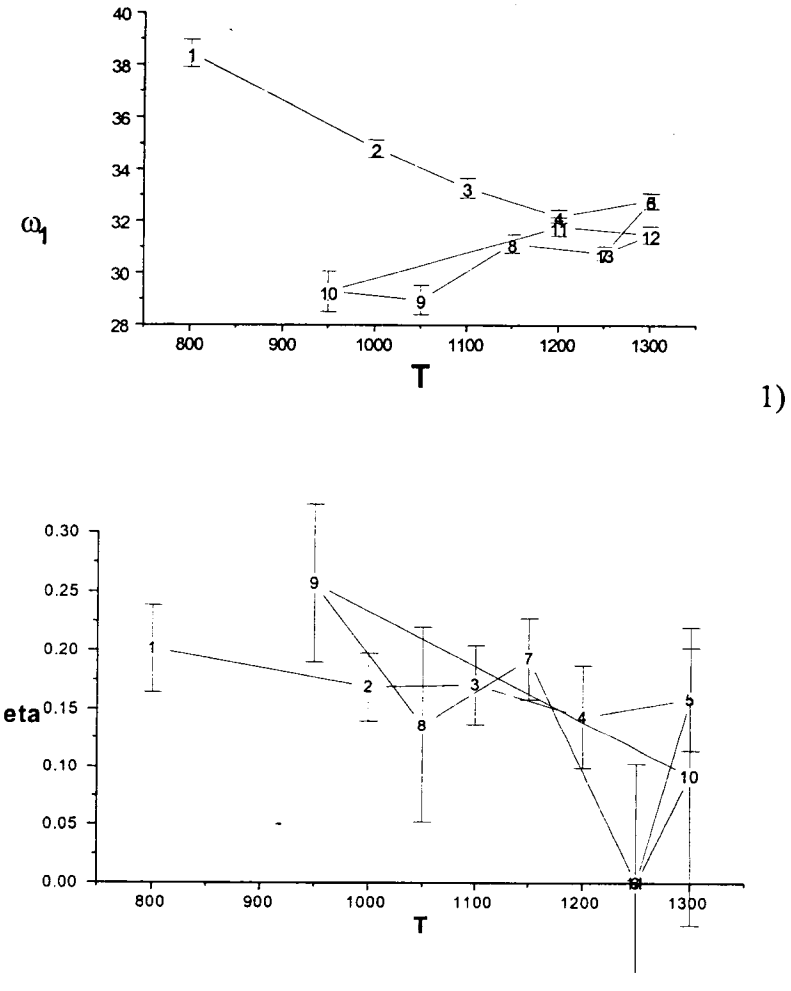

Figure 7.1.2 Temperature dependence of frequencies 1) and asymmetry parameter eta 2) for sample CeZr5 - 1% Ce-doped zirconia.

This sample was heated up to 1300°C. The statistics on this data are not very good, as is seen from the scatter of the data. The frequencies at 1300°C are not reproducible after the sample was cooled down, but at 1200°C frequency is reproducible. At low temperature lambda broadening was used for fitting the data (Fig.7.7.1)

This figure indicates that additional annealing occurs at high temperature but is consistent with conclusions drawn from Fig. 7.1.1.

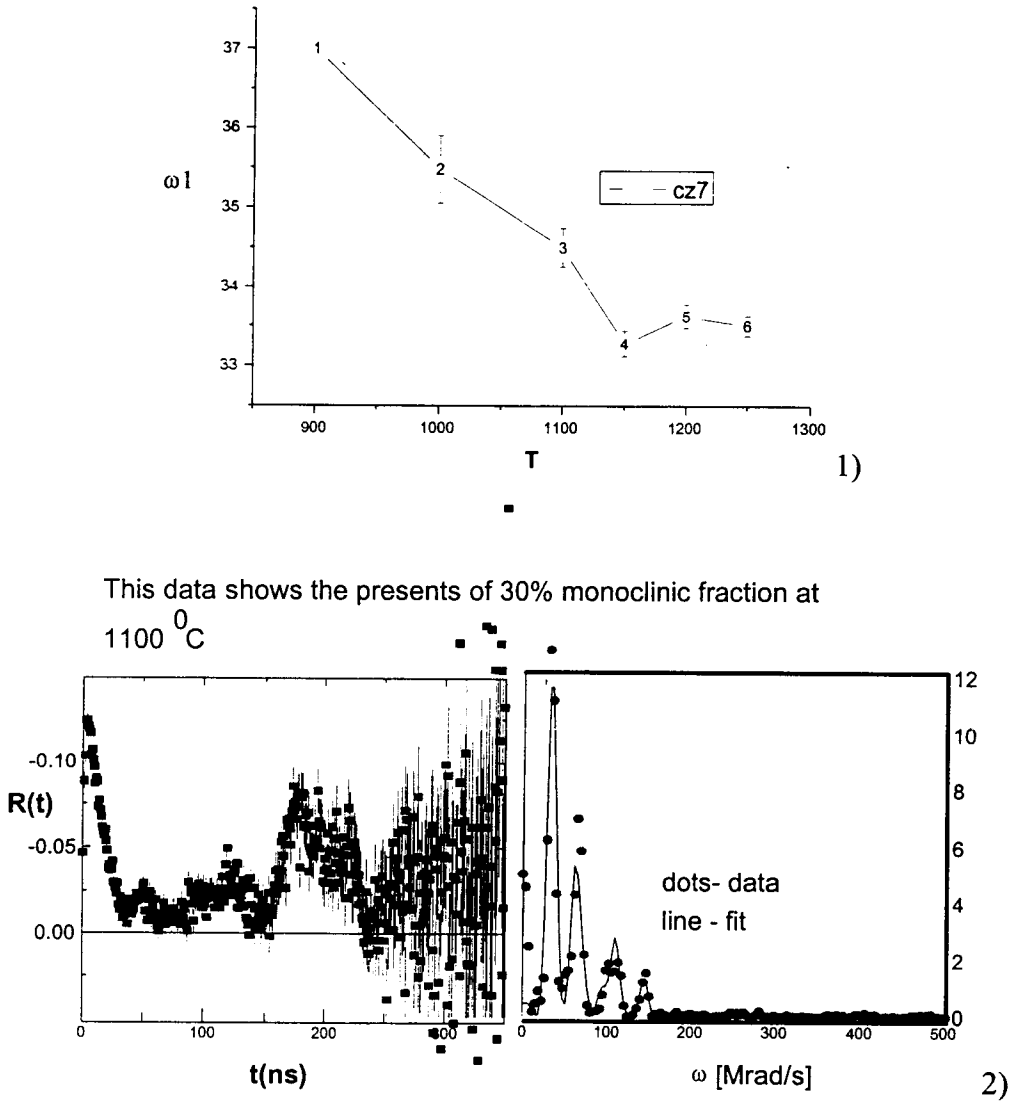

Figure. 7.1.3 Temperature dependence of frequencies 1) and PAC spectrum 2) for sample Cz7-1% Ce doped zirconia.

At 1000°C this sample had 60% tetragonal fraction and the rest was monoclinic, no missing fraction. At 1100°C the monoclinic fraction decreased to 25%, and at 1150°C the sample was fully tetragonal. The frequencies were the same from 1150°C to 1250°C. Delta at 1200°C was 5%. The same delta is found for all Ce doped samples, whereas for pure Zr it is close to 0%.

The monoclinic to tetragonal transformation occurs at a lower temperature than in pure zirconia, and the line broadeneing is larger than pure zirconia. Both effects are believed to be due to the cerium doping.

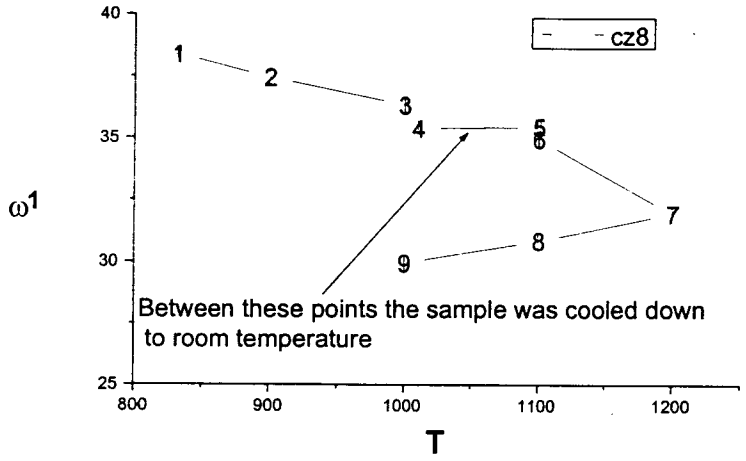

1)

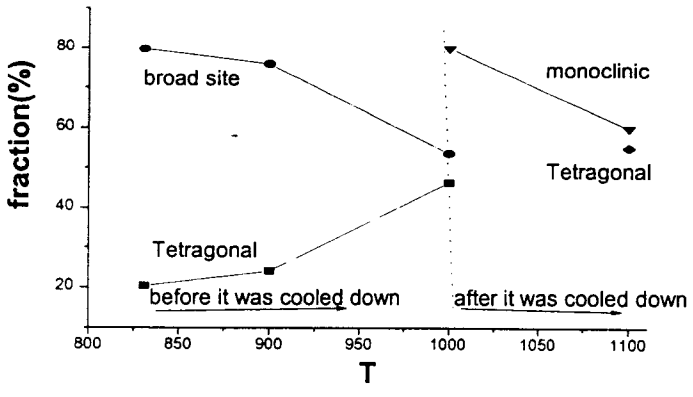

2)

Figure7.1.4 Temperature dependence of frequencies 1) and fraction of the tetragonal site 2) for sample CZ8 - 1% Ce doped zirconia.

The sample was taken up to 1000°C (it had 35% tetragonal fraction, 15% monoclinic and the rest was fitted to a broad site)and then cooled down to room temperature. After heating it back to 1000°C the sample was 80% monoclinic and the rest was fitted to a missing fraction. Then at 1100°C 35% of the sample transformed to the tetragonal phase and 65% remained monoclinic. At 1100°C the ratio tetragonal to monoclinic was 55/45. The frequencies of the tetragonal site remain the same as before cooling the sample. After 1200°C as the sample was cooled down the spectra were fitted with lambda broadening (Fig.7.7.1). This behavior is consistent with expectations for samples that are monoclinic below the equilibrium m/t transformation temperature.

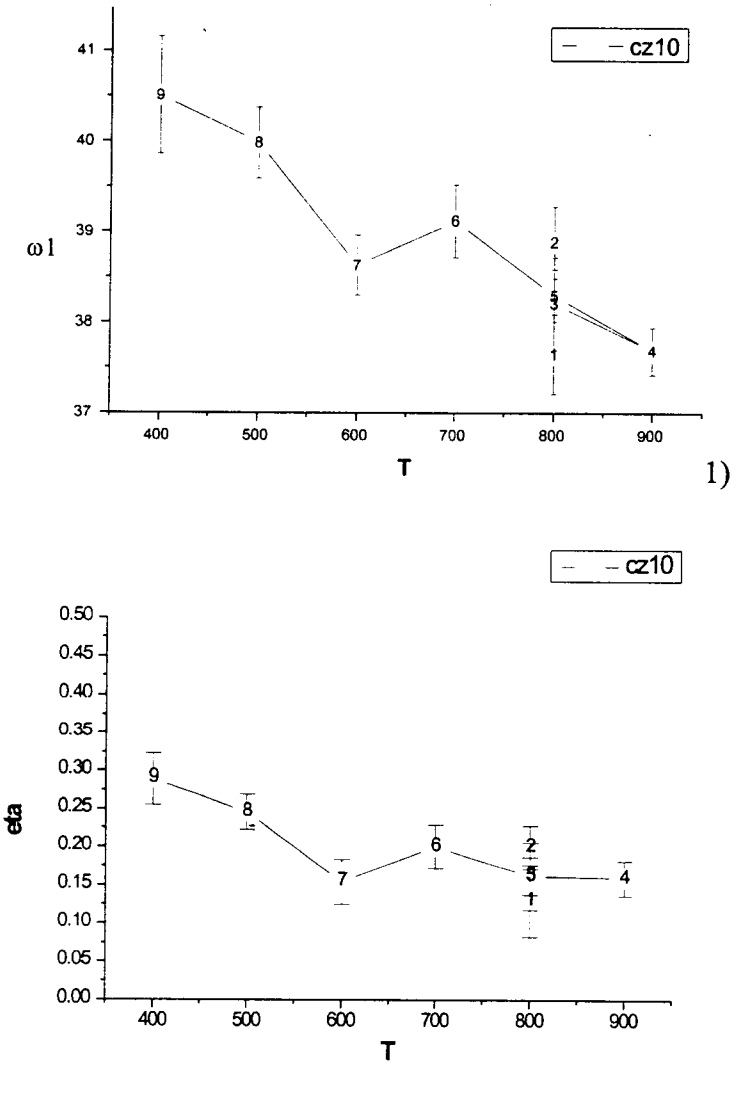

Figure 7.1.5 Temperature dependence of frequencies 1) and asymmetry parameter eta 2) for sample Cz10-1% Ce doped zirconia.

This sample shows typical behavior for the sample which went only up to 900° C. The ω_1 is reversible in this region. The frequency increases as a temperature goes down. Along with the tetragonal site there is a very broad site (missing fraction). The fraction of the tetragonal site at 800°C is 25% and increases up to 50% at 900°C and then drops with temperature to 30 % at 400°C. These data show that more indium dissolves into the zirconia as annealing temperature is increased. These data show that more indium dissolves into the zirconia as annealing temperature is increased. The reduction at low temperature is probably due to transformation of some of the tetragonal particles to monoclinic as the temperature is reduced. The monoclinic portions do not give good PAC spectra at low temperature, possibly because of "aftereffects"[6].

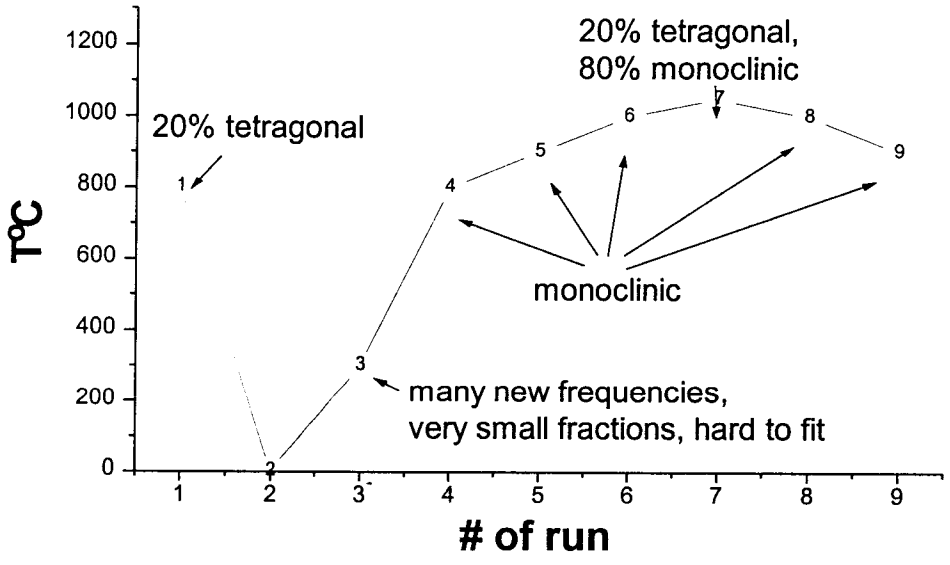

Figure. 7.1.6 Thermal history and corresponding fraction for each temperature for sample Cz 11-1% Ce-doped zirconia sample.

After calcining at 800°C, the fraction of tetragonal phase was 20% and the rest was fitted to a broad site. Then the sample was cooled down to room temperature. After heating the sample back to 800°C it was 40% monoclinic plus missing fraction. At 1000°C the monoclinic fraction increased to 80%. Then at 1050°C 20% of tetragonal phase appeared and the rest was monoclinic. After cooling the sample to 1000°C the tetragonal phase disappeared. We note that initially not all indium is dissolved into good crystalline zirconia. Only 20% "good site" is observed, and that is tetragonal. After cycling to room temperature, everything apparently converts to monoclinic. On heating to near the equilibrium m→t transition, tetragonal material appears again. This is apparently only marginally stable, since it converts to monoclinic when cooled again.

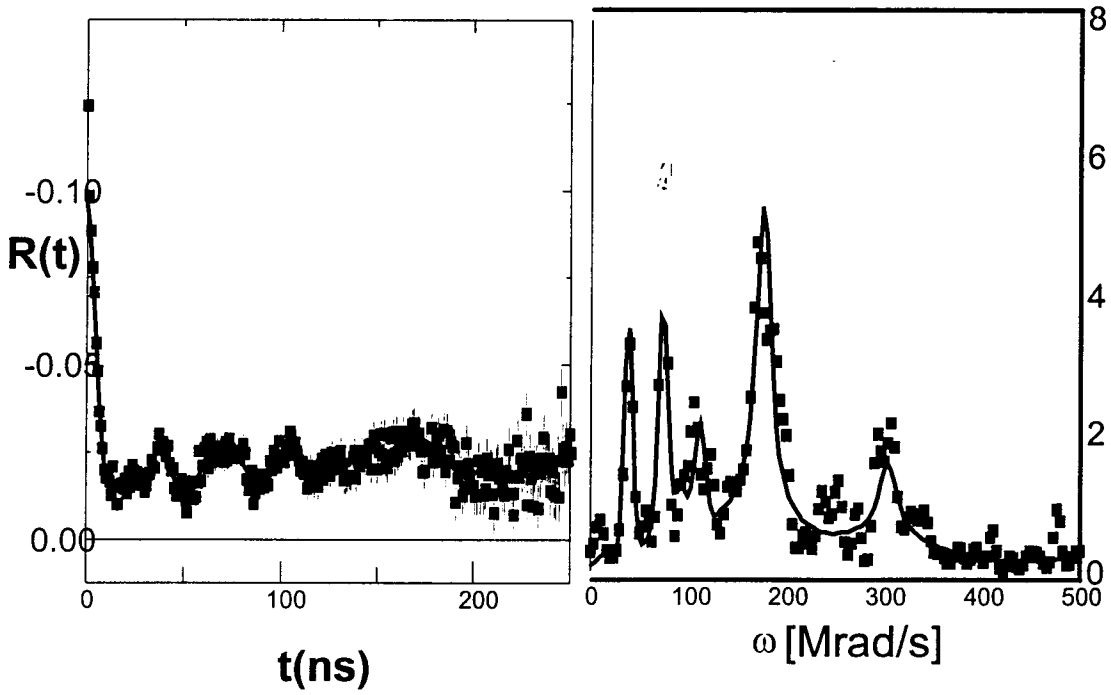

Figure. 7.1.7 PAC spectra of new sites at 450°C for Cz12 1%-Ce doped zirconia.

At 950°C this sample had 60% of tetragonal phase, and 40% missing fraction. Then the sample was cooled down, first to 700°C and then to 450°C. At 700°C it still had 60% tetragonal, and at 450°C the tetragonal fraction decreased to 10%,and two well defined new frequencies appeared. One had a frequency of ω_1=93 Mrad/s,

eta=0.25. The other had ω_1=180 Mrad/s, and eta=0.35. The spectrum at this temperature is shown on Fig. 7.1.7. This figure and later measurements show that most of the tetragonal phase converts to another phase, probably monoclinic at low temperature, and that the "monoclinic" material has a variety of PAC signatures that depend critically on exact thermal history. The purpose of this measurement was to search for tetragonal material with trapped vacancies that were static. The measurements were apparently not successful in doing so.

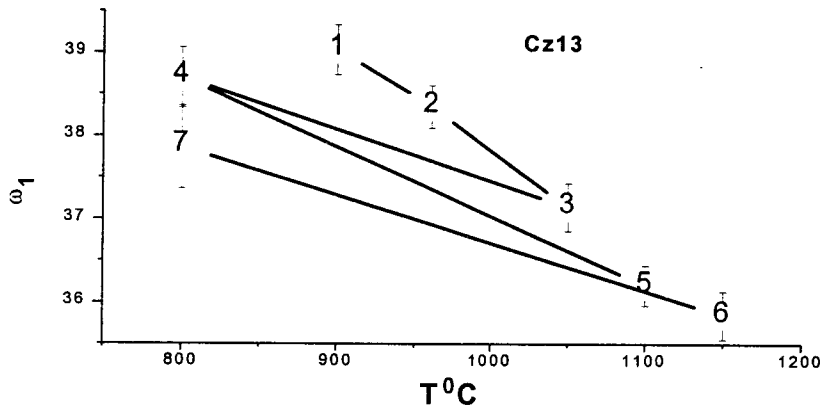

1)

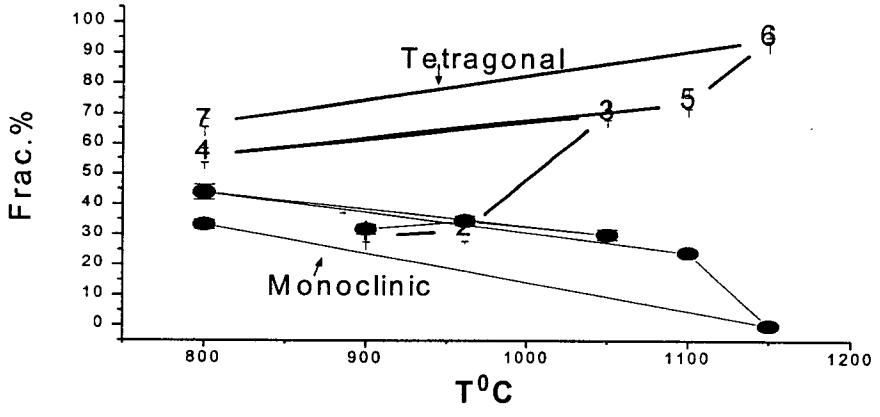

2)

Figure 7.1.8 Temperature dependence of frequencies for the tetragonal site 1) and fractions for tetragonal and monoclinic sites 2) for Cz13 is a 1% Ce-doped zirconia.

After calcining the Cz13 sample at 800°C the fraction of tetragonal phase was 30%, monoclinic fraction was 30% and 40% was fitted to a broad site. Then at 1050°C the broad site disappeared and the tetragonal fraction became 70% and the rest was monoclinic. Then the sample was cooled back to 800°C, the fraction of monoclinic site increased and the tetragonal fraction decreased by a small amount. Then at 1100°C the tetragonal fraction increased back to 70% and at 1150°C the sample was fully tetragonal. But after the sample was cooled back to 800°C the fraction of tetragonal phase decrease to 70%, and the remaining 30% transformed to monoclinic. Then the sample was cooled down to 500°C. As in the sample Cz12 new frequencies appeared, but there was no tetragonal site. The spectra at 500 was fitted to 15% of regular monoclinic with frequency 108 Mrad/s, 40% of the site with ω_1= 173 Mrad/s, eta=0.28, and 40% of the site with ω_1=195 Mrad/s, eta=0.3. (The parameters of these sites depend on the temperatures to which the sample was taken before cooling down.) Then the sample was heated to 800°C and then 900°C. It was 100% monoclinic at this temperature. These data are typical for samples cycled up through the m/t transformation temperature. The 500C data are another example of the irreproducibility of PAC spectra at low temperature.

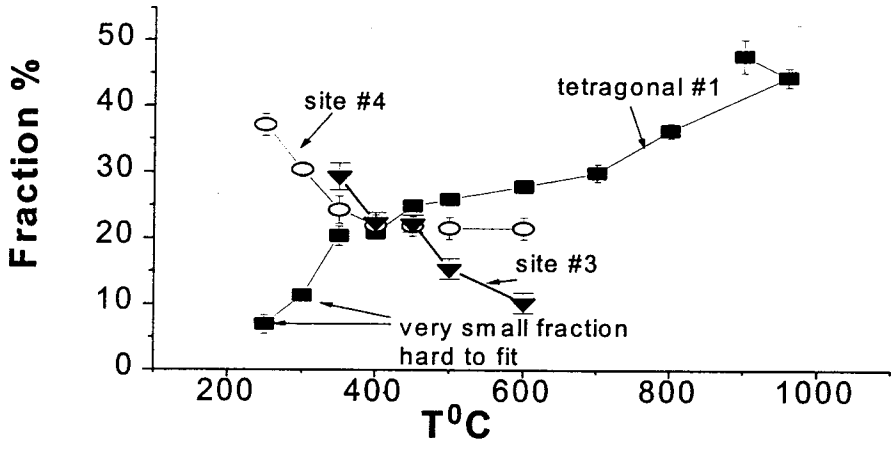

1)

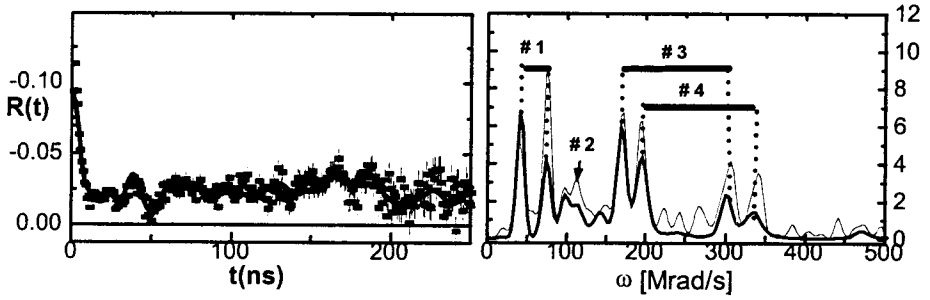

2)

Figure 7.1.9 Temperature dependence of fractions 1) and PAC spectra at 400°C 2) for Cz15 is 1% Ce-doped zirconia.

The maximum temperature this sample was taken is 960°C. Then this sample was gradually cooled down to 400°C while the data was accumulated. Figure 7.1.9 shows that new frequencies appeared at 600°C and their fraction increased as the temperature decreased. The new sites have parameters ω1=171 Mrad/s and eta=0.35 for the first one and ω1=196 Mrad/s and eta=.4 for the second.

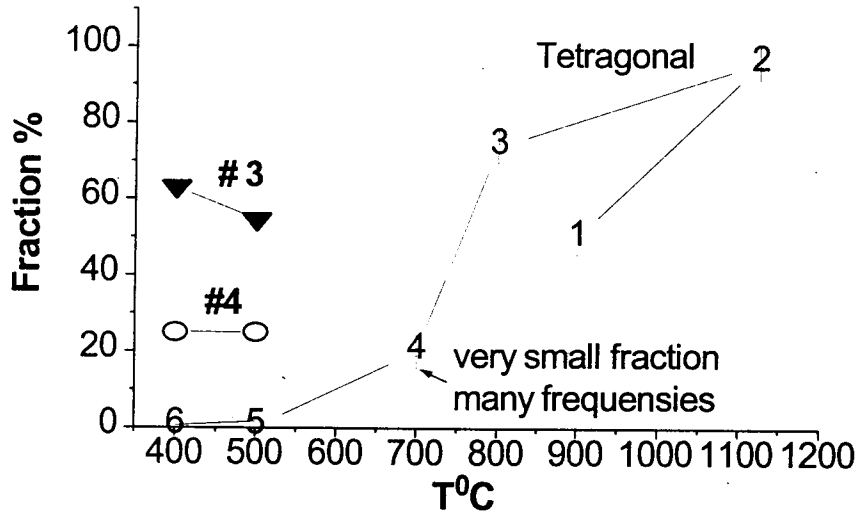

1)

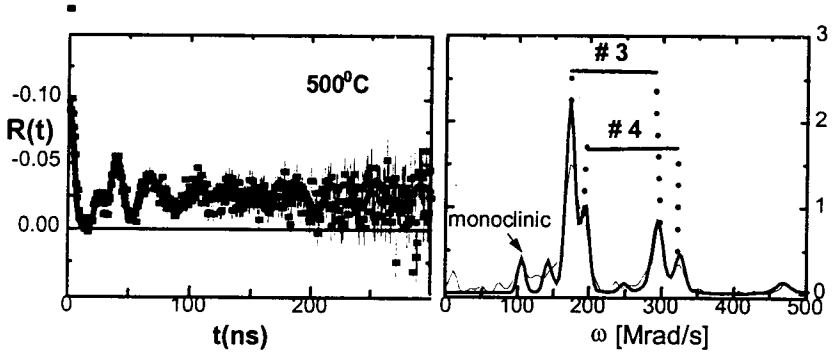

2)

Figure 7.1.10 Temperature dependence of fractions 1) and PAC spectra at 400°C 2) for Cz16 is 1% Ce-doped zirconia.

The maximum temperature this sample was taken to is 1125°C, which is higher than the Cz15 sample. And there is a significant difference between these two samples. After the sample was cooled down the tetragonal site disappeared at 700°C, and fractions of new sites at 500°C are bigger. Figures 7.1.9 and 7.1.10 show data collected

in a continued search for low temperature static trapped vacancies, as duscussed above for Fig. 7.1.7.

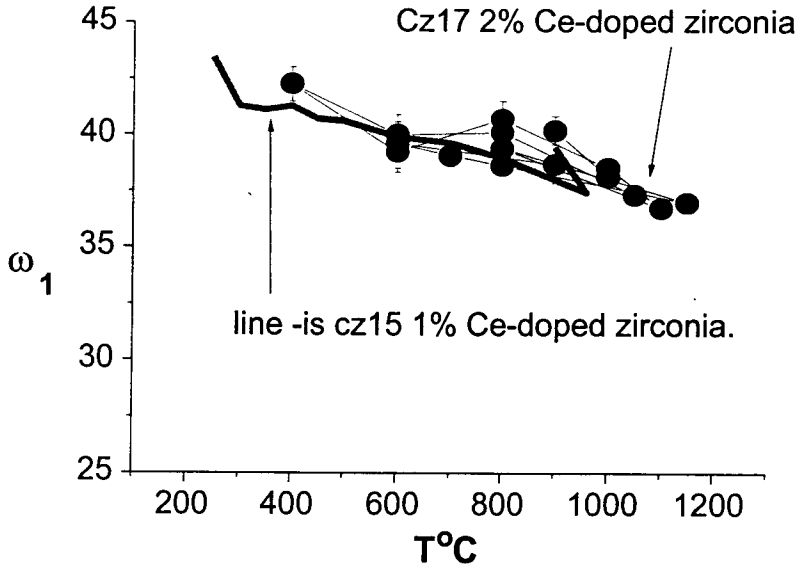

Figure 7.1.11 Temperature dependence of frequencies of the tetragonal site for Cz17-2% Ce-doped zirconia and Cz15-1% Ce-doped zirconia.

Well defined sites were obtained only when the sample was taken up to 900°C. Parameters of the tetragonal site were ω_1 = 40 Mrad/s and eta=.25 with fraction 20%. These are very close to those of the 1% Ce-doped samples. But instead of the usual monoclinic site with ω_1 = 110Mrad/s and eta=0.7 at this temperature along with a tetragonal a broad site with ω_1 = 50 Mrad/s appeared. At 1050°C the fraction of tetragonal phase increased up to 50%. Then when the sample was cooled down to 600° C the tetragonal fraction decreased to 40%, and the rest was fitted to 60% of broad site. At 400°C the broad site disappeared and the spectrum was fitted to 15% tetragonal phase, 25% monoclinic phase and 65% new site with ω_1 = 178 Mrad/s and eta=0.34

appear .Then back at 800°C the tetragonal fraction grew to 25%, monoclinic to 45% and new site decreased to 30%. At 1000°C the ratio became 40%/45%/15%. And then 1100°C three sites converted to 50% of tetragonal site and 50% of broad site. And as the sample was cooled again to 700°C and heated back to 1150°C the ratio of sites did not change even when the temperature decreased. But as the temperature decrease to 600°C three frequencies tetragonal, monoclinic and new with ω_1 = 178 Mrad/s and eta=0.34 appeared back with 20/30/50 ratio.

Summary: As the sample Cz17 was heated up for the first time from 900 to 1050°C there were two sites, broad and tetragonal. As the sample was cooled to 400°C three frequencies appear: tetragonal, monoclinic, and new site. When heated back up to 1100°C, the structure changed back to two frequencies (tetragonal and broad). After the sample was heated up to 1150°C and then cooled down to 600°C the spectrum changed to three frequencies (tetragonal, broad and monoclinic).

These measurements illustrate a complexity associated with obtaining homogeneous materials with both the cerium indium dissolved. Only after heating to 1150°C is a reasonably reproducible material obtained, but even this is altered if cooled too much.

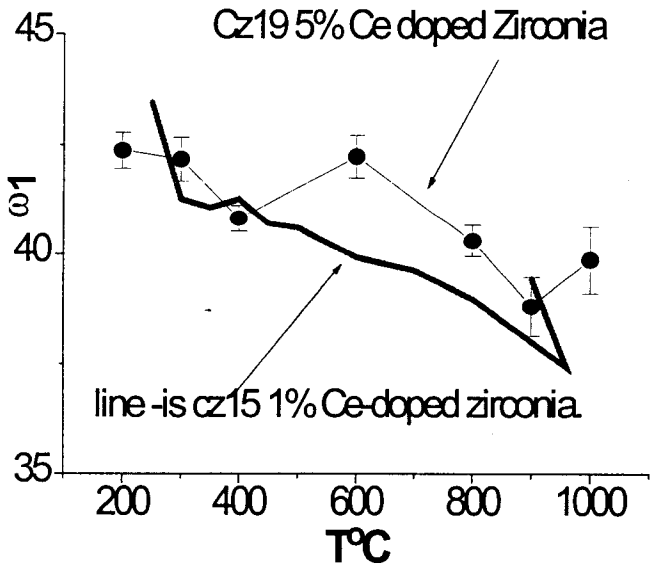

Figure 7.1.12 Temperature dependence of frequencies of the tetragonal site for Cz19-5% Ce-doped zirconia and Cz15-1% Ce-doped zirconia.

Cz 19 was fitted with two sites at 1000°C(the highest temperature this sample was taken) : with a sharp tetragonal site with ω_1= 40 Mrad/s , eta=0.2 and a broad site with ω_1=50 Mrad/s. Then after decreasing the temperature the frequencies of the broad site became 60 Mrad/s. The fraction of tetragonal site decreased from 70% at 1000°C to 20% at 100°C and another not well defined fraction appeared at 400°C .
Only one sample was made from 5% Ce doped solution. It showed that this heavily doped system is different from previous samples.

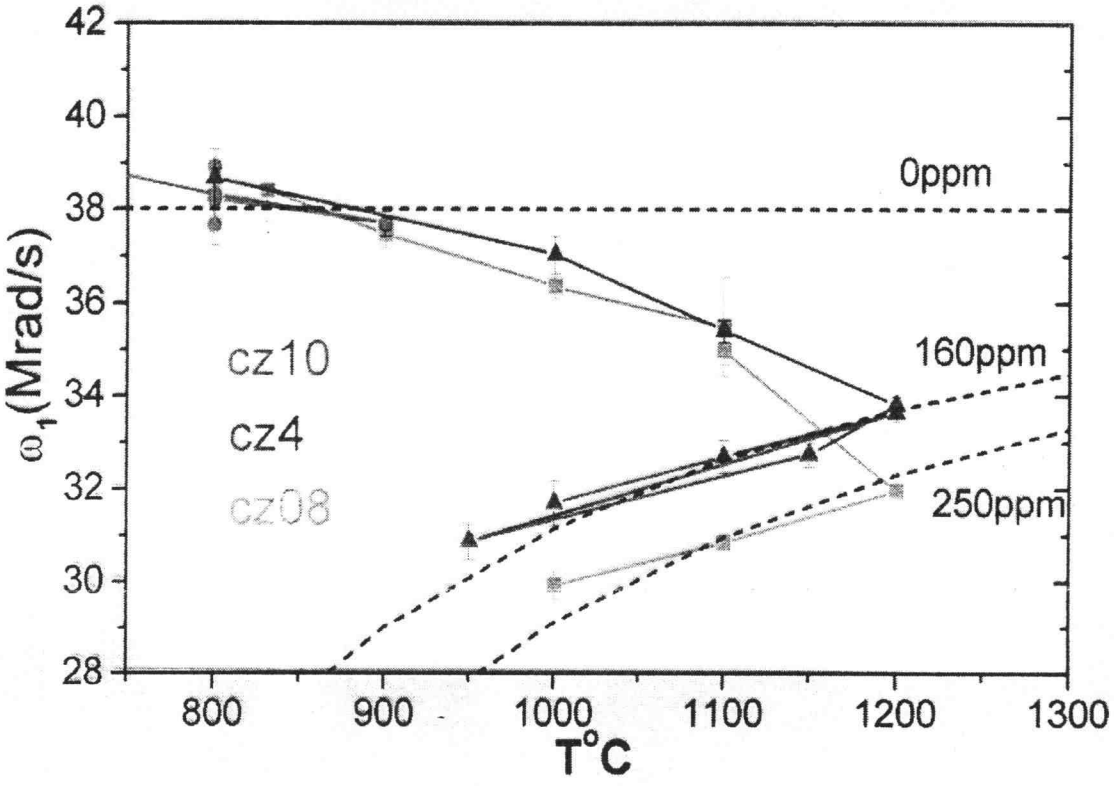

Figure 7.1.13 Temperature dependence of frequencies of the tetragonal site for Cz4, Cz08 and Cz10-1% Ce-doped zirconia samples.

Plot of frequency vs. temperature for a number of samples doped with 1% ceria. Note that the frequencies of samples are reproducible prior to being heated above 1000 °C but that the frequency drops irreversibly if the sample is heated to 1200°C. Our interpretation (see Section 2.5) is that there are very few oxygen vacancies below 1000°C but that vacancies are irreversibly incorporated if heated more. Samples heated to1200°C have a constant oxygen vacancy concentration when cycled to lower temperatures.

7.2 Pure zirconia.

Data are presented for pure zirconia powders that were prepared by various methods that are described in the chapter "Sample preparation". The purpose of this research was to investigate the influence of the precipitated methods on the oxygen vacancy concentration at 1200°C in tetragonal zirconia.

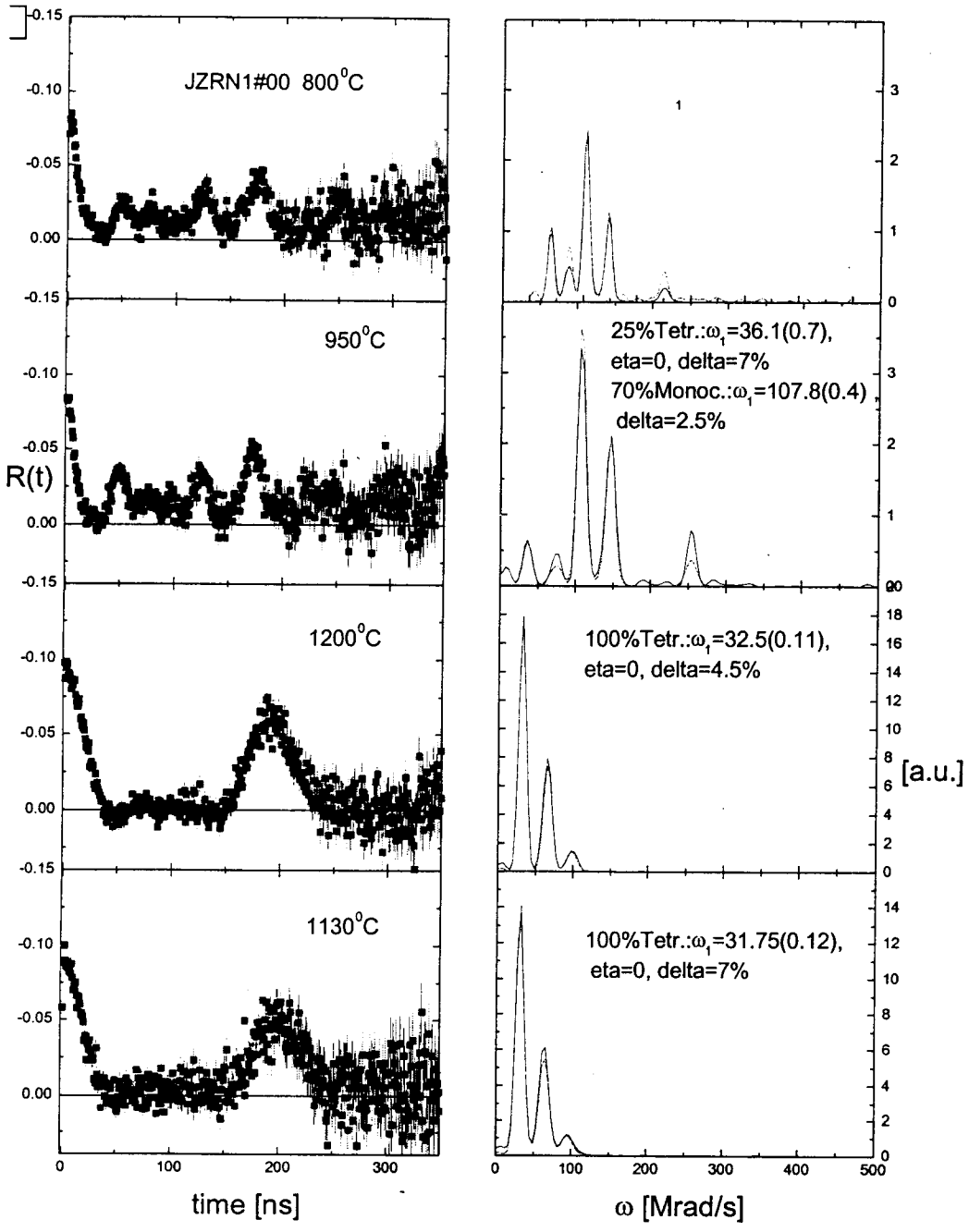

Figure.7.2.1 PAC spectra for Jzrn1 sample prepared by method #2.

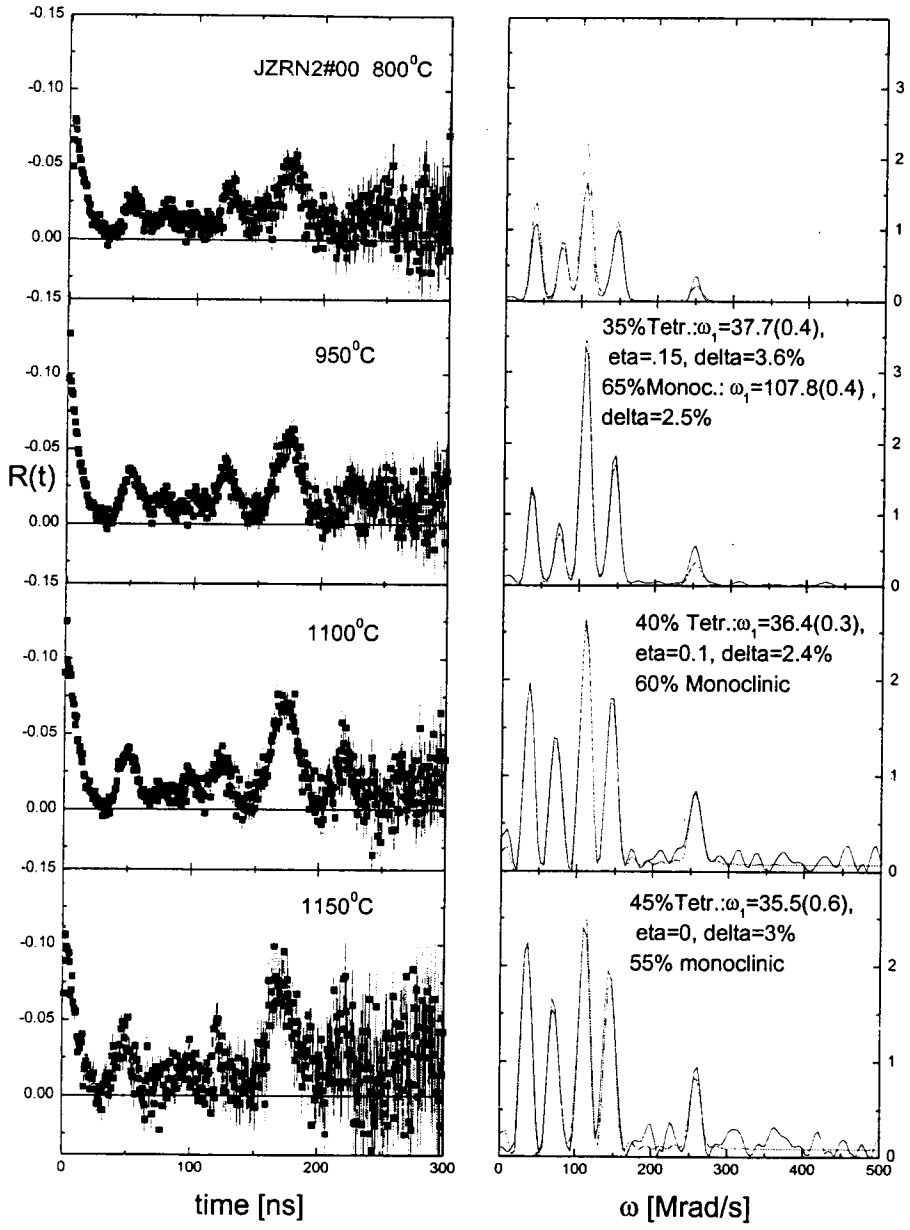

Figure.7.2.2 PAC spectra for Jzn2 pure zirconia sample prepared by method #2.

On the last two figures (Fig. 7.2.1 and 7.2.2) we can see that the pure zirconia samples prepared by method #2 had about 30% tetragonal as calcined at 900°C. Using method #1 the pure zirconia powders are fully monoclinic at this temperature. The behavior of the tetragonal frequency for these samples is similar to that of the 1% Ce-doped samples.

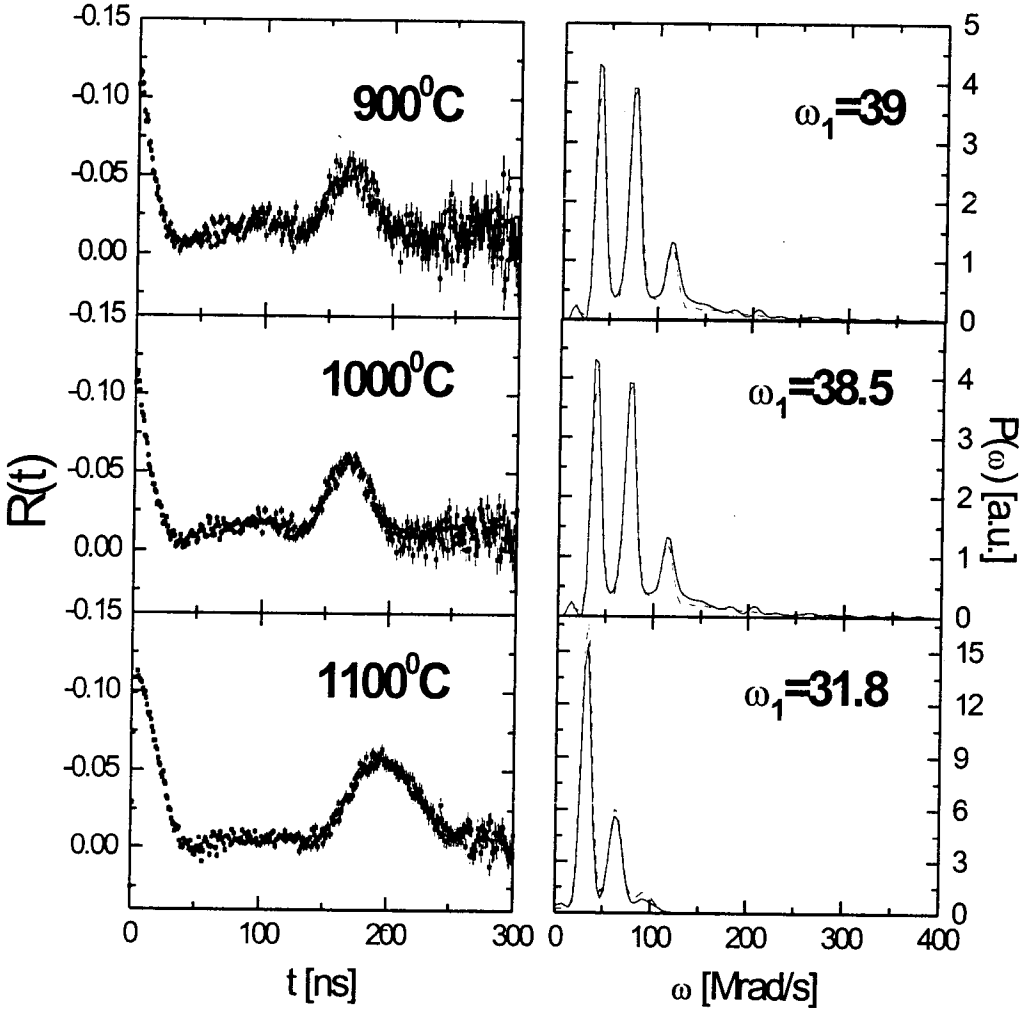

Figure.7.2.3 PAC spectra for Jzcl2-pure zirconia sample prepared by method #3.

The pure zirconia samples prepared by method #3 were fully tetragonal at the calcining temperature - 900°C, and the tetragonal frequency for this sample changed with temperature the same way as for the 1% Ce-doped samples. The PAC spectra for all methods of preparation are shown on Figure 7.2.6. It can be seen that method #1 produces the monoclinic structure for zirconia, method #2 produces from 30 to 40% tetragonal structure and the rest is monoclinic, and method #3 produces tetragonal structure for pure zirconia at 900°C.

The following experiment was made to investigate the influence of the rate of heating pure zirconia powders on phase stabilization. Samples jzcl2 and jzcl3 were portions of the same precipitate, made by method #3. Jzcl2 was heated from room temperature to 800°C with a 15deg/min heating rate. Jzcl3 was calcined at 400°C for 24 hours, then heated in 100°C steps to 800°C. It was held for at least 24 hours at each step. Spectra for these two samples are shown in figure 7.2.4.

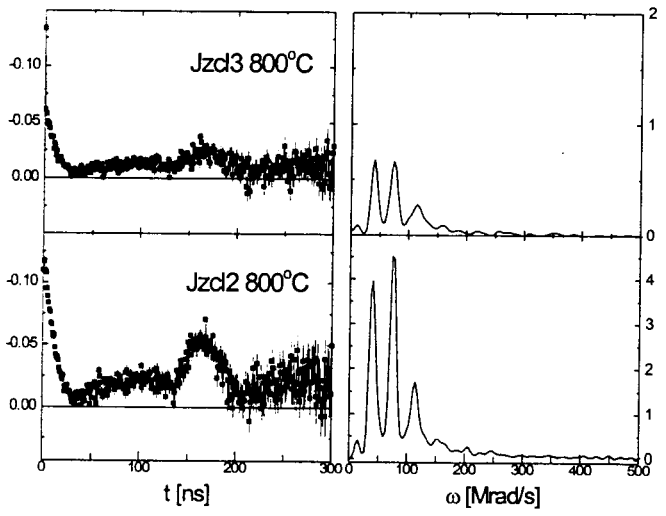

Figure.7.2.4 PAC spectra for Jzcl3 and Jzcl2 at 800°C

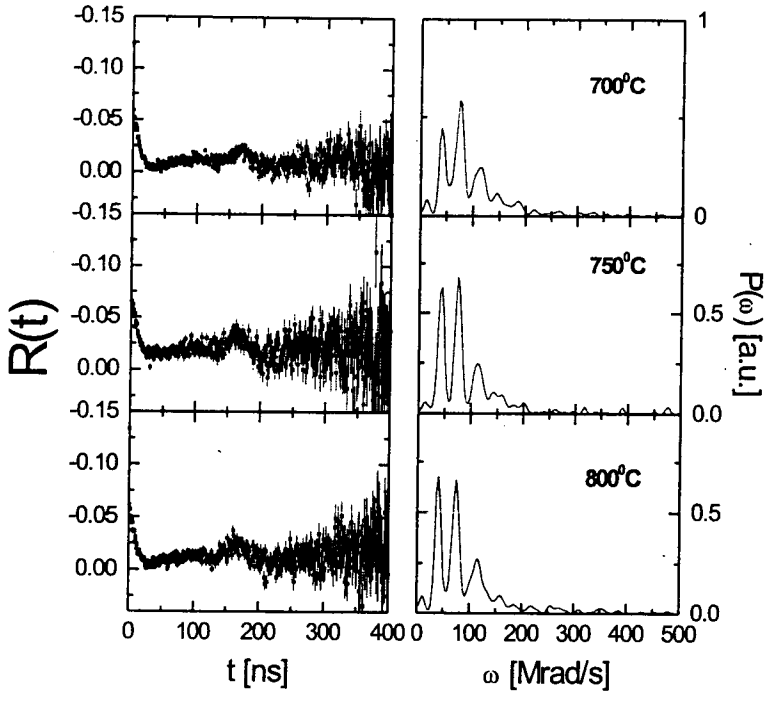

Figure7.2.5 PAC spectra for Jzcl3 sample prepared by method #3. Calcined at 400°C and heated up gradually with the step of 100°C. It was kept at each temperature at least 24 hours.

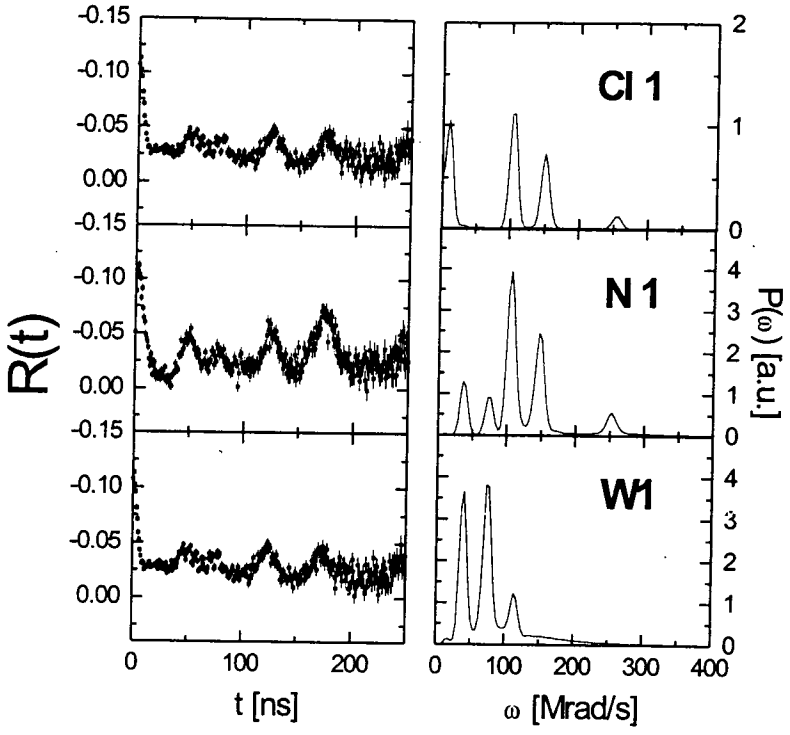

Figure 7.2.6 PAC spectra for three different sample preparation methods:#1-CL1,#2-N1,#3-W1.

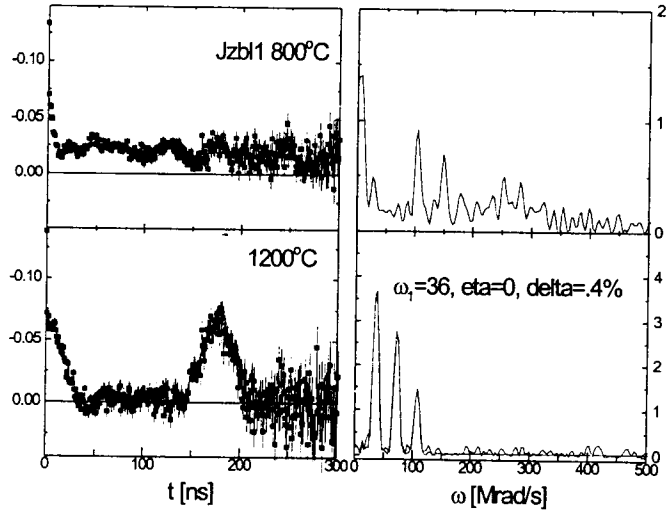

Figure.7.2.7 PAC spectra for Jzbl1 sample prepared by method #4.

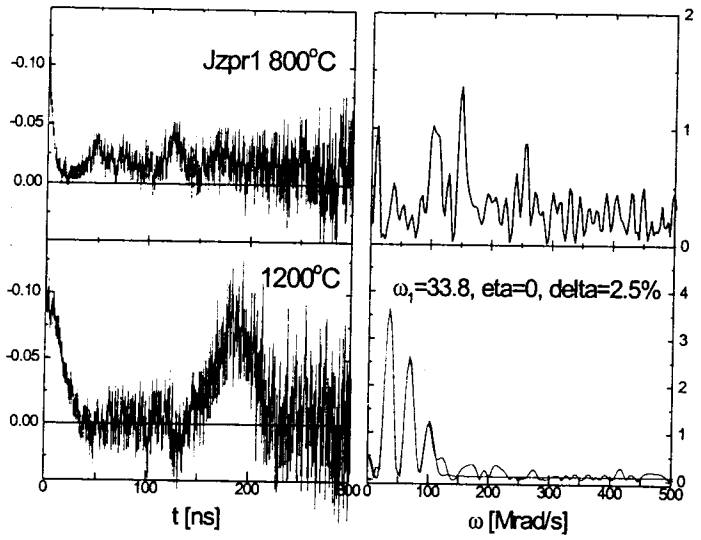

Figure.7.2.8 PAC spectra for Jzpr1 sample prepared by method #5.

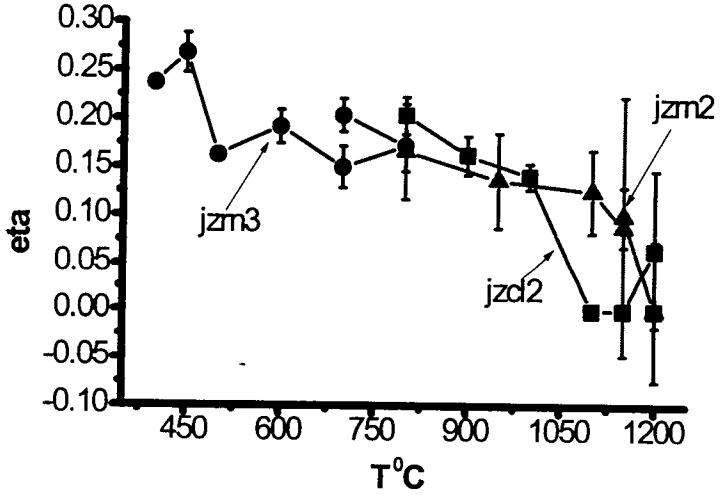

Figure 7.2.9 Temperature dependence of asymmetry parameter eta for jzrn2,jzrn3 and jzcl2. Jzrn2 and jzrn3 pure zirconia samples prepared by method #2, jzcl2 pure zirconia sample prepared by method #3.

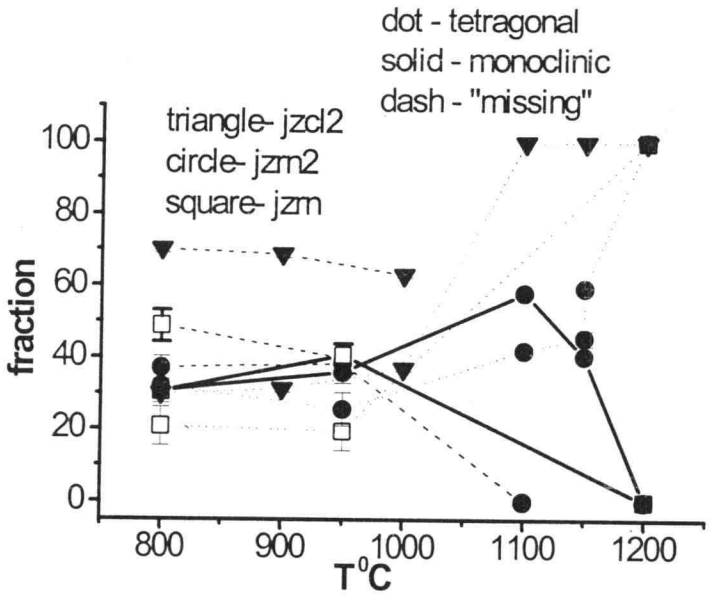

Figure.7.2.10 Temperature dependence of tetragonal, monoclinic and missing fractions for jzrn, jzrn2 and jzcl2. Jzrn and jzrn2 pure zirconia samples prepared by method #2, jzcl2 pure zirconia sample prepared by method #3.

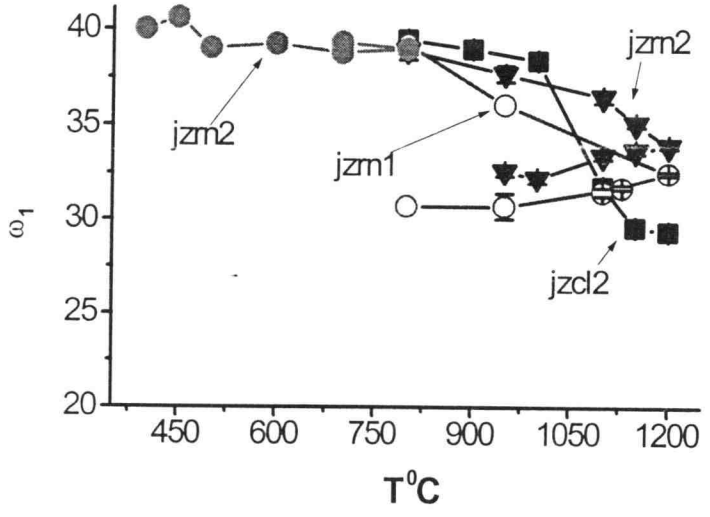

Figure.7.2.11 Temperature dependence of ω_1 for jzrn1, jzrn2, jzrn3 and jzcl2. First three samples were prepared by method #2, jzcl2 sample was prepared by method #3.

7.3 Nb-doped zirconia.

Nb-doped zirconia samples were studied by Han-Tzong Su [6]. We used a new method preparation #3, which is described in Chapter 5, for this research. By using this method of preparation we managed to stabilize 0.3% Nb-dopped zirconia powders at 900°C in the tetragonal phase.

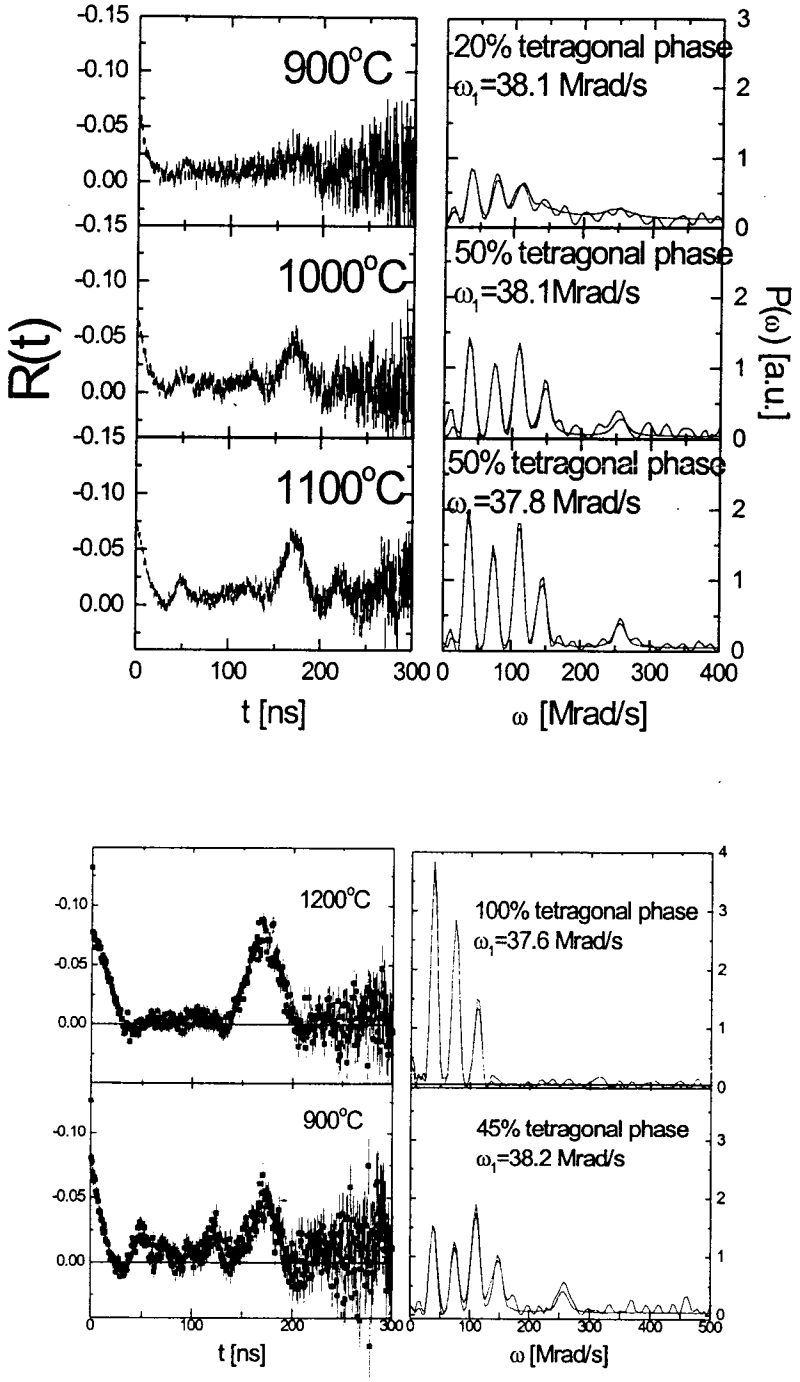

Figure 7.3.1. PAC spectra for Jznb2 .3% Nb doped zirconia sample prepared by method #3.

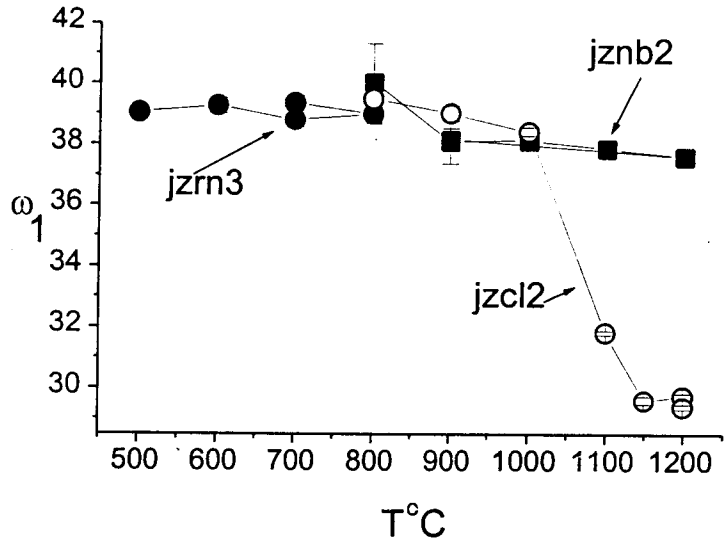

Figure 7.3.2 Temperature dependence of ω_1 of two pure zirconia samples: jzcl2 prepared by method #3, and jzrn3 prepared by method #2, and .3% Nb doped sample - jznb2

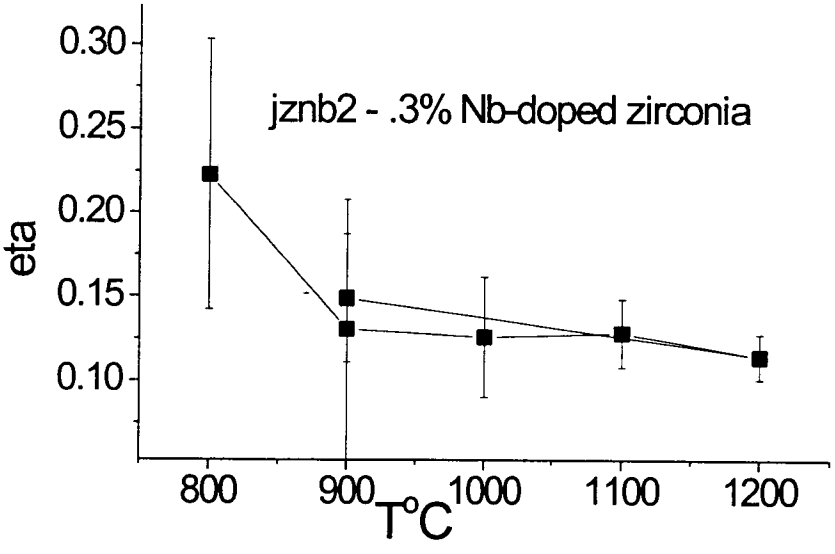

Figure 7.3.3 Temperature dependence of asymmetry parameter eta for the .3% Nb doped zirconia sample Jznb2.

7.4 Influence of atmosphere: argon and CO.

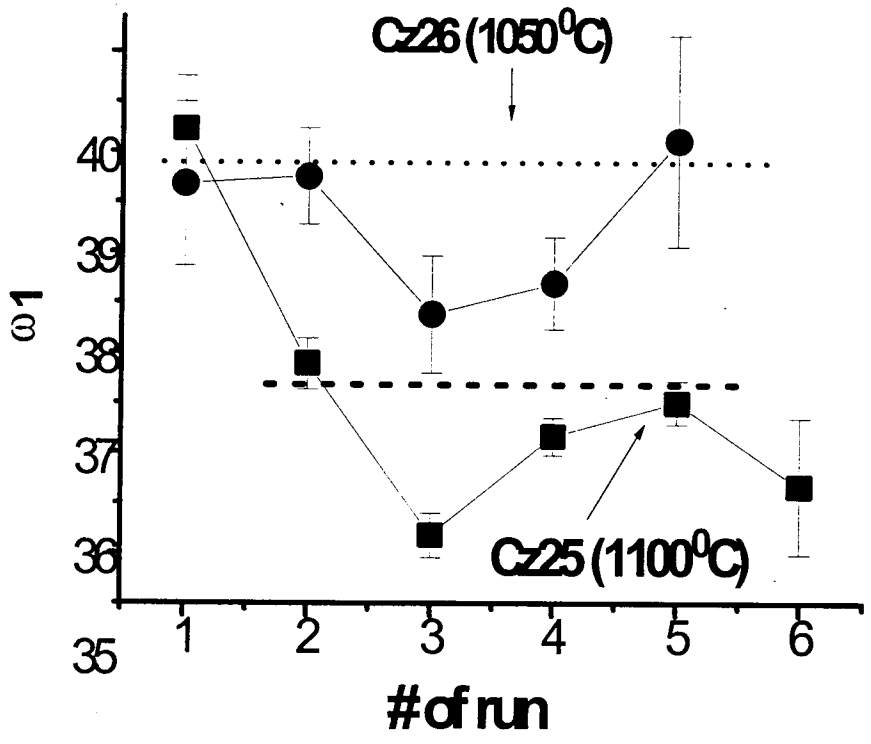

Figure 7.4.1 Dependence of tetragonal frequncy on the atmosphere for Cz 25 and Cz 26 1% Ce doped Zirconia.

The first and last runs for both samples were taken at 900°C. Then Cz 25 was taken to 1100°C and Cz 26 was taken to 1050°C. Run #2 was taken in air at these temperatures. Then run #3 was made under argon pressure at the same temperatures. Then for run #4 the argon flow was stopped. For sample Cz 26, air was flowed over the sample, but Cz 25 was left static. The data imply that the argon remained within the sample holder during run #4, so air was flowed during run #5 to assure that the sample was definitely in air.

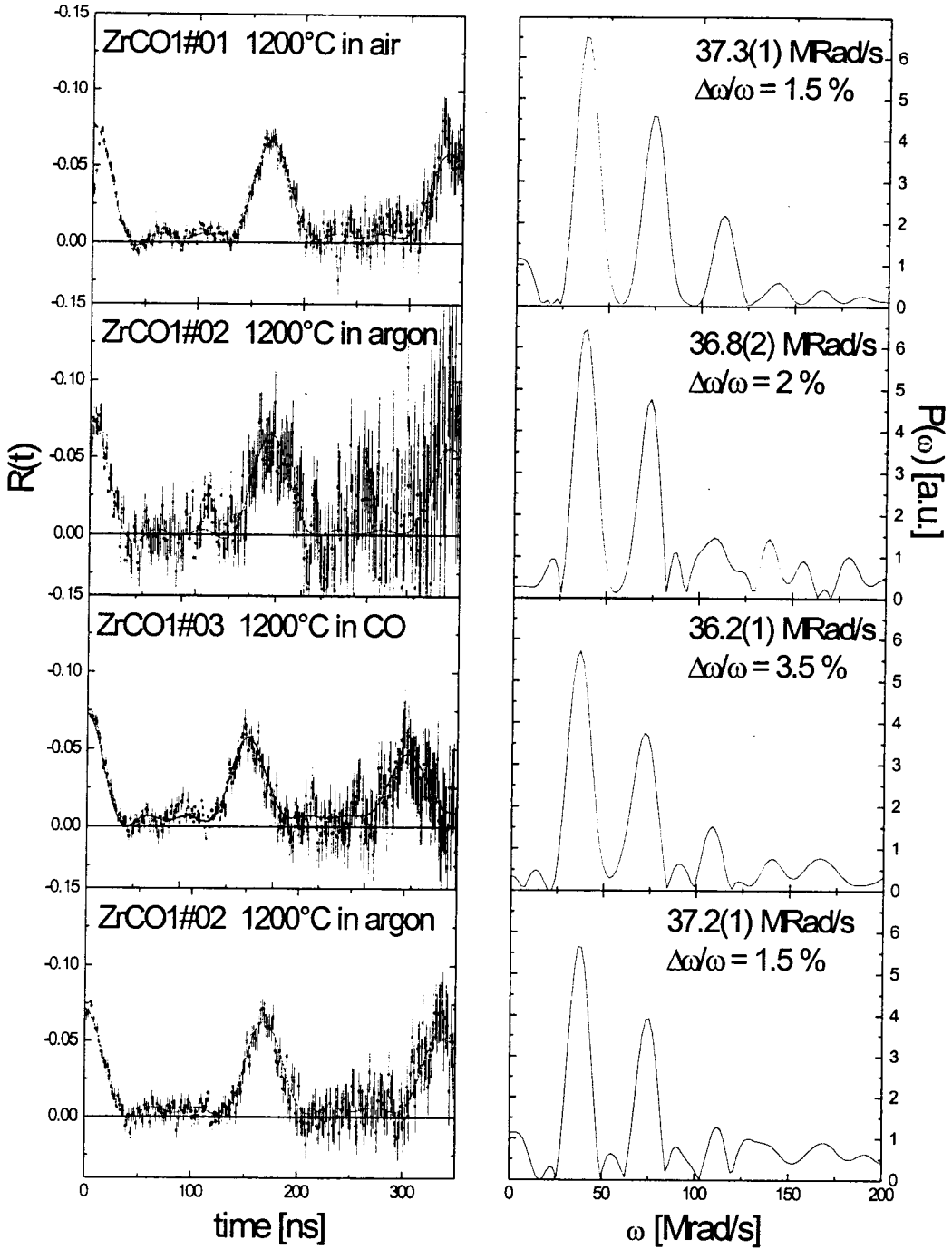

Figure 7.4.2 PAC spectra for ZrCO 0.3%Nb-doped zirconia sample prepared by method #3. At 1200°C CO was flowed through the system. The dependence of the tetragonal frequency on atmosphere is shown on the picture.

7.5 X-ray data.

Grain sizes (<100nm) were determined by X-ray line broadening measurements using a Siemens diffractometer with CuK_{α}-radiation. The X-ray spectra for pure zirconia samples are shown in the appendix section of this thesis. The average grain size was determined by the Warren-Averbach method using commercial software supplied by Siemens. Samples were prepared by various methods and calcined at the indicated temperatures. ZRCL samples were prepared by method#1. ZRN samples were prepared by method #2. ZRW samples were prepared by method #3. All x-ray data were collected after the sample had been cooled down to room temperature. The heating rate was 10 deg/min, and samples were calcined for 16 hours. Peaks related to tetragonal and monoclinic structures were observed. In order to retain the tetragonal phase at room temperature the powders can not be taken to too high temperature. That maximum temperature depends on the method of preparation.

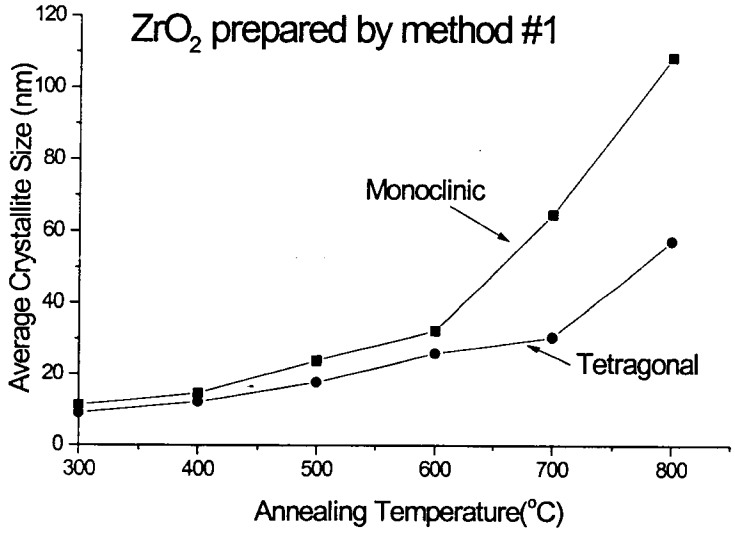

Figure 7.5.1 Increase of the average crystallite size for tetragonal and monoclinic phase with increasing annealing temperature.

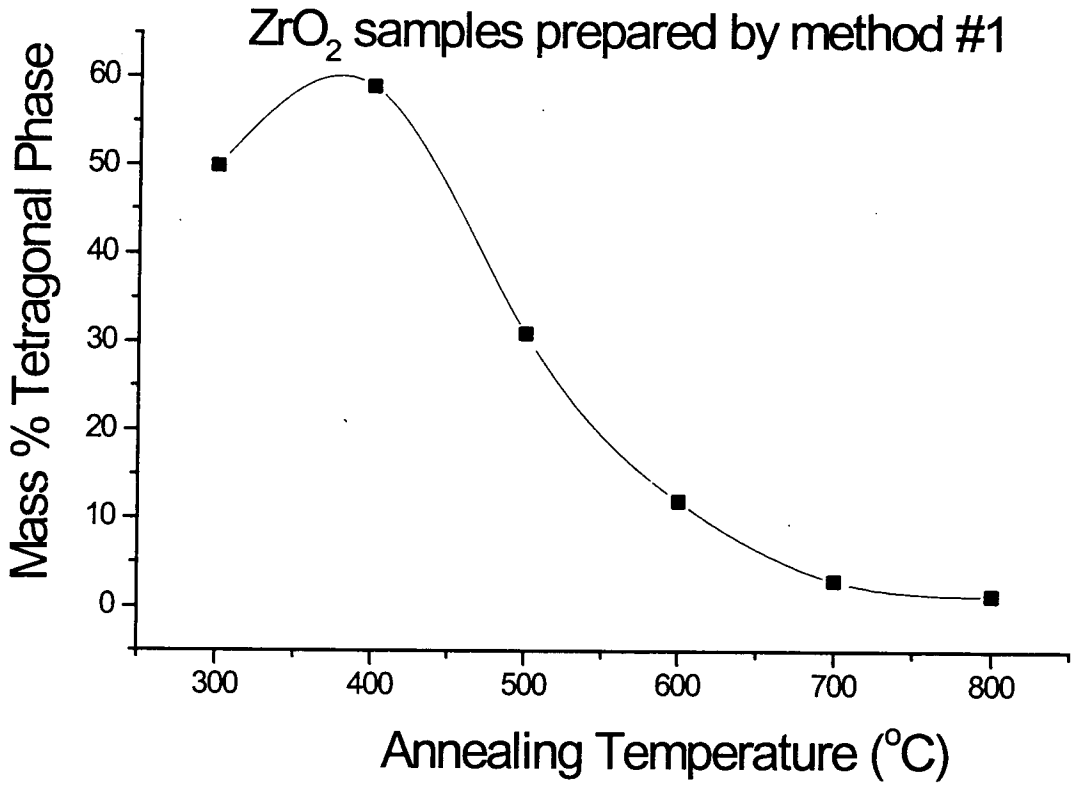

Figure 7.5.2. Dependence of tetragonal fraction on the annealing temperature.

7.6 SEM.

Powders from chloride and nitrate precursor solutions were calcined at two different temperatures 1000°C and 1200°C. As shown on Fig.7.6.1, the samples containing Cl have bigger grains at 1000°C then the chlorine-free samples. But at 1200°C the first sample has a porous structure in which the grains are connected to

each other by necks and average grain size is only slightly bigger than at 1000°C. In samples prepared by method #2 the grains are well sintered, and the average grain size of this sample is significantly larger than the other type of sample.

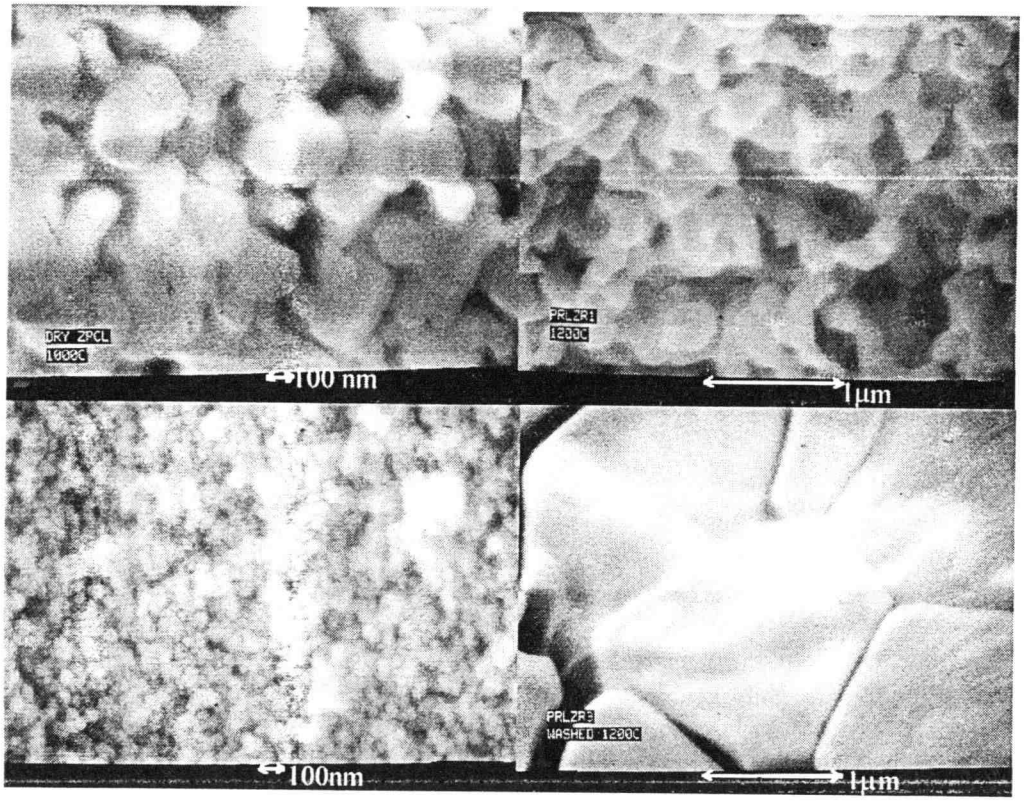

Figure.7.6.1 . SEM images of two samples at two different calcining temperatures 1000°C and 1200°C.
Top left: PR1ZR1 after being heated up to 1000C (The scale bar is 100 nm)
Top right: PR1ZR1 after 1200°C (scale bar is 1μm)
Lower left: PR1ZR3 after 1000°C (scale bar is 100 nm)
Lower right: PR1ZR3 after 1200°C (scale bar is 1μm)

Following the implications of a previous study [30] about the role of HCl in mass transport and the sintering process, a further set of experiments was performed. HCl was allowed to flow through the zirconia powder (sample PR1BCL2) continually as the sample was heated up. At 800°C the grain size was smaller than it was without flowing HCl (Fig.3). And at 1200°C the grains were even less sintered than in the PR1ZR1 sample and the necks between the grains were smaller. PAC measurements of the PR1BCL2 sample gave the smallest number of oxygen vacancies ever obtained in pure 1200°C tetragonal zirconia, approximately 80 ppm.

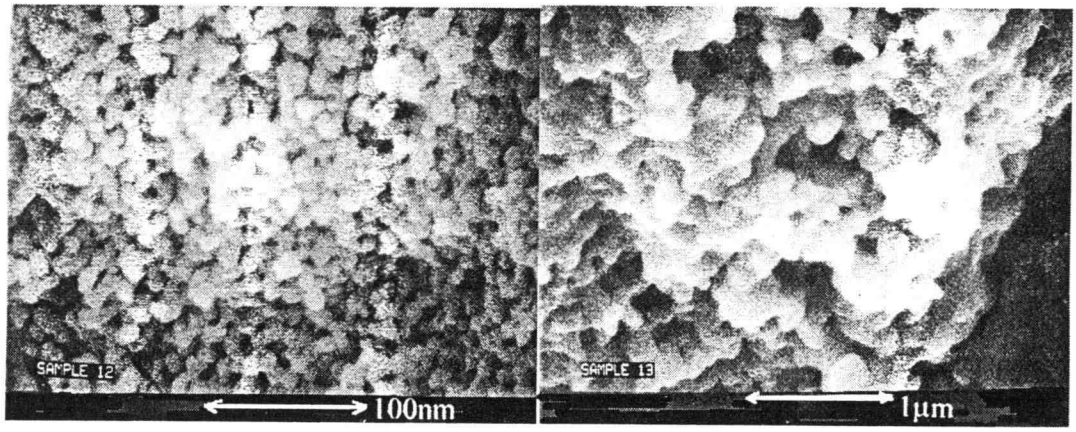

Figure 7.6.2. SEM images of PR1BCL2 sample at two different calcining temperatures 1000°C and 1200°C.
Left: the sample PR1BCL2 after being heated up to 1000°C (scale bar is 1μm)
Right: the same sample after 1200°C (scale bar is 1μm)

7.7 Damping parameter.

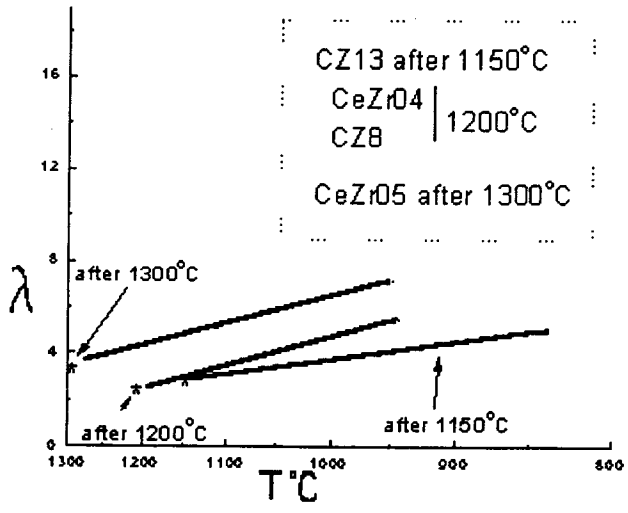

Figure 7.7.1 Damping parameter λ versus temperature.

Several PAC spectra for the samples that were heated to high temperatures were fitted with the λ broadening. This damping parameter is related to an actual fluctuation rate that corresponds to the hopping rate of the oxygen vacancy about the cadmium with a corresponding activation energy for zirconia [7, 60, 61].

8. DISCUSSION AND CONCLUSIONS.

8.1 Discussion.

Several different experiments were made for better understanding of the nature and behavior of oxygen vacancies in zirconia powders. Our primary technique PAC allows us to measure the average electric field gradient (efg) caused by trapped oxygen vacancies. The strength of this efg is used to determine the number of oxygen vacancies in tetragonal zirconia. The tetragonal phase in pure zirconia is stable in the range from 1200°C to 2370°C [1-3]. In order to measure oxygen vacancies at lower temperature we needed to stabilize the tetragonal phase by adding Ce, or by varying methods of preparation.

In analyzing the data for 1% ceria-doped zirconia several conclusions had been made:

1. 1% ceria-doped zirconia powders are tetragonal after calcining at 800°C and the change in the electric field gradient from 800°C to 1000°C is caused only by lattice expansion (Fig. 7.1.(1-5,8,11,12)). The frequencies of the samples at low temperature are close to those of the charge compensated zirconia (0.3% Nb-doped (Fig. 7.3.(1,2)).
2. The efg is not axially symmetric at all temperatures for Ce-doped samples (Fig.7.1.(1,2,5)).
3. After 1000°C the change in the efg can not be explained only by lattice expansion. In this range additional oxygen vacancies appear and do not subsequently disappear when the temperature is reduced again (Fig. 7.1.(1- 4,8,11,12)).
4. After the samples were heated up to 1200°C the oxygen vacancy concentration became independent of temperature (Fig. 7.1.(1-4)). Even after a tetragonal to monoclinic and back to tetragonal transformation, the sample has the same number of vacancies as it had the first time at 1200°C (Fig. 7.1.1, 7.1.4, 7.1.8)
5. As the samples were cooled down from temperature not greater than 1050°C several new well-defined frequencies were observed (Fig. 7.1.(7,9,10)). The fraction of these new sites seemed to be strongly related to the highest temperature to which the sample had been taken.

6. By increasing the doping level from 1% to 2% we changed the symmetry of the lattice somewhat, but the strength of the efg remained the same. At 5% the frequencies of the tetragonal site at low temperature increased (Fig. 7.1.(11,12)). The increase may be due to the lattice change with the presence of high concentration of alien atoms.

In order to investigate the influence of the dopants on the behavior of pure zirconia, several methods of sample preparation were used to eliminate contamination in our powders. The initial source solutions contained N or Cl elements in addition to Zr.

1. Precipitates prepared by method #1 contained a significant amount of chlorine. After calcining at temperatures below 800°C x-ray diffraction indicates that these samples had some tetragonal fraction (Chapter 7.5). However above 800°C tetragonal grains transformed to monoclinic (Fig.7.2.6) and at 1200°C had the lowest concentration of oxygen vacancies (Fig. 7.2.11).
2. A significant amount of Cl was also found in the samples prepared by method #4 and #5. As for samples prepared by the first method, the samples were monoclinic after 800°C (Fig.7.2.(7,8)).
3. Samples prepared by method #2 also were formed as tetragonal crystals (Chapter 7.5) and at 800°C the ratio of tetragonal to monoclinic was about 40/60 (Fig.7.2.1, 7.2.2), but the samples prepared by method #3 were fully tetragonal at this temperature (F ig. 7.2.10).
4. At low temperature the tetragonal frequencies of pure zirconia for method #2 and #3 are close to those of 1% Ce-doped samples.
5. The asymmetry parameter eta is non-zero for metastable tetragonal zirconia (below 1200°C), but as the sample was heated up to the stable tetragonal region (above 1200°C) eta becomes zero (Fig. 7.2.9).

Some of the Nb-doped samples were prepared by method #3, which allowed us to keep the sample partially tetragonal from 900°C up to 1200°C (Fig. 7.3.1).

1. The frequencies of the Nb-doped sample were the same as for pure zirconia samples (Fig.7.3.2). This allows us to conclude that there are no vacancies in the pure zirconia sample present up to 1000°C.
2. The asymmetry parameter eta is non zero at all temperatures for the 0.3% Nb-doped zirconia sample.(Fig. 7.3.3).

Several experiments were done trying to induce additional oxygen vacancies by reduced oxygen partial pressure (Chapters 4 and 7.4)

1. The influence of flowing argon on the 1% Ce-doped zirconia at two different temperature is shown on fig. 7.4.1. The relative drop in the frequency for tetragonal site in zirconia at 1050°C and 1100°C is the same. The concentration of oxygen vacancies increased when argon flowed and then recovered after air was added to the system. At 1200°C, however, the addition of argon to the system did not change the oxygen vacancy concentration.
2. R. Platzer measured PAC spectra with CO flowing over the 0.3% Nb-doped zirconia sample at 1200°C. This sample was prepared by method #3 (Fig.7.4.2). With this considerable reduction of oxygen below atmospheric pressure, he managed to increase the oxygen vacancy concentration at 1200°C.

8.2 Implications of the data.

8.2.1 Zirconia that is tetragonal at 800°C.

The above discussion for materials that are tetragonal at 800°C can be summarized by the following observations.

1. At low temperature the PAC frequencies of tetragonal zirconia behave very similarly for all materials. If stabilization is achieved by heavy doping, there are shifts and line-broadening due to the presence of dopants but no obvious differences in the essential physics. One material included in this group is Nb-doped zirconia that has no oxygen vacancies. The implication is that there are no detectable oxygen vacancies in our pure or lightly doped zirconia powders.
2. Vacancies are incorporated as the samples are heated above 1050°C, the temperature at which sintering becomes important. The oxygen vacancies in samples that have been heated to 1200°C remain when cooled.
3. We see no vacancy concentration dependence on the atmosphere for samples containing no +5 valent elements such that there are a substantial number of vacancies at 1200°C.
4. In several instances, samples that had been heated to a maximum temperature of 1050°C or 1100°C contained a vacancy density that was small (<100 ppm) but

measurable. A reduced oxygen pressure increased the oxygen vacancy density by a measurable amount in these samples.

5. Samples that are tetragonal at 800°C are well-sintered after being heated to1200°C (Fig. 7.6.1)

8.2.2 Zirconia that is monoclinic at 800°C.

PAC gives no information about the oxygen vacancies in monoclinic zirconia. We can determine the oxygen vacancy concentration in samples that are monoclinic at low temperature only after the monoclinic to tetragonal phase transition in zirconia near 1170°C. The data on these materials is summarized by the following points.

1. Samples that were monoclinic below 1170°C are very poorly sintered at 1200°C and contain few vacancies.
2. As shown in Fig.7.6.2 [59], flowing Cl in the system as the samples are sintering retards the densification of the grains. These samples had the smallest density of oxygen vacancies.

8.2.3 The excess oxygen vacancy concentration.

In the course of this work it was found that the excess from the expected value of the oxygen vacancy concentration was not caused by the presence of the impurities in the samples; this was proved by NAA experiments. The only straightforward way to explain the high concentration of oxygen vacancies in zirconia is by the existence of negatively charged extrinsic defects. These defects can be caused by inclusion in grains as the grains are sintered. This is presently our hypothesis based on the experimental results represented in Chapter 7.

We plan to look at our samples using Transmission Electron Microscopy, in collaboration with the TEM group directed by Prof. Janet Rankin of Brown University. This will allow us to see the arrangement of the atoms in the grains.

Future investigations of the influence of the pH on the stabilization and grain growth are required to complete the picture of the formation of the oxygen vacancies.

Future work needs to be done to test the hypotheses made after this work, that monoclinic powders at 800°C do not sinter well as they are heated up to 1200°C and

that they contain small amounts of oxygen vacancies at high temperature. Another hypothesis is that pure tetragonal zirconia powders at low temperature are well sintered by 1200°C, and contain the large amounts of oxygen vacancies concentration at high temperature.

Future study also should be done in the low temperature region where several new PAC frequencies were found for samples as they were cooled down from temperatures around 1000°C.

BIBLIOGRAPHY.

[1] *International Table for Crystallography*, Vol. A, edited by T. Hahn, D. Reidel, Publishing Co., Dordrecht (1987).

[2] R. W. G. Wyckoff, *Crystal Structures*, Vol.2, John Wiley and Sons, New York (1960).

[3] R. N. Patil and E. C. Subbarao, *Axial thermal expansion of ZrO_2 and HfO_2 in the range room temperature to 1400°C*, J. Appl. Cryst. 2, 281 (1969).

[4] C. Garvie, R. H. Hannink and R.T. Pascoe, *Ceramic steel?*, Nature 258, 703 (1975)

[5] H.-T. Su, R. Wang, H. Fuchs, J. Gardner, W. Evenson, J. Sommers, *Study of oxygen vacancies in ceramics by perturbed angular correlation spectroscopy*, J. Am. Ceram. Soc. 73, 3215-19 (1990).

[6] H.T. Su, PhD Thesis, *Perturbed Angular Correlation Spectroscopy of Oxide Ceramics at High Temperature*, Dept. of Physics, Oregon State University, 1989.

[7] M. O. Zacate, PhD Thesis, *A Microscopic Study of the Interaction Between Aliovalent Dopants and Native Defects in Group IV Oxides: Indium and Cadmium in Ceria and Zirconia.*, Dep. of Physics, Oregon State University, 1997.

[8] S. L. Jones and C. J. Norman, *Effect of chemical and heat treatment on the tetragonal-to-monoclinic transformation of zirconia*, J. Mater. Res., Vol.8, No. 1, Jan (1993) 163-168.

[9] R. Srinivasan et al., *Factors influencing the stability of the tetragonal form of zirconia*, J. Mater. Res. 11 (4), Jul/Aug 583-588 (1986).

[10] A. Clearfield ,*The mechanism of hydrolytic polymerization of zirconyl solution*, J. Mater. Res. Vol. 5, No. 1 , Jan (1990) 161-162.

[11] B. H. Davis, *Effect of pH on Crystal Phase of ZrO_2 Precipitated from solution and calcined at 600°C*, Commun. Of the Amer. Cer. Soc. August (1984) C-168.

[12] R. P. Denkewicz et al., *Hydrothermal crystallization kinetics of m-ZrO_2 and t-ZrO_2*, J. Mater. Res., Vol. 5, No. 11, Nov (1990), 2698-2705.

[13] M. M. R. Boutz et al., *Yttria-Ceria Stabilized Tetragonal Zirconia Polycrystals: Sintering, Grain Growth and Grain Boundary Segregation*, J. of the European Cer. Soc. 13 (1994) 89-102.

[14] B. Garvie J.Phys.Chem. 69 (1965) 1238, J. Phys. Chem. 82 (1978)218.

[15] E. Bailey et al., Trans. J. Br. Ceram. Soc. 71 (1972)25.

[16] Murase and Kato, J, Am. Ceram. Soc., 62 (1979)527.

[17] T. Sato et al., Thermochim. Acta 34 (1979)211 .

[18] A. Clearfield, Ignor. Chem. 3,146 (1964).

[19] A.Clearfield, Rev. Pure Appl. Chem. 14. 91 (1964).

[20] A. Clearfield et al., Acta Crystallogr. 9, 555(1956).

[21] Muha and et al., J. Chem. Phys. 33, 194 (1960).

[22] J. S. Johnson et al., J. Am. Chem. Soc. 78,3937 (1956).

[23] R. Fryer, J. L. Hutchenson, and R. Paterson, J. Colloid Interface Sci. 34, 238 (1970).

[24] A. Bleier and R. and R.M. Cannon, in Letter Ceramics Through Chemistry, 2. Edited by C.J.Brinker, D.E. Clark, And D. R. Ulrich (Mater. Res. Soc. , Pittsburgh, PA, 1986), p.71.

[25] R. Srinivasan et al. *Cristallization and Phase Transformation Process in Zirconia: An in situ High-Temperature X-ray Diffraction Study*, J. Am. Ceram. Soc., 75[5]1217-22 (1992).

[26] M. Bychi et al. *Crystallization of zirconia under hydrothermal conditions* , J. Am. Ceram. Soc. 78[12] 3397-3400 (1995).

[27]M.A. Blesa et al., J.Mater. Sci. 20, 4501 (1985).

[28] Goran Srefanic et al., Croatica chemica acta CCACAA 69(1) 223-239 (1996).

[29] Livage, K. Doi and C. Mazieres *Nature and Termal Evolution of Amorphous Hydrated Zirconium Oxide.,* J, Am. Cer. Soc. Vol 51, No.6 349-353, 1968

[30] M.J Readey and D.W. Readey J. Am. Ceram. Soc.69 [7]580-82 (1986).

[31] D. E. Collins and et al. ,Journal of the European Ceramic Society 15 (1995) 1119-1124.

[32] J. Rankin, B. W. Sheldon, Material Science and Engineering A204 (1995) 48-53.

[33] Srinivasan et al. *Critical Particle Size and Phase Transformation in Zirconia : Transmission Electron Microscopy and X-ray Diffraction Studies*, J. Am. Ceram. Soc., 73[11]3528-30(1990).

[34] X. Turrillas, P. Barnes , and D. Hausermann J. Mater. res., Vol.8, No. 1, Jan 1993.

[35] J. Anwar, Ph.D. Thesis, University of London (1990).

[36] G. T. Mamott, P. Barnes and et al., J. Mater. Sci. 26, 4054 (1991).

[37] G. S. A. M. Theunissen et al. "Effect of dopants on the sintering behavior and stability of tetragonal zirconia." J. of Europ. Ceram. Soc. 9(1992)251-263.

[38] Aswndi et al. Metastability of tetragonal zirconia powders. J. Am. Ceram. Soc. 68 (3) (1985) 135-9.

[39]Igawa et al. *Crystal structure of metastable tetragonal zirconia by neutron powder diffraction study.* J. Am. Ceram. Soc. 76(10)(1993) 2673-6.

[40]Gravie R, *The occurrence of metastable tetragonal zirconia as a crystallite size effect.* J.Phys. Chem. 69(4) (1965) 1238-43.

[41] Ackermann R. *High -temperature phase diagram for the system Zr-0.* J. Am. Ceram. Soc. 60[1]7-8(1977)341-5.

[42] P. Aldebert and J.-P. Traverse *Structure and Ionic Mobility of Zirconia at High Temperature* , J. Am. Ceram. Soc. 68 [1] 34-40 (1985).

[43] Mary Sue Kaliszewski and Arthyr H. Heuer, *Alcohol Interaction with Zirconia Powders*, J. Am. Ceram. Soc. ,73[6]1504-509(1990).

[44] M. J. Readey and et al., *Processing and Sintering of Ultrafine MgO-ZrO2 and (MgO, Y2O3)-ZrO2 powders*, J. Am. Ceram. Soc., 73[6]1499-503(1990).

[45] S. L. Jones and C. J. Norman , *Dehydration of Hydrous Zirconia with Methanol*, J. Am. Ceram. Soc. 71[4]C-190-C-191(1988).

[46] C. E. Scott and J. S. Reed *Analysis of Cl^- Ions Laundered from Submicron Zirconia Powders* , Ceramic Bulletin Vol.57, No.8(1978).

[47] Tsugio Sato and Masahiko Shimada *Transformation of Ceria-Doped Tetragonal Zirconia Polycristals by Annealing in Water*, Am. Ceram. Sos. Bull., **64** [10] 1382-84 (1985).

[48] H. Jaeger. *Perturbed Angular Correlation Investigation of Zirconia Ceramics. PhD theses* , Oregon State University, March 1987.

[49] Yet-Ming Chaing, Dunbar Birnie III and W.David Kingery Physical Ceramics, Wiley 1997.

[50] Wei-E Wang and Donald R. Olander *Thermochemistry of the U-O and Zr-O Systems,* J. Am. Ceram. Soc. 76[5]1242-48 (1993).

[51] L. A. McClaine and C. P. Coppel , *Electrical Conductivity Studies of Tetragonal Zirconia,* J. Electrochem. Soc. , 113,80 (1966).

[52] J. Xue, *Nonstoichiometry and Point Defecr Structure of Monoclinic and Tetragonal Zirconia ...*, J. Electrochem. Soc. , 138,36 (1991) .

[53] S. Aronson , *Oxidation and Equilibrium in Nonstoichiometric Zirconium Dioxide Powder*, J. Electrochem. Soc. , 108, 312 (1961).

[54] *Nuclear Methods and Applications*, by Gunter Schatz and Alois Weidinger, Wiley; 1996.

[55] *Theory of Defects in Solids* by A.M. Stoneham, Clarendon Press, Oxford, 1975.

[56] Randy Lunquist. I*ndium Donor Complexes with Native Point Defects in Zinc Selenide.* PhD thesis, Oregon State University, June 1994

[57] H. Jaeger, J. A. Gardner, H. T. Su, and R. L. Rasera. *Microcomputer-controlled perturbed angular correlation spectrometer.* Rev. Sci. Instrum., 58(9):1694-1698, September 1987

[58] Kanthal Corporation, 119 Wooster Street, P. O. Box 281, Bethel, CT 06801-0281.

[59] E. Karapetrova et al., *Oxygen Vacancy Concentration Dependence on Processing in Nanostructural Zirconia* , paper for MS degree, July, 1997, to published in J. Amer. Ceram. Soc.

[60] Hui Guan, *Models of Perturbed Angular Correlation in Fluctuating Electric Field Gradients.* PhD thesis , Brigham Yound University, April 1994.

[61] William E. Evenson, John A. Gardner, Ruiping Wang, Han-Tzong Su, and Alex G. McKale, *PAC Analysis of defect motion by Blume's Stochastic model for I=5/2 electric quadrupole interactions.* Hyperfine Interactions, 62, 283-300, 1990.

[62] A. Abragam and R. V. Pound. *Influence of electric and magnetic fields on angular correlations.* Phys. Rev., 92(4)943, November 1953.

APPENDICES

APPENDIX I:

X-RAY SPECTRA FOR PURE ZIRCONIA.

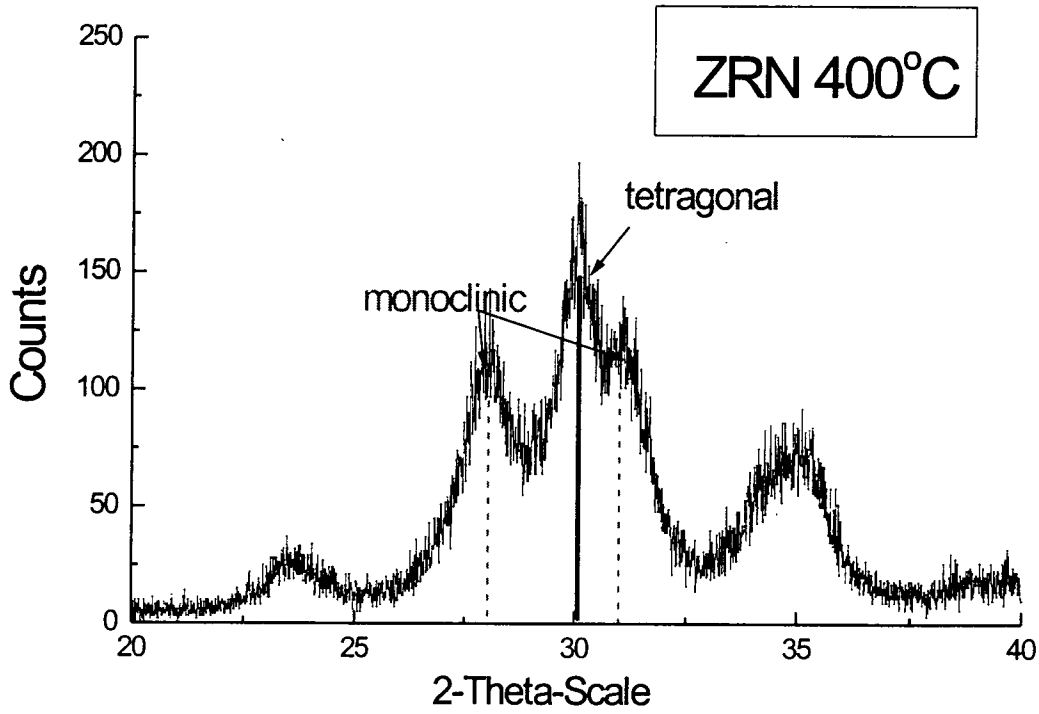

Figure.A-1 X-ray spectra for sample ZRN after calcining at 400°C.

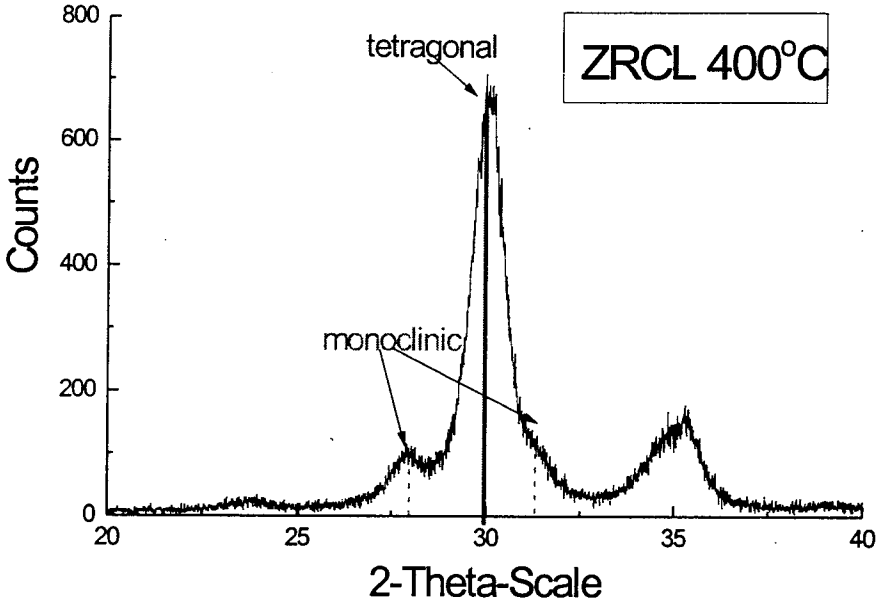

Figure.A-2 X-ray spectra for sample ZRCL after calcining at 400°C

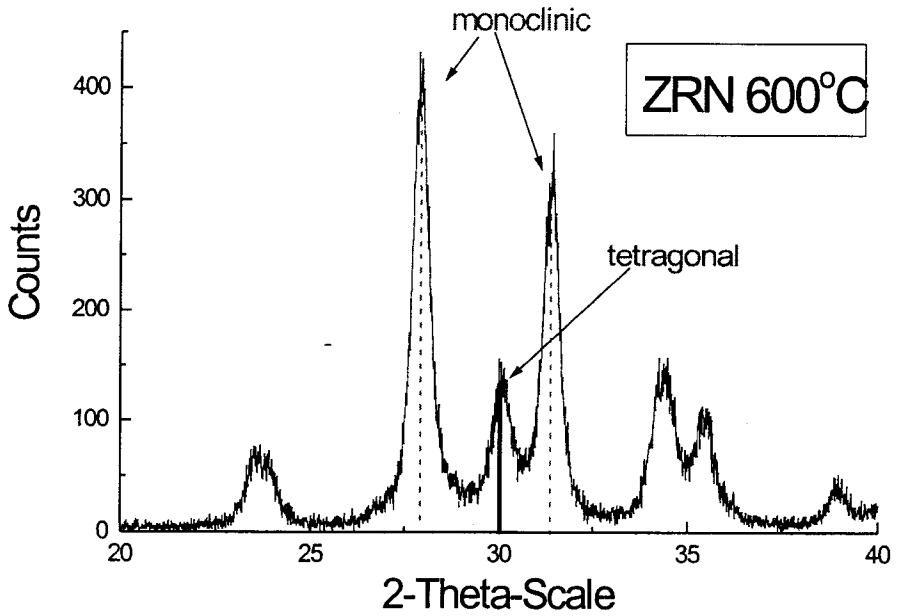

Figure A-3 X-ray spectra for sample ZRN after calcining at 600°C

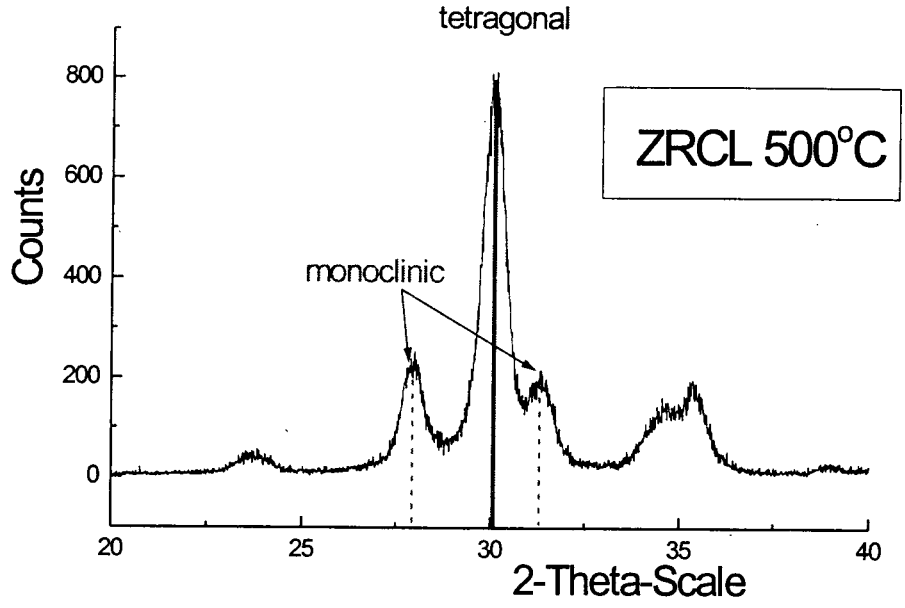

Figure A-4 X-ray spectra for sample ZRCL after calcining at 500°C

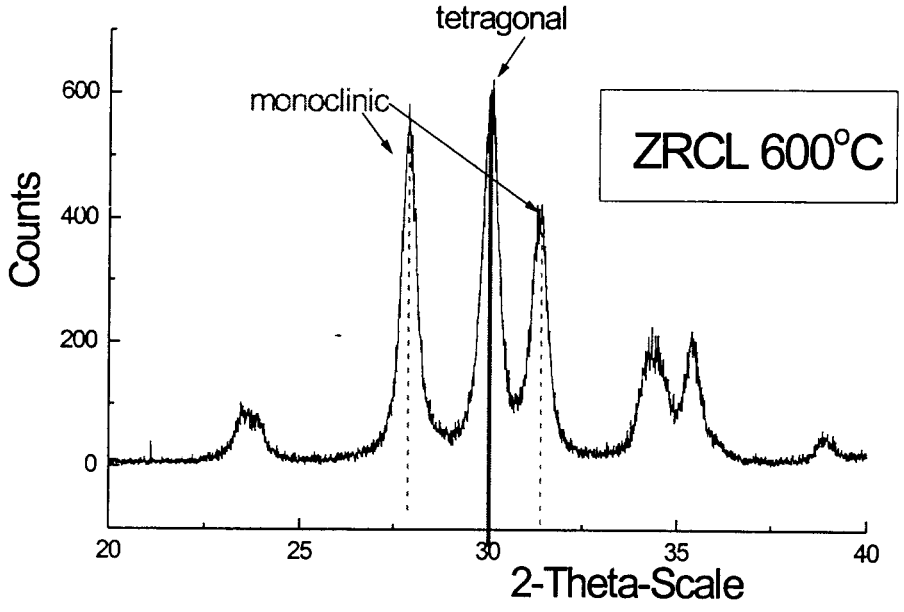

Figure A-5 X-ray spectra for sample ZRCL after calcining at 600°C

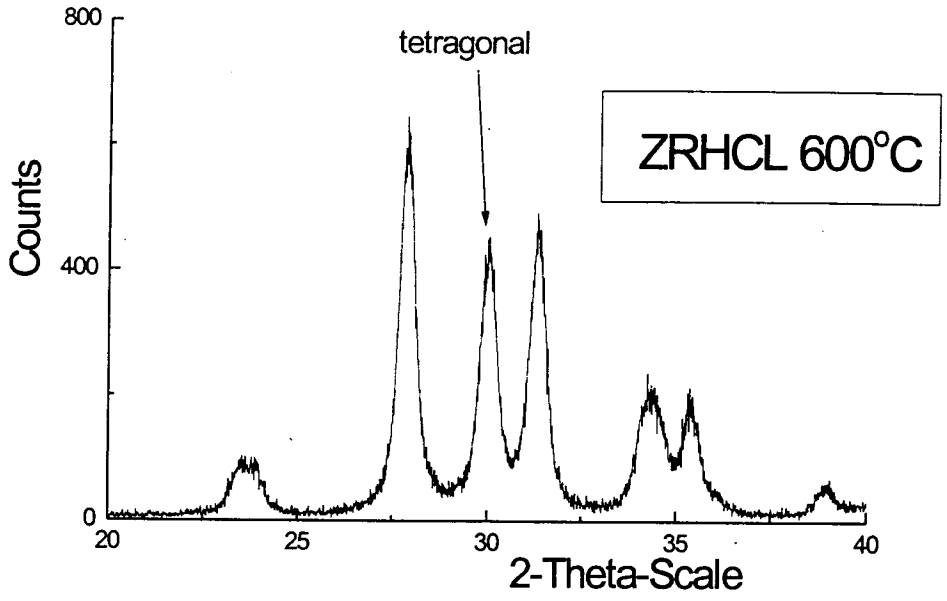

Figure A-6 X-ray spectra for sample ZRHCL after calcining at 600°C. This sample containg Hf.

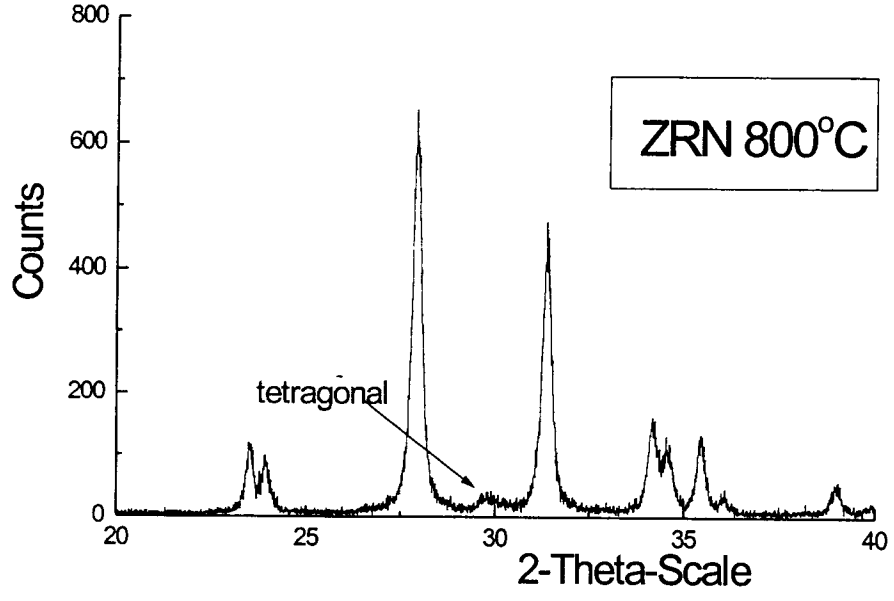

Figure A-7 X-ray spectra for sample ZRN after calcining at 800°C.

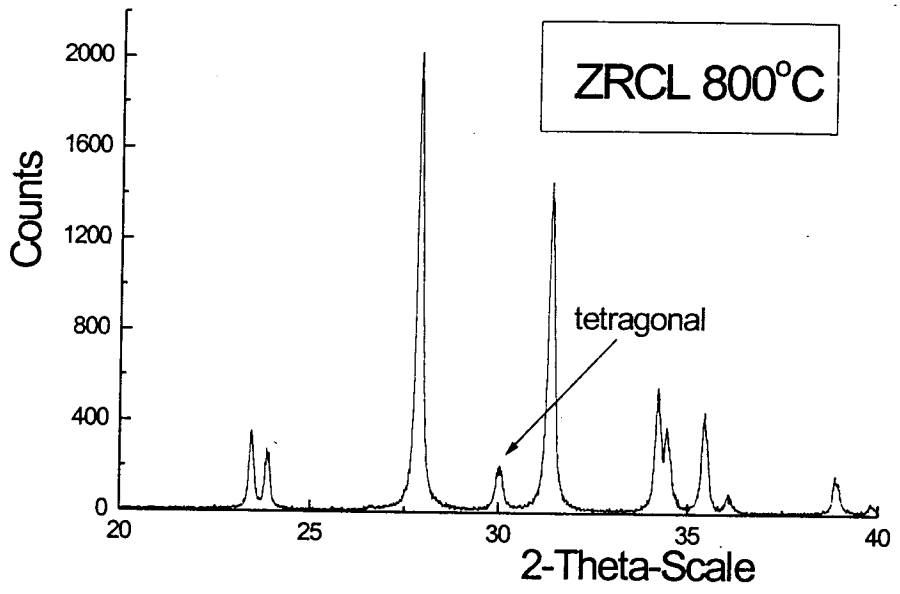

Figure A-8 X-ray spectra for sample ZRCL after calcining at 800°C

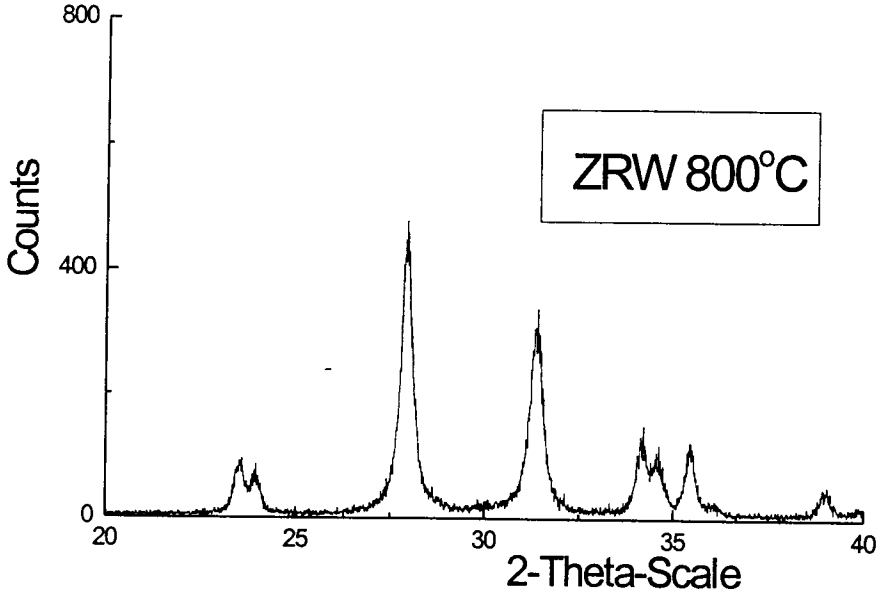

Figure A-9 X-ray spectra for sample ZRW after calcining at 800°C

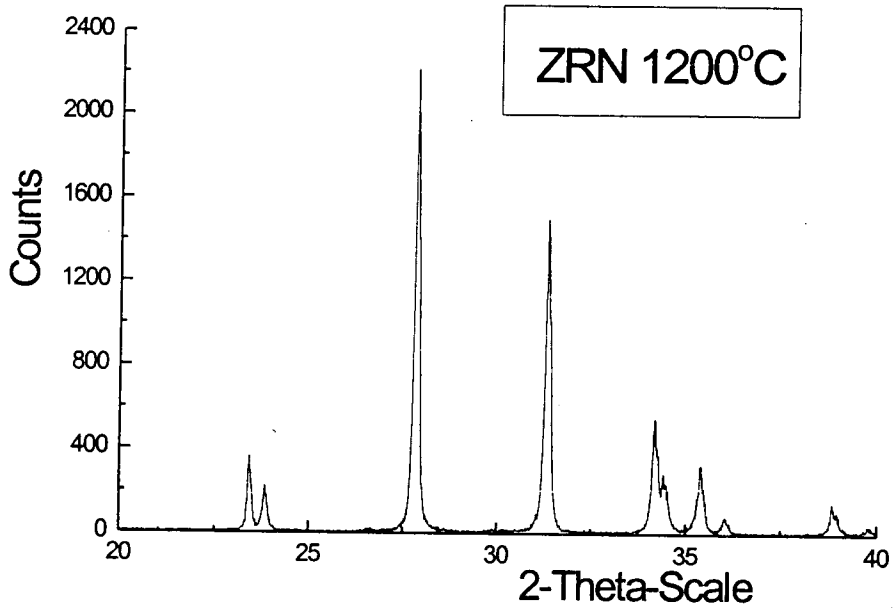

Figure A-10 X-ray spectra for sample ZRN after calcining at 1200°C

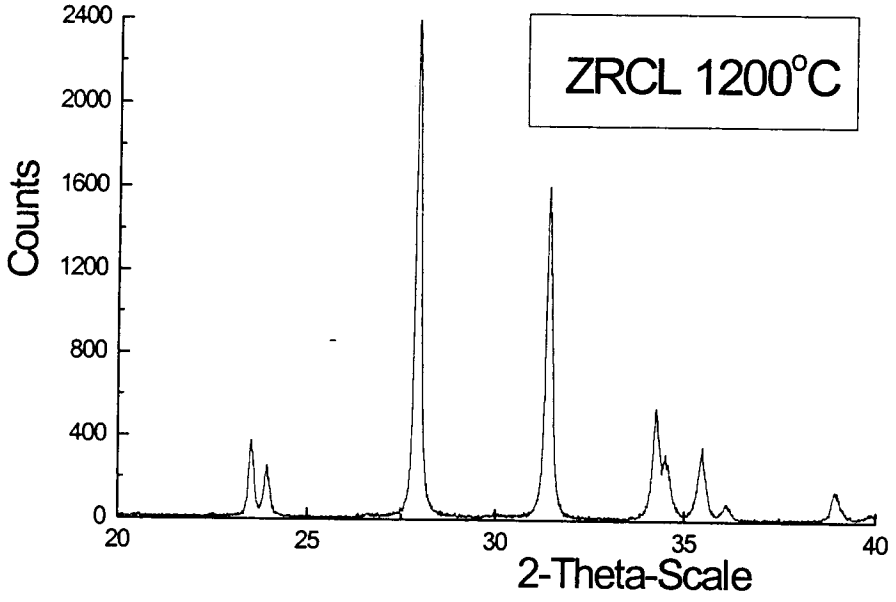

Figure A-11 X-ray spectra for sample ZRCL after calcining at 1200°C

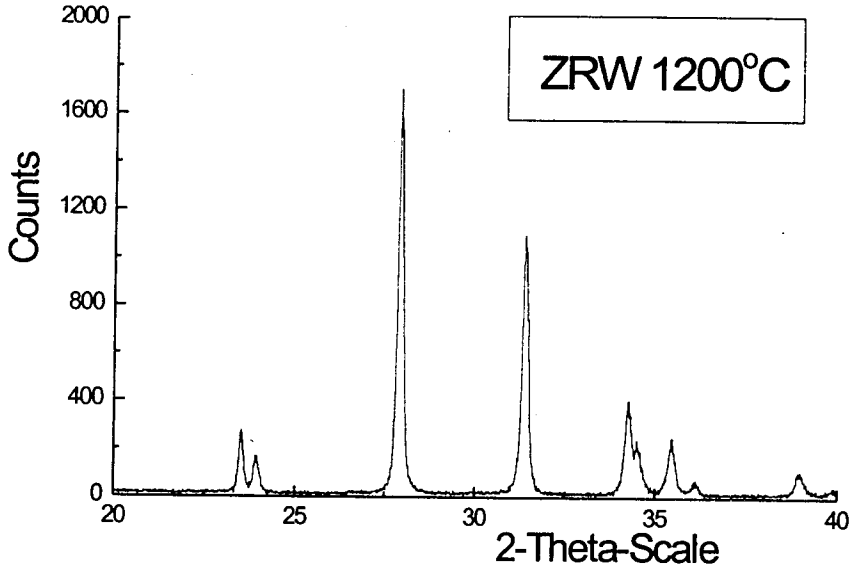

Figure.A-12 X-ray spectra for sample ZRW after calcining at 1200°C

APPENDIX II:

DESCRIPTION OF THE SAMPLES.

1. CeZr4 - 1% Ce-doped zirconia. Prepared by method #1. Was used for PAC measurements.
2. CeZr5 - 1% Ce-doped zirconia. Prepared by method #1. Was used for PAC measurements.
3. CZ7 - 1% Ce-doped zirconia. Prepared by method #1. Was used for PAC measurements.
4. CZ8 - 1% Ce-doped zirconia. Prepared by method #1. Was used for PAC measurements.
5. CZ10 - 1% Ce-doped zirconia. Prepared by method #1. Was used for PAC measurements.
6. CZ11 - 1% Ce-doped zirconia. Prepared by method #1. Was used for PAC measurements.
7. CZ12 - 1% Ce-doped zirconia. Prepared by method #1. Was used for PAC measurements.
8. CZ13 - 1% Ce-doped zirconia. Prepared by method #1. Was used for PAC measurements.
9. CZ15 - 1% Ce-doped zirconia. Prepared by method #1. Was used for PAC measurements.
10. CZ16 - 1% Ce-doped zirconia. Prepared by method #1. Was used for PAC measurements.
11. CZ17 - 2% Ce-doped zirconia. Prepared by method #1. Was used for PAC measurements.
12. CZ19 - 5% Ce-doped zirconia. Prepared by method #1. Was used for PAC measurements.
13. Jzrn1 – pure zirconia sample. Prepared by method #2. Was used for PAC measurements.
14. Jzrn2 – pure zirconia sample. Prepared by method #2. Was used for PAC measurements.
15. Jzrn3 – pure zirconia sample. Prepared by method #2. Was used for PAC measurements.

16. Jzcl2 – pure zirconia sample. Prepared by method #3. Was used for PAC measurements.
17. Jzcl3 – pure zirconia sample. Prepared by method #3. Was used for PAC measurements.
18. Jzbl1 – pure zirconia sample. Prepared by method #4. Was used for PAC measurements.
19. Jzpr1 – pure zirconia sample. Prepared by method #5. Was used for PAC measurements.
20. Jznb2 – 0.3% Nb doped zirconia samples. Prepared by method #3. Was used for PAC measurements.
21. PR1ZR1 – pure zirconia sample. Prepared by method #1. Was used for PAC and SEM measurements.
22. PR1ZR3 – pure zirconia sample. Prepared by method #3. Was used for PAC and SEM measurements.
23. PR!BCL2 – pure zirconia sample. Prepared by method #1. Was used for PAC and SEM measurements.